

~~CONFIDENTIAL~~

Copy 252
RM L50L12

NACA RM L50L12

7223

TECH LIBRARY KAFB, NM
0143761

~~CONFIDENTIAL~~
NACA

RESEARCH MEMORANDUM

INVESTIGATION OF THE EFFECTS OF GEOMETRIC
CHANGES IN AN UNDERWING PYLON-SUSPENDED EXTERNAL-STORE
INSTALLATION ON THE AERODYNAMIC CHARACTERISTICS OF A
45° SWEEPBACK WING AT HIGH SUBSONIC SPEEDS

By Kenneth P. Spreemann and William J. Alford, Jr.

Langley Aeronautical Laboratory
Langley Field, Va.

CLASSIFIED DOCUMENT

This document contains information affecting the National Defense of the United States within the meaning of the Espionage Act, U.S.C. 1831, the transmission or the revelation of its contents in any manner to an unauthorized person is prohibited by law. Information so classified may be imparted only to persons in the Army, Navy, and naval services of the United States, appropriate civilian officers and employees of the Federal Government who have a legitimate interest therein, and to United States citizens of known loyalty and discretion who are authorized therefor.

NATIONAL ADVISORY COMMITTEE FOR AERONAUTICS

WASHINGTON
March 5, 1951

319.98/13

~~CONFIDENTIAL~~

~~CONFIDENTIAL~~

Classification cancelled (or changed to) **Unclassified**

By Authority: **NASA Techn. Info. Office ENL**

By.....

GRADE OF OFFICER MAKING CHANGE) **NK**

DATE **10 Apr 94**

94 11 Jan 56

1
NACA RM L50L12[REDACTED]
NATIONAL ADVISORY COMMITTEE FOR AERONAUTICS

RESEARCH MEMORANDUM

INVESTIGATION OF THE EFFECTS OF GEOMETRIC
CHANGES IN AN UNDERWING PYLON-SUSPENDED EXTERNAL-STORE
INSTALLATION ON THE AERODYNAMIC CHARACTERISTICS OF A
45° SWEEPBACK WING AT HIGH SUBSONIC SPEEDS

By Kenneth P. Spreemann and William J. Alford, Jr.

SUMMARY

An investigation has been made in the Langley high-speed 7- by 10-foot tunnel through a Mach number range of 0.41 to 0.96 to determine the effects of external-store fineness ratio, store shape, store chordwise position, pylon thickness, pylon length, and pylon sweep angle on the aerodynamic characteristics of a number of underwing pylon-suspended external stores in combination with a 45° sweptback semispan wing and fuselage. The Reynolds number range of this investigation was from about 0.50×10^6 to 0.75×10^6 . The store profiles corresponded to NACA 65A-series bodies of revolution, the pylons were NACA 64A-series airfoil sections, and the wing was an NACA 65A006 airfoil section parallel to the free stream.

The results showed that in the range of external-store fineness ratios investigated (4 to 12) and for the particular mounting used in this investigation, the lowest installation drag per unit of store volume was obtained with a store of fineness ratio 8. Variations in pylon length showed that for a particular chordwise location of the store and pylon, the least interference drag was obtained with a pylon of about 25 percent of the local wing chord in length. Decreases in pylon thickness, particularly from 30 to 20 percent of the pylon chord, also resulted in large reductions in drag, especially at the higher Mach numbers. It appeared, in general, however, that the most effective means of obtaining minimum drag for the store installation was to position the store in extreme forward or rearward chordwise locations by mounting the store on swept pylons.

[REDACTED]

[REDACTED]

INTRODUCTION

The use of external stores on high-speed airplanes has been frequently accompanied by severe losses in performance and stability and control because of the adverse interference effects produced by the store installation. These adverse interference effects are largely dependent on the magnitudes and locations of the peak negative pressures of the component parts of the external-store installation in combination with the peak negative pressures of the wing. It is apparent that the changes in the peak-negative-pressure characteristics of the store components can be affected by such store geometric parameters as store fineness ratio, store shape, store chordwise position, pylon thickness, pylon length, and pylon sweep angle.

Investigations have been made to determine the effects of several of these geometric parameters on the interference of external-store installations (references 1 to 5). The results have indicated the need for an investigation of systematized changes in installation geometry. The present paper presents the results of such an investigation by showing the effects of changes in some of the geometric parameters on which the interference depends.

The investigation was made on an inboard underwing pylon-suspended external-store installation on a model with a 45° sweptback semispan wing over a Mach number range that generally extended from 0.41 to 0.96.

COEFFICIENTS AND SYMBOLS

The system of axes employed, together with an indication of the positive forces, moments, and angles, is presented in figure 1. The pitching-moment coefficients are referred to the 25-percent-chord point on the mean aerodynamic chord. Pertinent coefficients and symbols used in this paper are defined as follows:

- C_L lift coefficient (Twice semispan lift/ qS)
- C_m pitching-moment coefficient (Twice semispan pitching moment/ $qS\bar{c}$)
- C_D drag coefficient (Twice semispan drag/ qS)
- C_{D_S} theoretical drag coefficient of stores alone based on model wing area
- ΔC_D increment of drag coefficient due to external-store installation
 $(C_{D_{\text{model} + \text{store installation}}} - C_{D_{\text{model}}})$

-Z	lift, pounds
-X	drag, pounds
M	pitching moment, foot-pounds
M	free-stream Mach number
M_B	drag-break Mach number (free-stream Mach number at which $\frac{\partial C_D}{\partial M} = 0.1$)
V	free-stream velocity, feet per second
a	distance between wing chord line and center line of store, feet
q	dynamic pressure, pounds per square foot $\left(\frac{1}{2}\rho V^2\right)$
ρ	mass density of air, slugs per cubic foot
S	twice wing area of semispan model, 0.125 square foot
\bar{c}	mean aerodynamic chord (M.A.C.) of wing, 0.181 foot; based on relationship $\frac{2}{S} \int_0^{b/2} c^2 dy$ (using theoretical tip)
c	local wing chord measured streamwise, feet
c_p	pylon chord measured perpendicular to pylon quarter-chord line, feet
b	twice span of semispan model, 0.866 foot
y	spanwise distance from plane of symmetry, feet
R	Reynolds number $(\rho V \bar{c} / \mu)$
μ	absolute viscosity, pound-seconds per square foot
α	angle of attack relative to wing chord line, degrees
Λ	angle of pylon quarter-chord line sweep, degrees (positive, sweepback)
l_s/d	external-store fineness ratio

l_p/c	pylon length, presented in percent of local wing chord
t/c_p	pylon thickness, presented in percent of pylon chord
x/c	store chordwise position (positive, aft of wing leading edge), presented in percent of local wing chord
l	length of body, feet
d	maximum diameter of body, feet
t	maximum pylon thickness, feet
x	chordwise distance between nose of store and wing leading edge at spanwise location of store, feet

Subscripts:

f	basic fuselage
s	store
p	pylon (when referred to pylon length it is minimum distance between wing lower surface and store upper surface)

APPARATUS AND MODELS

The investigation was conducted in the Langley high-speed 7- by 10-foot tunnel using a semispan model mounted on a reflection-plane plate, located 3 inches from the tunnel wall in order to bypass the wall boundary layer (figs. 2 and 3). The semispan model was provided with an end plate that was attached to the fuselage at the plane of symmetry. To prevent fouling of the model, a clearance of approximately $\frac{1}{32}$ inch was maintained between the fuselage end plate and the reflection-plane plate. Forces and moments were measured by means of an electrical strain-gage balance system mounted outside the tunnel. The balance system was enclosed in a sealed container to minimize leakage of air from outside the tunnel test section into the flow field of the model.

Basic Model

The basic semispan model consisted of a wing-fuselage combination. The wing was made of beryllium copper and had 45° of sweepback referred to the quarter-chord line, aspect ratio 4, taper ratio 0.6, and an

NACA 65A006 airfoil section parallel to the free stream. The fuselage, which was made of brass, was half a body of revolution of actual fineness ratio 10 (and basic fineness ratio 12), the ordinates of which are given in table I. A two-view drawing of the wing-fuselage combination is presented in figure 2 and photographs of the model in figure 3.

Stores

The external stores were bodies of revolution of fineness ratios 4, 6, 8, 10, and 12. The variations in store fineness ratio were made by changing the diameters of the stores while maintaining a constant store length. The store profiles corresponded to NACA 65A-series airfoil sections. The ordinates are given in table II.

The fineness-ratio-6 store was modified to effect a change in shape of the rear portion of the store by reflexing the store center line so that the upper surface of the store followed closely the contour of the rear part of the wing lower surface and in plan form was fan-shaped. The ordinates of this store are presented in table III.

Pylons

The three variables of pylon geometry investigated were thickness, length, and sweep angle. All the pylons had NACA 64A-series airfoil sections perpendicular to the leading edges and were of 1.0- and 1.5-inch chord. The 1.0-inch-chord pylons were used only in the store shape and store chordwise position phases of the investigation.

The pylon thicknesses (in terms of pylon chord) were 10, 20, and 30 percent. The pylon ordinates are given in table IV.

The pylon lengths based on the minimum distance between the wing lower surface and the store upper surface in percent of the wing local chord were 9.45, 18.9, and 37.8.

Configurations

The external-store installation was an inboard underwing pylon-suspended type of installation. The installation was such that a single geometric parameter could be varied independently, except for the store chordwise position parameter wherein it was also necessary to sweep the supporting pylons.

The store fineness ratios investigated were 4 to 12 at $\frac{l_p}{c} = 9.45$ percent and 4 to 8 at $\frac{l_p}{c} = 37.8$ percent. The fineness-ratio stores are

shown in figure 4 located on the test model and a photograph of the fineness-ratio-4 store on the model is given in figure 3(a).

The store-shape phase of the investigation consisted of a fineness-ratio-6 body of revolution and the fantail-shaped body on a pylon of $\frac{t}{c_p} = 20$ percent and $\frac{l_p}{c} = 9.45$ percent. The fantail-shaped store is shown in figure 5 installed on the model. In figure 3(b) is a photograph of the model with the fantail store.

The fineness-ratio-6 store was located at three chordwise positions such that the distance between the nose of the store and the wing leading edge based on the wing local chord was 141.3 percent and 41.1 percent ahead of the wing leading edge and 40.0 percent behind the wing leading edge. (See fig. 6.) A photograph of the model with the store in the most forward position is presented in figure 3(c).

The fineness-ratio-6 store was utilized for the investigations of the three pylon variables; thickness, length, and sweep angle. The pylon thicknesses of 10, 20, and 30 percent were investigated at $\frac{l_p}{c} = 9.45$ percent and $\frac{l_p}{c} = 37.8$ percent.

The three pylon lengths of $\frac{l_p}{c} = 9.45, 18.9,$ and 37.8 percent were investigated at $\Lambda = 0^\circ$ for 10 and 20 percent thickness and at $\Lambda = 45^\circ$ for 10 percent thickness. Figure 7 shows the pylons and store installed on the model.

The pylon sweep angles of $0^\circ, 30^\circ,$ and 45° were investigated at $\frac{l_p}{c} = 18.9$ percent for two thicknesses, $\frac{t}{c_p} = 10$ percent and 20 percent. The pylons were swept about the intersection of the pylon quarter-chord line and the wing lower surface. The external store remained in the same vertical and chordwise location for each group of pylon sweep angles. Figure 8 shows the installation of the external store and swept pylons on the model.

The pylons and stores were checked for installation accuracy and found to be aligned within $\pm 0.5^\circ$ of the plane of symmetry of the model (vertical plane) and within $\pm 0.2^\circ$ of the wing chord line (horizontal plane).

TESTS AND RESULTS

Lift, pitching moment, and drag measurements were obtained through an angle-of-attack range that usually extended from -2° to 10° . The test Mach number range generally extended from 0.41 to 0.96. The test Reynolds numbers over this Mach number range are presented in figure 9.

The figures showing the results of the investigation are tabulated as follows:

Model parameter	Basic data figures	Summary figures				
		C_D against M	ΔC_D against M	M_B	$(L/D)_{max}$	$\left(\frac{\partial C_m}{\partial C_L}\right)$ and $\left(\frac{\partial C_L}{\partial \alpha}\right)$ against M
Basic model	10	17	--	--	--	18
Store fineness ratio	11	19	20	21	22	23
Store shape	12	24	25	--	--	26
Store chordwise position	13	27	28	29	30	31
Pylon thickness	14	32	33	34	35	36
Pylon length	15	37	38	39	40	41
Pylon sweep angle	16	42	43	44	45	46

It should be noted that summary figures of drag-break Mach numbers and maximum lift-drag ratios were not presented for the external-store-shape phase of the investigation because the fantail-shaped store did not readily lend itself to any common basis for systematic geometric comparison; however, point values of M_B are presented in figure 24.

The slopes of the pitching-moment coefficient ($\partial C_m / \partial C_L$) and of the lift coefficient ($\partial C_L / \partial \alpha$) were generally measured through a lift-coefficient range of 0 to 0.4. The rate of change in pitching-moment coefficient with lift coefficient at a constant Mach number ($\partial C_m / \partial C_L$) is a measure of the aerodynamic-center location relative to the quarter-chord point of the mean aerodynamic chord.

Corrections have been applied to the lift and drag coefficients presented herein to account for the effects of the residual air-flow leakage from within the reflection-plane-plate support into the flow field of the model. The pitching-moment coefficients were found to be

virtually unaffected by this induced air flow into the flow field of the model. The corrections were determined from tests of a wiper-type sponge seal which was located between the model support and the reflection-plane plate. It was impractical to test with the sponge seal in all the time because the seal required adjustment for each angle of attack.

No corrections have been made in these data to account for the fuselage end-plate tares. Drag coefficients presented include the drag due to the fuselage base pressure. Jet-boundary and tunnel blocking corrections were considered negligible because the model was very small in size compared to the tunnel.

DISCUSSION

Basic Model

The basic wing-fuselage data are presented (figs. 10, 17, and 18) for comparison with the results obtained on the model with the external-store installation. Discussion of the basic-model results is presented in the following sections and is limited to a presentation of the points necessary for analysis of the effects of changes in the geometry of the external-store installation.

External-Store Fineness Ratio

Drag characteristics.- An illustration of the effects of changes in store fineness ratio is shown in figures 20(a) and 20(b) where increases in store fineness ratio are seen to produce substantial reductions in the drag coefficients of the installation. With the short pylon, interference effects appear to produce excessive installation drag coefficients for external stores of fineness ratios less than 6. The data also indicate that only small reductions in the installation drag coefficient can be expected with store fineness ratios above 12. With the long pylon (which effectively locates the pressure field of the store at a greater distance from the pressure field of the wing) large reductions in the installation drag coefficients result for the range of store fineness ratios for which interference appeared to produce excessive drag coefficients, particularly at an angle of attack.

In order to evaluate the installation drag coefficient per unit of external-store capacity, figure 20(c) was prepared. The model was assumed to be 1/45 scale for calculations of the volumetric capacities of the stores. The results show that the stores with fineness ratios between 6 and 10 produced the minimum drag per unit volume and that a fineness ratio of about 8 was the optimum. In general, the reductions in ΔC_D at the

lower fineness ratios, using the long pylon, resulted in shifting the point of minimum drag coefficient per unit volume to lower fineness ratios. It appears that for Mach numbers below the drag break a lower drag coefficient per unit volume was obtained with a fineness-ratio-4 store on the long pylon than with the optimum fineness-ratio store of 8 on the short pylon.

In order to provide a quantitative indication of the importance of interference, the increments in drag coefficient due to the external-store installation have been compared to the calculated drag coefficients of the isolated body (shown in fig. 20(b)), and the results plotted as a function of store fineness ratio are presented in figure 20(d) for a representative Mach number of 0.8. The theoretical body alone drag coefficients were calculated by the method of reference 6 utilizing the theoretical velocity distributions over the surfaces of the bodies calculated by means of reference 7. The calculations were based on an assumed transition-point location of 25 percent of the store length for all fineness ratios. It is seen, figure 20(d), that the installation drag coefficient at a fineness ratio of 4 with the short pylon is from 4 to 6 times greater than the drag coefficient of the isolated body over a lift-coefficient range of 0 and 0.3; whereas at a fineness ratio of 12 it is only 50 percent greater than the drag of the isolated body.

The reduction in interference produced by lengthening the pylon is shown to affect a reduction in installation drag coefficient, that is, from 1 to 2 times the drag of the isolated body at fineness ratio 4. It is to be noted however, that with the longer pylon the fineness-ratio-8 store (highest fineness-ratio store investigated on the long pylon) produced higher installation drag coefficients at zero lift coefficient than with the short pylon. The lower installation drag coefficients with the short pylon at zero lift coefficient and store fineness ratios greater than 5 are particularly evident in figure 20(d).

Drag-break Mach number.- The variations of drag-break Mach number M_B , with store fineness ratio, (fig. 21), show that large reductions in M_B accompany excessive installation drag coefficients resulting largely from the serious interference effects of the low fineness-ratio stores. A progressive increase in M_B resulted from increases in store fineness ratio. At the highest store fineness ratio investigated the drag-break Mach number and, consequently, the expected buffet Mach number (reference 1) of the wing-fuselage external-store installation was only 0.01 to 0.03 less than M_B of the basic wing-fuselage combination (fig. 17) over the lift-coefficient range from 0 to 0.3.

It would seem evident that the best store installation will depend somewhat on the tactical mission of the aircraft. For example, an external-store installation employing a high-fineness-ratio external store and short

pylon (which gives low installation drag coefficients at low lift coefficients and comparatively high drag-break Mach numbers) is of interest for airplanes designed for high-speed operations. However, an external store of low fineness ratio (to provide large tank capacity) on a long pylon, which gives low installation drag coefficients per unit volume at lower speeds but which has comparatively low drag-break Mach numbers, would be of interest for long-range aircraft having lower speed requirements.

Maximum lift-drag ratios.- The maximum lift-drag ratios (fig. 22) of the model with the external-store installation employing a short pylon increase with increasing store fineness ratio, particularly for store fineness ratios of 4 and 6. The $(L/D)_{\max}$ of the fineness-ratio-4 store on the short pylon was from 48 percent at low Mach numbers to 32 percent at high Mach numbers of the $(L/D)_{\max}$ for the fineness-ratio-12 store. In the low Mach number range the highest maximum lift-drag ratios, which were obtained with a fineness-ratio-12 store, compare favorably with the $(L/D)_{\max}$ of the basic model. (See fig. 22(a).) With the long pylon the $(L/D)_{\max}$ values (fig. 22(b)) were generally higher throughout the external-store fineness-ratio range investigated. These results also show that the maximum lift-drag ratios for the model with all fineness-ratio external-store configurations whether on the short or long pylon were always reduced by increasing Mach number in contrast to the basic model on which the maximum lift-drag ratios were virtually unaffected by changes in Mach number.

Aerodynamic-center location.- Comparison of the $(\partial C_m / \partial C_L)$ curves for the model with the external-store fineness-ratio installation (fig. 23) with the $(\partial C_m / \partial C_L)$ curve for the basic model (fig. 18) shows that the external-store installation produced a forward or destabilizing change in the aerodynamic-center location. Below the drag-break Mach number, the maximum forward shift was obtained with the fineness-ratio-4 store and was of the order of 8 to 9 percent of the mean aerodynamic chord. The minimum change was obtained with the fineness-ratio-12 store and was about 4 percent of the mean aerodynamic chord.

Lift-curve slope.- The lift-curve slopes of the model with the external-store installation (fig. 23) compared favorably with the lift-curve slope of the basic model (fig. 18) except in the case of the fineness-ratio-4 store at $\frac{l_p}{c} = 9.45$ percent. With the fineness-ratio-4 store on the short pylon, the lift-curve slope was slightly less than that of the basic model.

External-Store Shape

Drag characteristics.- The effect of the modification (fantail-shaped store) to the fineness-ratio-6 body of revolution on the drag coefficients of the external-store installation is shown in figures 24 and 25(a). At low Mach numbers the modified fineness-ratio-6 store produced higher installation drag coefficients than the basic fineness-ratio-6 body. However, with increasing Mach number the installation drag coefficient of the fantail store approached values approximately equal to those of the basic body of revolution. It should be noted that the modification produced a store of greater volume than the basic fineness-ratio-6 body of revolution. A comparison of the installation drag coefficients on the basis of volumetric capacities is presented in figure 25(b). It can be seen that the installation drag coefficients per unit volume of the fantail-shaped store was substantially lower than that of the body of revolution at the higher Mach numbers. At a Mach number of 0.90 the reduction was of the order of 22 percent of the drag coefficient per unit volume of external-store capacity of the basic fineness-ratio-6 body installation.

Drag-break Mach number.- The modified store shape also showed an increase in the drag-break Mach number (fig. 24) compared to the fineness-ratio-6 body of revolution (about 0.015 to 0.03 throughout the lift-coefficient range investigated). Similar results have been obtained on such a store installation on a model with an unswept wing (reference 2).

Aerodynamic-center location.- The modification gave an aerodynamic-center shift of about 3 to 4 percent rearward of that of the basic fineness-ratio-6 installation (fig. 26) and resulted in an aerodynamic-center location of only 1.5 percent ahead of that of the basic wing-fuselage combination (fig. 18). The fantail-shaped store caused less change in aerodynamic-center location than any store installation investigated.

Lift-curve slope.- Below the drag-break Mach number the modified body showed an increase in lift-curve slope over that of the basic wing-fuselage combination (figs. 18 and 26), whereas the basic fineness-ratio-6 store produced a slight decrease.

Store Chordwise Position

Drag characteristics.- The effects of external-store chordwise location on the drag characteristics of the external-store installation with the fineness-ratio-6 body of revolution is presented in figures 27 and 28. The results presented in this section include, in addition to the effects of store chordwise position, the effects of pylon sweep because it was necessary for structural reasons to sweep the pylon

suspension member to achieve the extreme forward and aft positions of the external store. An examination of these data reveals that extreme chordwise positions of the external store gave substantially lower installation drag coefficients throughout the Mach number range investigated than the store located so that the peak negative pressure of the external store was near the peak negative pressure of the wing ($\frac{x}{c} = -41.1$ percent). At the higher Mach numbers where adverse interference effects are more pronounced, the forward- and rearward-located stores produced installation drag coefficients of about 25 to 50 percent of the drag coefficients of the midpositioned store installation. Of the two extreme chordwise store positions, the rear position gave the lowest installation drag coefficients. It is interesting to note that in this position the drag coefficients of the external-store installation (fig. 28) were equal to or less than the calculated drag coefficient of the isolated body of revolution (fig. 20(b)) up to a Mach number of 0.8. It then appears that particularly favorable interference effects exist for this chordwise location of the external store. It is also apparent that, of all the external-store geometric parameters investigated, extreme chordwise location of the stores was the most effective means of reducing the store-installation drag. A previous investigation of extreme chordwise-positioned external stores shows similar results for a model with an unswept wing (reference 2).

Drag-break Mach number.- The results presented in figure 29 show that external-store chordwise location had an appreciable effect on the drag-break Mach numbers of the model with the external-store installation. An increase in M_B is shown to accompany either a forward or rearward movement of the store from the middle chordwise position. The increase in drag-break Mach number is from 0.06 to 0.09 over the lift-coefficient range from 0 to 0.3. The forward and aft chordwise-located stores reduced M_B about 0.05 to 0.06 compared with the basic model.

Maximum lift-drag ratios.- The variations of the maximum lift-drag ratios of the model with the external store in the several chordwise positions are presented in figure 30. These results show that increases in $(L/D)_{max}$ accompany either forward or rearward movement of the external store from the middle position. It also appears that increases in Mach number effect reductions in the maximum lift-drag ratios for any chordwise position of the store, whereas the basic model $(L/D)_{max}$ was practically constant for all test Mach numbers.

Aerodynamic-center location.- Comparison of the $(\partial C_m / \partial C_L)$ curves of the model with several chordwise locations of the external store (fig. 31) with the $(\partial C_m / \partial C_L)$ curve of the basic model (fig. 18) indicates that the minimum forward movement of the aerodynamic center was incurred with the extreme aft-located store and was about 2 percent of the mean aerodynamic

chord. The maximum forward movement of the aerodynamic center was obtained with the extreme forward position of the store. In this position, the aerodynamic center was about 8 percent of the mean aerodynamic chord ahead of the aerodynamic-center location of the basic model.

It should be noted that no attempt has been made in these data to consider changes in the center-of-gravity location that may be expected from such extreme chordwise positions of the external store.

Lift-curve slope.- Below the drag-break Mach number, only small variations in lift-curve slope were apparent due to changes in the store chordwise position (fig. 31), and these values of the model with the external-store installation compared favorably with the lift-curve slope of the basic model (fig. 18).

Pylon Thickness

Drag characteristics.- As may have been expected, decreasing the pylon thickness for both pylon lengths (figs. 32 and 33) resulted in noticeable reductions in the installation drag coefficients. The largest reductions were obtained between pylon thicknesses of 30 and 20 percent. It appeared that, in general, reductions in pylon thickness below 10 percent may be expected to result in only small further reductions in the installation drag coefficients. It is also important to note that, under the conditions where interference effects resulted in high installation drag coefficients with the short pylon (at the greater pylon thicknesses and higher Mach numbers), increasing the pylon length produced even higher installation drag coefficients.

Drag-break Mach number.- The variations of drag-break Mach number with pylon thickness for the installation with the short and the long pylons are presented in figure 34. These data show that an increase in drag-break Mach number accompanies a reduction in pylon thickness and that the increases with the short pylon are small compared to those for the installation utilizing the long pylon. It may also be observed that the highest drag-break Mach number, obtained with the 10-percent-thick pylon, was given by the installation with the short pylon.

Maximum lift-drag ratios.- The variations with pylon thickness of the maximum lift-drag ratios for the model with the external-store installation, presented in figure 35, show that the maximum lift-drag ratios are increased with reductions in pylon thickness and that the largest increases occur for the installation with the long pylon.

Aerodynamic-center location.- A study of figure 36 shows that the variations in pylon thickness generally produced destabilizing

shifts in the aerodynamic-center locations of about 2 to 3 percent of the mean aerodynamic chord. The changes in aerodynamic-center location were about 5 to 8 percent of the mean aerodynamic chord compared to the mean-aerodynamic-center location of the basic model (fig. 18). The thinnest short pylon gave the minimum destabilizing shift which amounted to about 5 to 6 percent of the mean aerodynamic chord ahead of the aerodynamic-center location of the basic model.

Lift-curve slope.- The variations in lift-curve slopes of the model due to changes in pylon thickness, presented in figure 36, show that the external-store installation with the lowest pylon thickness gave a lift-curve slope that compared favorably with that of the basic model (fig. 18). It is also shown that increases in pylon thickness generally produced decreases in lift-curve slope. The largest reductions in lift-curve slope due to increasing the pylon thickness were observed for the longer pylon installation and thickest pylon.

Pylon Length

Drag characteristics.- The effects of changes in pylon length on the drag coefficients of the external-store installation are shown in figures 37 and 38. It appears that, with pylons of 10-percent thickness and 0° sweep angle, a pylon length of about 25 percent of the local wing chord gave the lowest installation drag coefficients. It should be observed that at zero lift coefficient and 0.50 Mach number the installation drag coefficient at about $\frac{l_p}{c} = 25$ percent (fig. 38(b)) was approximately equal to the theoretical drag coefficient of the body alone (fig. 20(b)). It is also apparent that pylon lengths below this optimum introduce detrimental interference effects due to the proximity of the peak negative pressure of the external store to the peak negative pressure of the wing. On the other hand, lengths beyond this optimum (from consideration of the additional pylon, wetted area) appear to produce pylon drag in excess of any reductions in the interference drag of the installation.

Increasing the thickness of the pylons to 20 percent resulted in general increases in installation drag coefficients throughout the range of pylon lengths investigated. The results indicate that at a Mach number of 0.50 the optimum pylon length was also about 25 percent of the local wing chord (fig. 38(b)), but as the Mach number was increased the minimum installation drag coefficients were obtained with pylons less than 25 percent length.

Comparison of the results obtained on a 45° swept pylon of varying lengths (figs. 37(c) and 38) with the results obtained on the unswept pylon of varying lengths (figs. 37(a) and 38) illustrates the reductions in installation drag coefficients that occur with pylon sweep at the

longer pylon lengths. However, these results are believed to be of limited design interest because the additional weight and critical aeroelastic properties of such a pylon configuration would not suggest preference over a short unswept pylon configuration with equally low installation drag coefficients.

Drag-break Mach number.- The effects of changes in pylon length on the drag-break Mach number of the model with the external-store installation, presented in figure 39, show that lengthening the pylon on the two 10-percent-thick configurations appears to cause only minor changes in the drag-break Mach number, although the values of M_B with the 45° swept pylon were generally higher than those obtained on the unswept pylon. However, the drag-break Mach numbers were noticeably decreased with increased pylon length for the 20-percent-thick group of pylon lengths (fig. 39(b)), about 0.06 in the range of lengths investigated. It may also be observed (fig. 39) that the effect of lift on the drag-break Mach numbers appeared to be reasonably constant with variations in pylon length regardless of pylon thickness or pylon sweep angle.

Maximum lift-drag ratios.- Changes in pylon length appeared to have negligible effects on the maximum lift-drag ratios, (fig. 40), for all three groups of pylon lengths investigated. However, as previously indicated in the discussion of pylon thickness, the maximum lift-drag ratios were substantially reduced by increasing the pylon thickness from 10 to 20 percent.

Aerodynamic-center location.- A study of the $(\partial C_m / \partial C_L)$ values for the pylon lengths investigated (fig. 41) shows that variations in pylon length had negligible effect on the aerodynamic-center location. All pylon lengths investigated produced large destabilizing shifts in the aerodynamic-center locations (fig. 41) which were about 7 to 8 percent of the mean aerodynamic chord, compared to the basic model (fig. 18).

Lift-curve slope.- In general, the lift-curve slopes for all pylon lengths investigated (fig. 41) compared favorably with that of the basic model (fig. 18), and were not greatly affected by changes in pylon length.

Pylon Sweep Angle

Drag characteristics.- The results obtained with a 10-percent-thick pylon, $\frac{t_p}{c} = 18.9$ percent, (figs. 42(a) and 43) show that sweeping the pylon did not produce any substantial changes in the external-store installation drag coefficients. Increasing the pylon thickness to 20 percent gave approximately the same trends of installation drag coefficients (figs. 42(b) and 43) as the 10-percent-thick pylon except that the values

of drag were generally higher for the 20-percent-thick pylons. In consideration of the effects of pylon length previously discussed, it appears that the pylon length used for this investigation of pylon sweep angle was lower than that for which pylon sweep effects reductions in the installation drag coefficients. It should be noted that the streamwise chord of the pylon was lengthened with sweep angle.

Drag-break Mach number.- The drag-break Mach numbers with the 10-percent-thick pylon (fig. 44(a)) were virtually unaffected by pylon sweep; however, with the thick pylon the drag-break Mach numbers (fig. 44(b)) were increased about 0.015 by sweeping the pylon from 0° to 45° .

Maximum lift-drag ratios.- The maximum lift-drag ratios (fig. 45) were practically constant with pylon sweep angle for both pylon thicknesses investigated.

Aerodynamic-center location.- A study of figure 46 shows that the aerodynamic-center location was varied about 2 percent by sweeping the pylon and, compared with that of the basic model (fig. 18), was generally shifted forward about 5 to 7 percent of the mean aerodynamic chord.

Lift-curve slope.- The lift-curve slopes were virtually unaffected by sweeping the pylons (fig. 46) and were generally slightly lower than that of the basic wing-fuselage combination (fig. 18).

Pylon Chord Length

Insufficient data were obtained to make a complete analysis of the effects of pylon chord length and, for this reason, figures devoted to the comparison of pylon chord lengths were not included. However, results of the effects of two pylon chord lengths (1.0 and 1.5 inches) with the fineness-ratio-6 body of revolution (figs. 25(a) and 38(a)) show that slightly lower installation drag coefficients were obtained with the 1.0-inch-chord pylon at $\frac{l_p}{c} = 9.45$ percent. At a longer length, $\frac{l_p}{c} = 18.9$ percent, (figs. 28(a) and 38(b)) the difference was negligible in installation drag coefficients. Higher drag-break Mach numbers (figs. 24 and 39(b)) were also obtained with the shorter pylon chord at $\frac{l_p}{c} = 9.45$ percent. The drag-break numbers (figs. 29 and 39(b)) were identical for both chord lengths at $\frac{l_p}{c} = 18.9$ percent.

An examination of $(\partial C_m / \partial C_L)$ in figures 26 and 41(b) indicates that for $\frac{l_p}{c} = 9.45$ percent the ratio of pylon chord to the local wing chord

was an important factor in the stability contribution of underwing pylon-suspended external-store installations. It may be observed that the aerodynamic-center location generally was moved about 2.0 to 4.5 percent of the mean aerodynamic chord farther forward with the 1.5-inch-chord pylon. With the longer pylons, $\frac{l_p}{c} = 18.9$ percent, the $(\partial C_m / \partial C_L)$ values in figures 31 and 41(b) indicated little change in the aerodynamic-center location for the two pylon chord lengths.

A study of figures 26 and 41(b) for $\frac{l_p}{c} = 9.45$ percent and figures 31 and 41(b) for $\frac{l_p}{c} = 18.9$ percent indicates that there is little change in lift-curve slope with changes in pylon chord length.

CONCLUSIONS

The following conclusions are based on a wind-tunnel investigation of the effects of changes in geometry of an underwing pylon-suspended external-store installation on the aerodynamic characteristics of a semispan wing-fuselage model with a 45° sweptback wing:

1. Variations in external-store fineness ratio from 4 to 12, when the store length was held constant, indicated that aerodynamic interference resulted in excessive installation drag coefficients and low drag-break Mach numbers for fineness ratios less than 6 and that a store of fineness ratio of 8 on the shorter of the two pylons used for this investigation produced the minimum installation drag coefficients per unit of external-store volume.
2. Modifying the rear portion of a body of revolution by reflexing the store center line toward the wing lower surface and flattening the rear portion in plan form resulted in less drag per unit of store volume and higher drag-break Mach numbers than the original body of revolution. This modification also produced the least change in the aerodynamic-center location.
3. The most effective means of minimizing the adverse effects of interference to obtain low installation drag coefficients was to position the store in extreme forward or rearward chordwise location by means of swept pylons.
4. Reductions in pylon thickness ratio from 30 to 20 percent of the pylon chord gave large reductions in installation drag coefficients and higher drag-break Mach numbers. Less significant changes in these characteristics were obtained with pylon thickness ratios below 20 percent of the pylon chord.

5. Variations in pylon length from 9.45 to 37.8 percent of the local wing chord showed that for the particular chordwise location investigated, the minimum installation drag coefficients were obtained with a pylon that was about 25 percent of the local wing chord in length.

6. For a given chordwise location of the store, variations in pylon sweep angle from 0° to 45° showed that sweep was effective in reducing the installation drag coefficients only at the longest pylon length investigated (about 38 percent of the local wing chord).

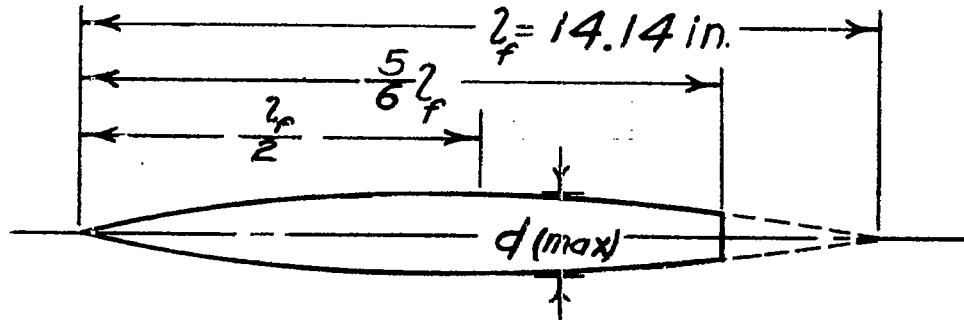
Langley Aeronautical Laboratory
National Advisory Committee for Aeronautics
Langley Field, Va.

REFERENCES

1. Silvers, H. Norman, and Spreemann, Kenneth P.: Correlation of Wind-Tunnel and Flight Determinations of the Buffet Speed of an Airplane Equipped with External Stores. NACA RM L7E20, 1948.
2. Silvers, H. Norman, and Spreemann, Kenneth P.: Wind-Tunnel Investigation of a Wing-Fuselage Combination with External Stores. NACA RM L7K20, 1948.
3. Silvers, H. Norman, and Spreemann, Kenneth P.: Effect of Airfoil Section and Tip Tanks on the Aerodynamic Characteristics at High Subsonic Speeds of an Unswept Wing of Aspect Ratio 5.16 and Taper Ratio 0.61. NACA RM L9J04, 1949.
4. Spreemann, Kenneth P., and Silvers, H. Norman: Experimental Investigation of Various Wing-Mounted External Stores on a Wing-Fuselage Combination Having a Sweptback Wing of Inverse Taper Ratio. NACA RM L9J06, 1950.
5. Silvers, H. Norman, and Spreemann, Kenneth P.: Experimental Investigation of Various External-Store Configurations on a Model of a Tailless Airplane with a Sweptback Wing. NACA RM L9K25, 1950.
6. Heaslet, Max. A., and Nitzberg, Gerald E.: The Calculation of Drag for Airfoil Sections and Bodies of Revolution at Subcritical Speeds. NACA RM A7B06, 1947.
7. Young, A. D., and Owen, P. R.: A Simplified Theory for Streamline Bodies of Revolution, and Its Application to the Development of High-Speed Low-Drag Shapes. R. & M. No. 2071, British A.R.C., 1943.

TABLE I.- FUSELAGE ORDINATES

[Basic fineness ratio 12; actual fineness ratio 10 achieved by cutting off rear one-sixth of body; $\bar{c}/4$ located at $l_f/2$]

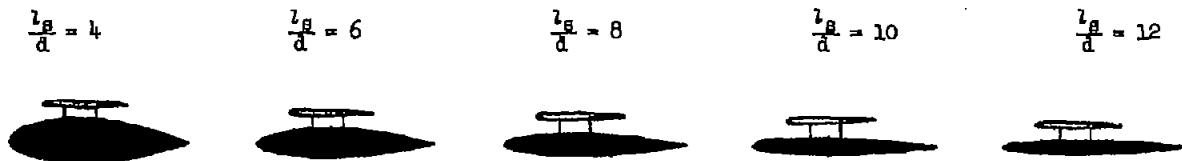


Ordinates, percent length			
Station	Radius	Station	Radius
0	0	45.0	4.143
.5	.231	50.0	4.167
.75	.298	55.0	4.130
1.25	.428	60.0	4.024
2.5	.722	65.0	3.842
5.0	1.205	70.0	3.562
7.5	1.613	75.0	3.128
10.0	1.971	80.0	2.526
15.0	2.593	83.33	2.083
20.0	3.090	85.0	1.852
25.0	3.465	90.0	1.125
30.0	3.741	95.0	.439
35.0	3.933	100.0	0
40.0	4.063		

L.E. radius = 0.05

TABLE II.- ORDINATES, IN PERCENT LENGTH, FOR FIVE NACA 65A-SERIES BODIES OF REVOLUTION USED AS EXTERNAL STORES

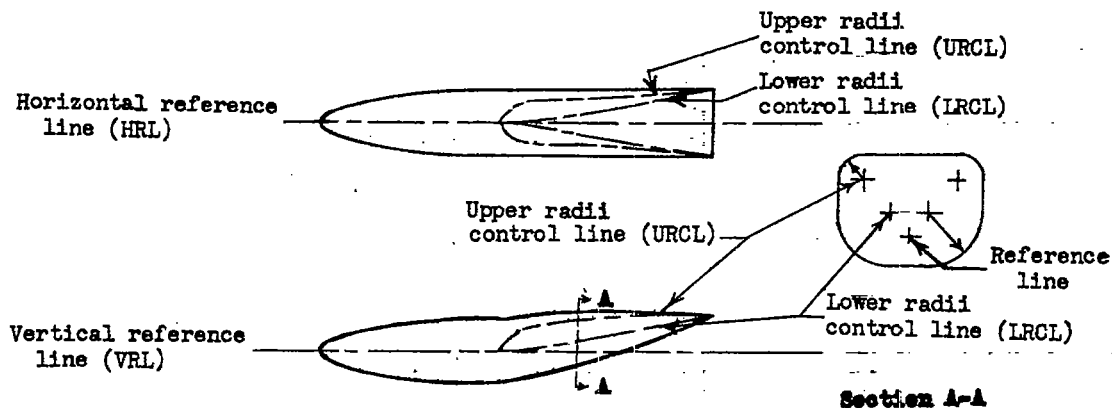
[$l_B = 5.0$ in.]



Station	Radius	Radius	Radius	Radius	Radius
0	0	0	0	0	0
.5	1.92	1.28	.96	.76	.64
.75	2.32	1.54	1.16	.92	.78
1.25	2.96	1.98	1.48	1.18	.98
2.5	4.06	2.70	2.02	1.62	1.36
5.0	5.46	3.64	2.72	2.18	1.82
7.5	6.62	4.42	3.32	2.66	2.22
10.0	7.60	5.06	3.80	3.04	2.54
15.0	9.14	6.10	4.58	3.66	3.06
20.0	10.32	6.88	5.16	4.12	3.44
25.0	11.20	7.48	5.60	4.48	3.74
30.0	11.86	7.90	5.92	4.74	3.96
35.0	12.28	8.18	6.14	4.92	4.10
40.0	12.48	8.32	6.24	5.00	4.16
45.0	12.46	8.30	6.22	4.98	4.16
50.0	12.16	8.10	6.08	4.86	4.06
55.0	11.58	7.72	5.80	4.64	3.86
60.0	10.76	7.18	5.38	4.30	3.60
65.0	9.74	6.50	4.88	3.90	3.26
70.0	8.58	5.72	4.30	3.44	2.86
75.0	7.28	4.86	3.64	2.92	2.42
80.0	5.88	3.92	2.94	2.36	1.96
85.0	4.42	2.96	2.22	1.78	1.48
90.0	2.98	1.98	1.48	1.18	1.00
95.0	1.52	1.00	.76	.60	.50
100.0	.06	.04	.02	.02	.02
L.E. rad.	1.60	1.06	.80	.64	.54
T.E. rad.	.06	.04	.02	.02	.02

TABLE III.- ORDINATES, IN PERCENT LENGTH, FOR FANTAIL-SHAPED BODY

$$[l_s = 5.0 \text{ in.}]$$



Station reference →	LRCL VRL	URCL VRL	Upper ordinate VRL	Lower ordinate VRL	LRCL HRL	URCL HRL	Ordinate HRL
0	0	0	0	0	0	0	0
.5	0	0	1.28	-1.28	0	0	±1.28
.75	0	0	1.50	-1.50	0	0	±1.50
1.25	0	0	1.96	-1.96	0	0	±1.96
2.5	0	0	2.70	-2.70	0	0	±2.70
5.0	0	0	3.64	-3.64	0	0	±3.64
7.5	0	0	4.42	-4.42	0	0	±4.42
10.0	0	0	5.01	-5.01	0	0	±5.01
15.0	0	0	6.10	-6.10	0	0	±6.10
20.0	0	0	6.87	-6.87	0	0	±6.87
25.0	0	0	7.49	-7.46	0	0	±7.48
30.0	0	0	7.90	-7.90	0	0	±7.90
35.0	0	0	8.18	-8.18	0	0	±8.16
40.0	0	0	8.34	-8.34	0	0	±8.34
45.0	0	0	8.30	-8.30	0	0	±8.34
47.5	.01	3.11	8.41	-8.19	±.20	±3.00	±8.34
50.0	.02	4.62	8.62	-8.09	±.30	±4.50	±8.34
52.5	.50	6.00	9.04	-7.30	±.50	±5.20	±8.34
55.0	.76	6.66	9.26	-6.96	±.70	±5.60	±8.34
60.0	1.50	7.40	9.70	-5.68	±1.20	±5.60	±8.34
65.0	2.60	8.00	10.20	-3.90	±1.80	±5.80	±8.34
70.0	3.30	8.20	10.20	-2.41	±2.50	±6.00	±8.34
75.0	4.30	8.70	10.20	-.55	±3.20	±6.40	±8.34
80.0	5.20	8.95	10.20	1.28	±4.20	±6.70	±8.34
85.0	6.20	9.20	10.20	3.24	±5.20	±7.00	±8.34
90.0	7.10	9.30	10.10	5.14	±6.10	±7.50	±8.34
95.0	8.30	9.50	10.00	7.30	±7.20	±7.80	±8.34
100.0	9.30	9.30	9.30	9.30	±8.30	±8.30	±8.34
L.E. rad.	.04						

TABLE IV.- ORDINATES, IN PERCENT CHORD, FOR NACA 64A-SERIES AIRFOIL SECTIONS
USED AS PYLONS

$[c_p = 1.0 \text{ in. and } 1.5 \text{ in.}]$

$\frac{t}{c_p} = 10 \text{ percent}$

$\frac{t}{c_p} = 20 \text{ percent}$

$\frac{t}{c_p} = 30 \text{ percent}$



Station	Ordinate	Ordinate	Ordinate
0	0	0	0
.5	±.81	±1.61	±2.41
.75	±.97	±1.94	±2.91
1.25	±1.22	±2.45	±3.67
2.5	±1.69	±3.37	±5.07
5.0	±2.33	±4.65	±6.98
7.5	±2.81	±5.61	±8.41
10.0	±3.20	±6.40	±9.60
15.0	±3.81	±7.62	±11.44
20.0	±4.27	±8.55	±12.81
25.0	±4.61	±9.21	±13.83
30.0	±4.84	±9.67	±14.51
35.0	±4.97	±9.93	±14.91
40.0	±4.99	±9.99	±15.32
45.0	±4.89	±9.79	±14.68
50.0	±4.69	±9.37	±14.05
55.0	±4.39	±8.77	±13.17
60.0	±4.02	±8.04	±12.06
65.0	±3.60	±7.19	±10.79
70.0	±3.13	±6.25	±9.38
75.0	±2.62	±5.25	±7.87
80.0	±2.10	±4.21	±6.31
85.0	±1.58	±3.17	±4.75
90.0	±1.06	±2.13	±3.19
95.0	±.54	±1.08	±1.62
100.0	±.02	±.04	±.06
L.E. rad.	.69	1.37	2.06
T.E. rad.	.02	.05	.07



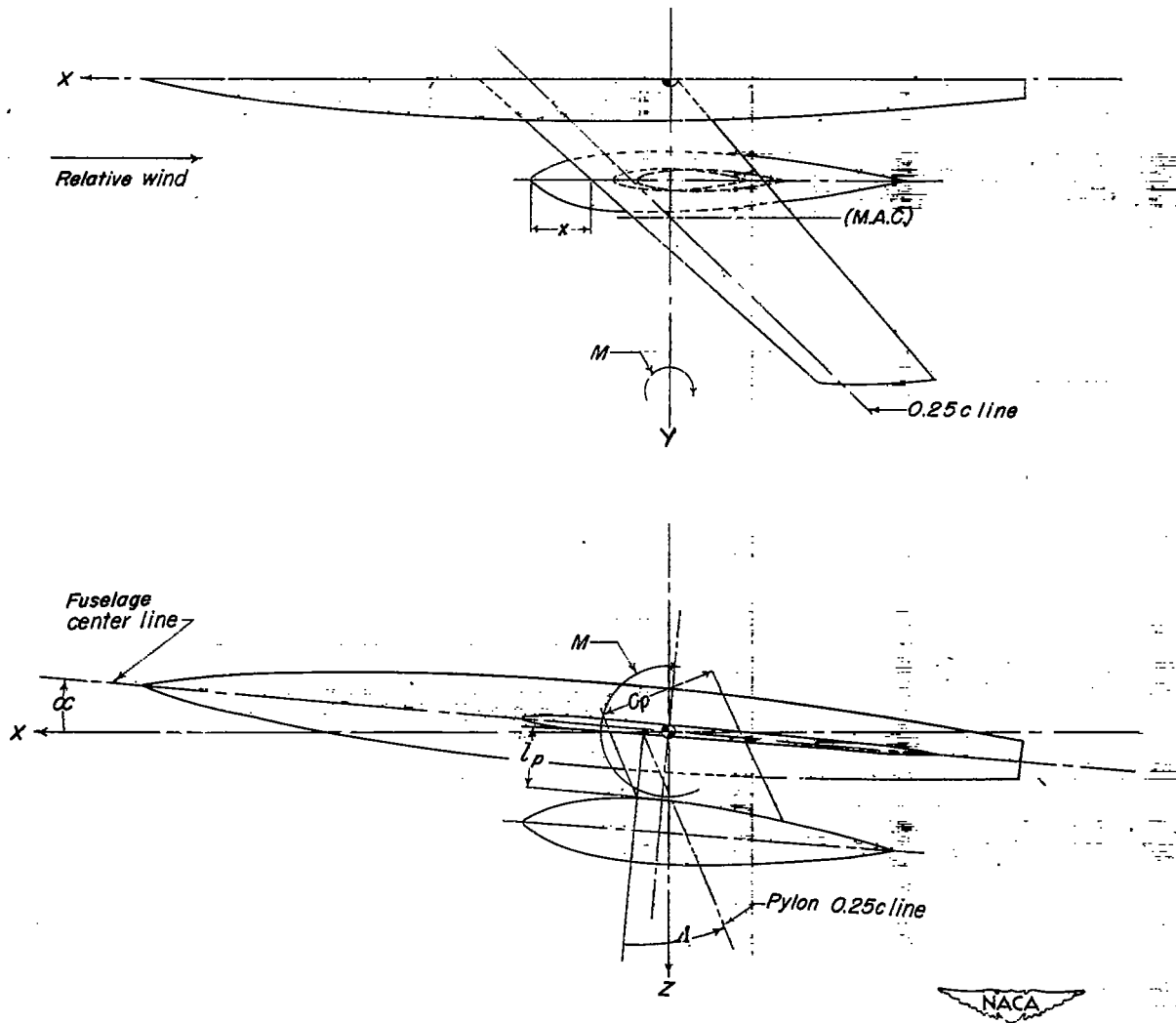


Figure 1.- System of axes. Positive values of forces, moments, and angles are indicated by the arrows.

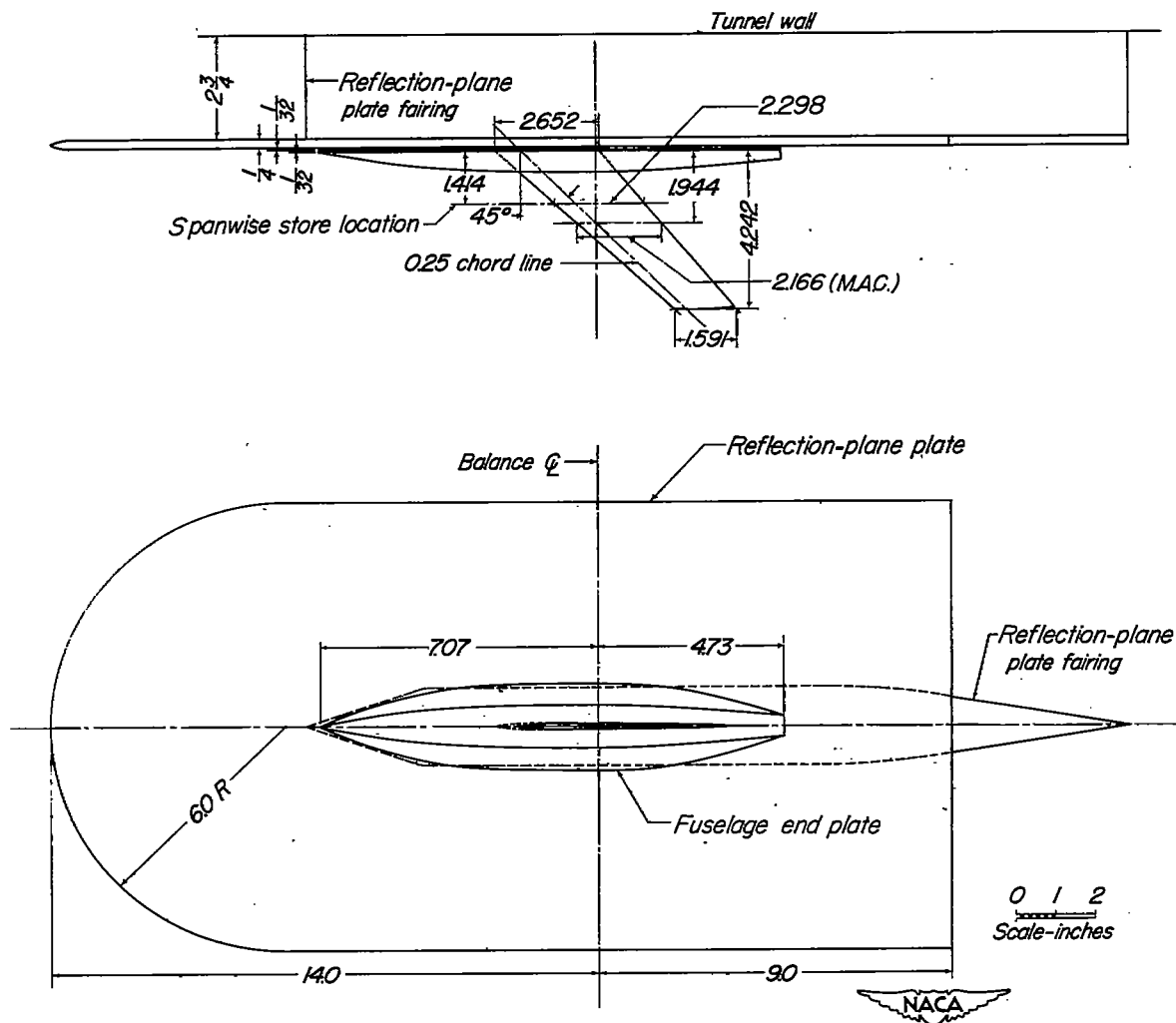
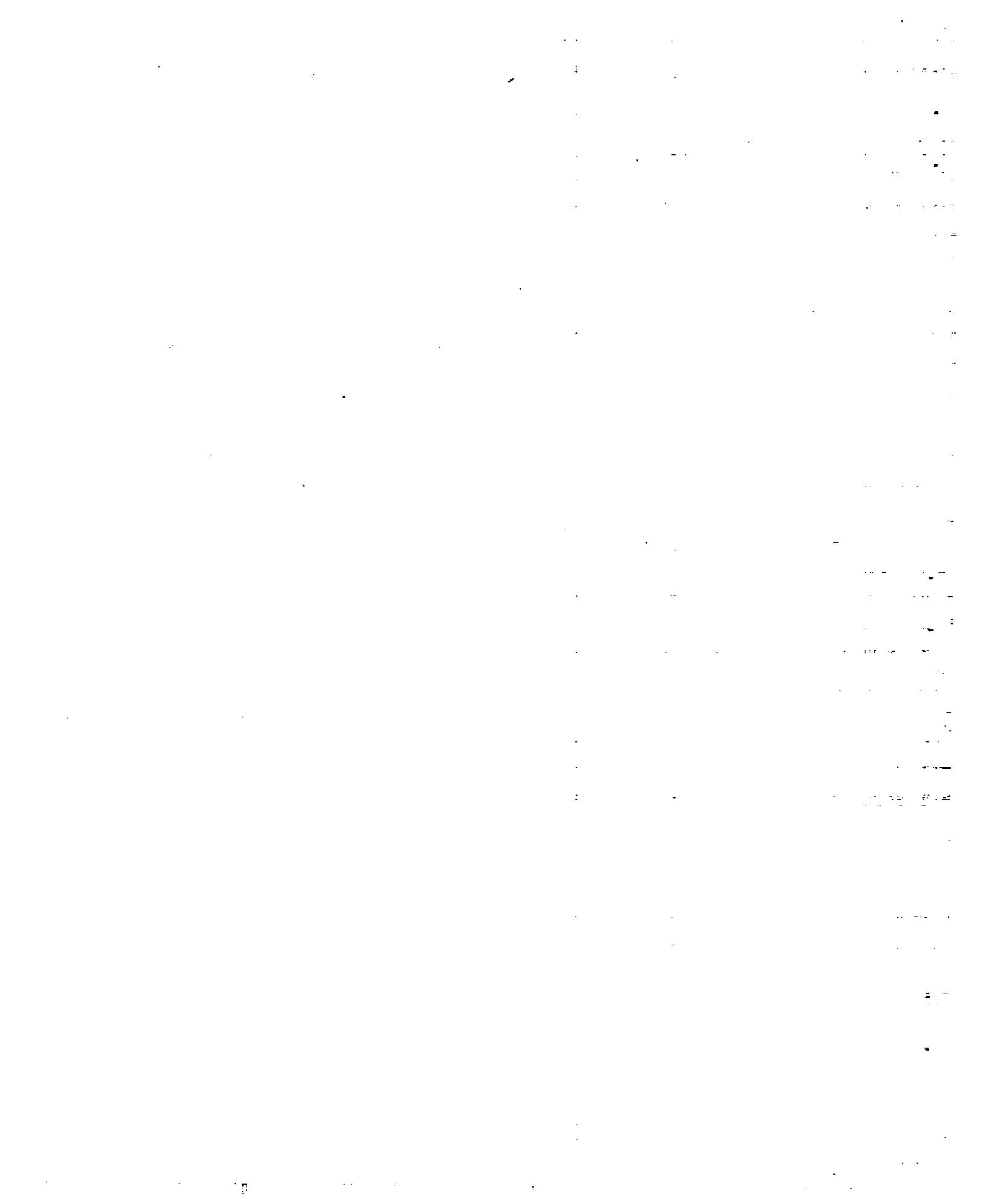
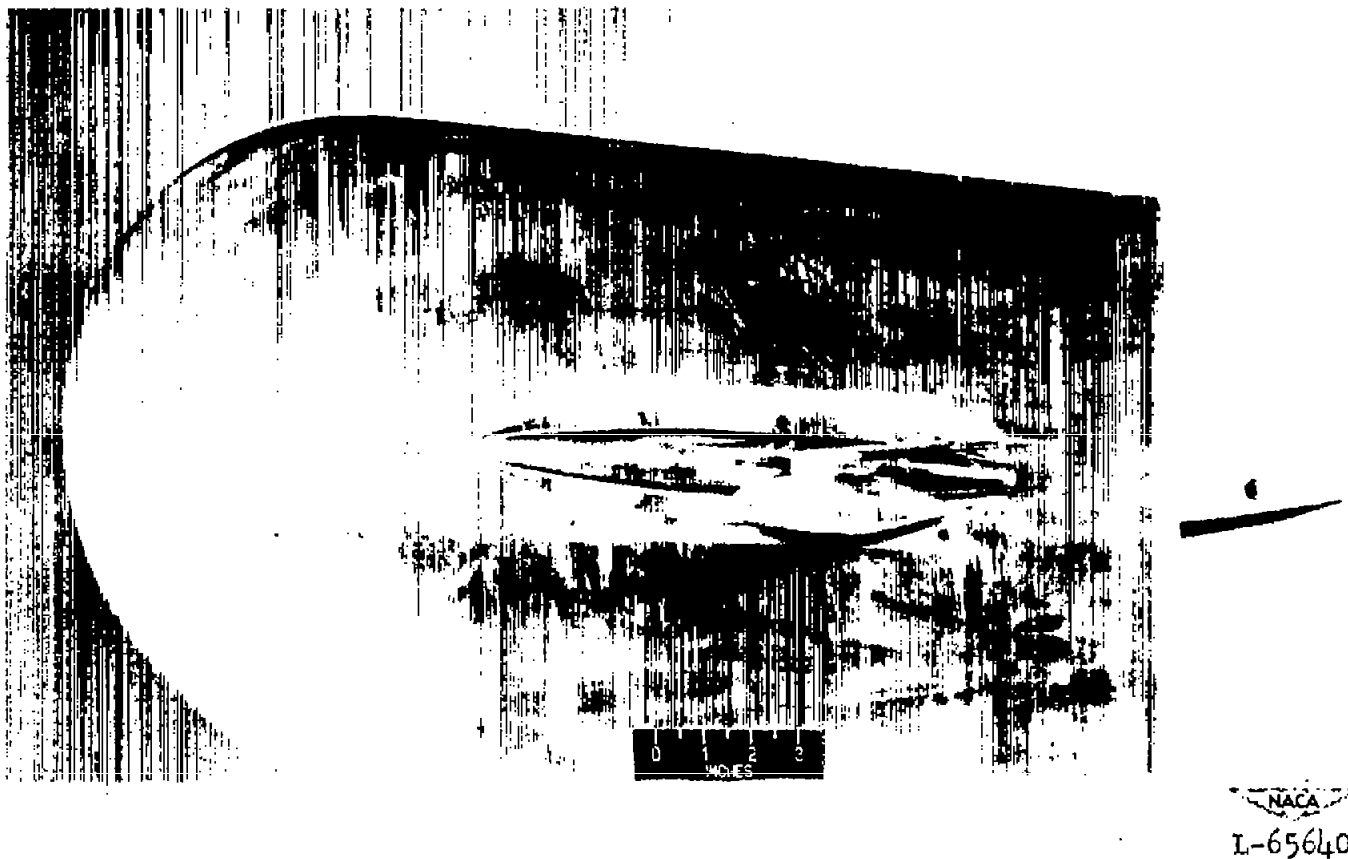


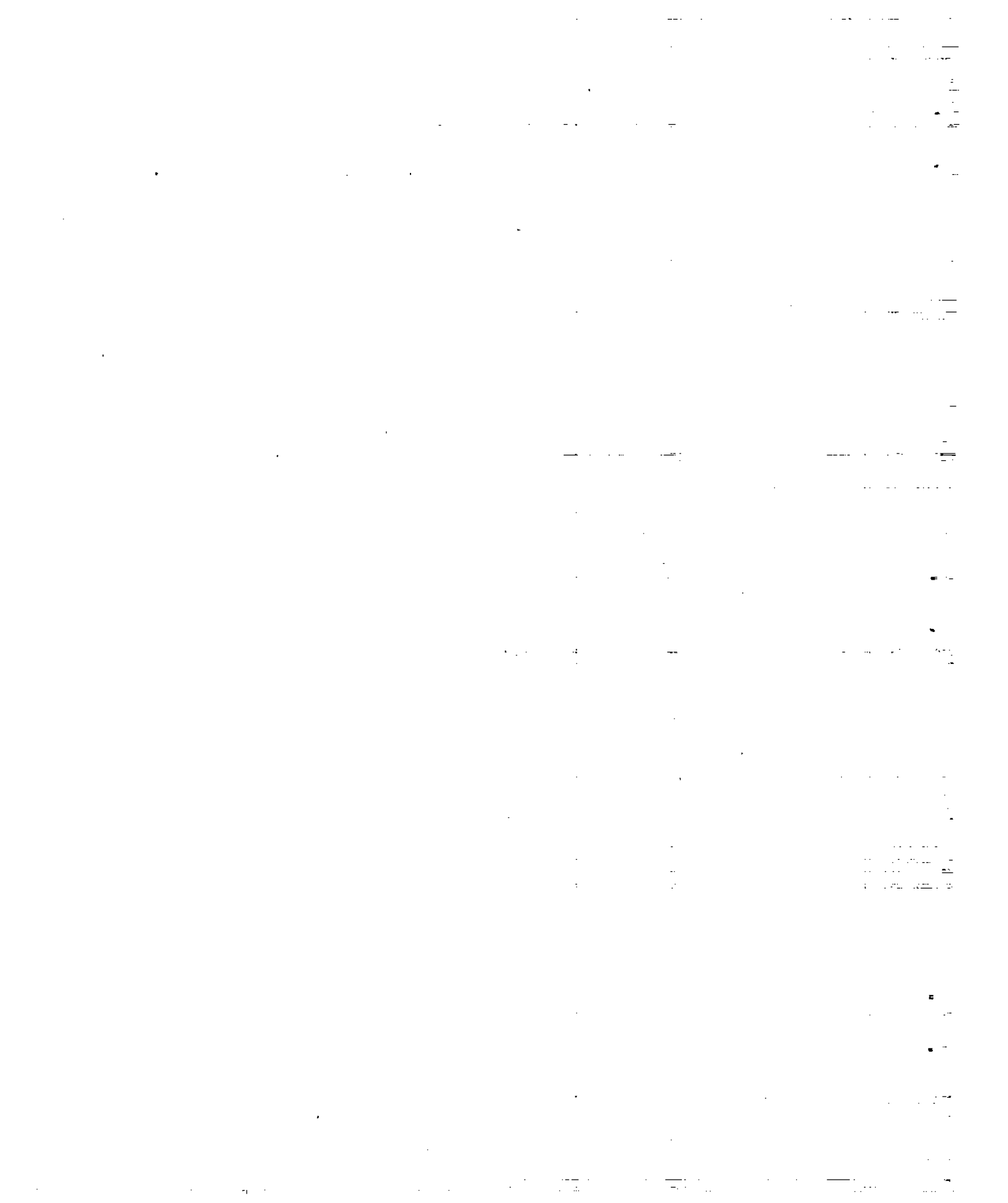
Figure 2.- Two-view drawing of the basic semispan model with 45° sweptback wing, aspect ratio 4, taper ratio 0.6, and an NACA 65A006 airfoil section.

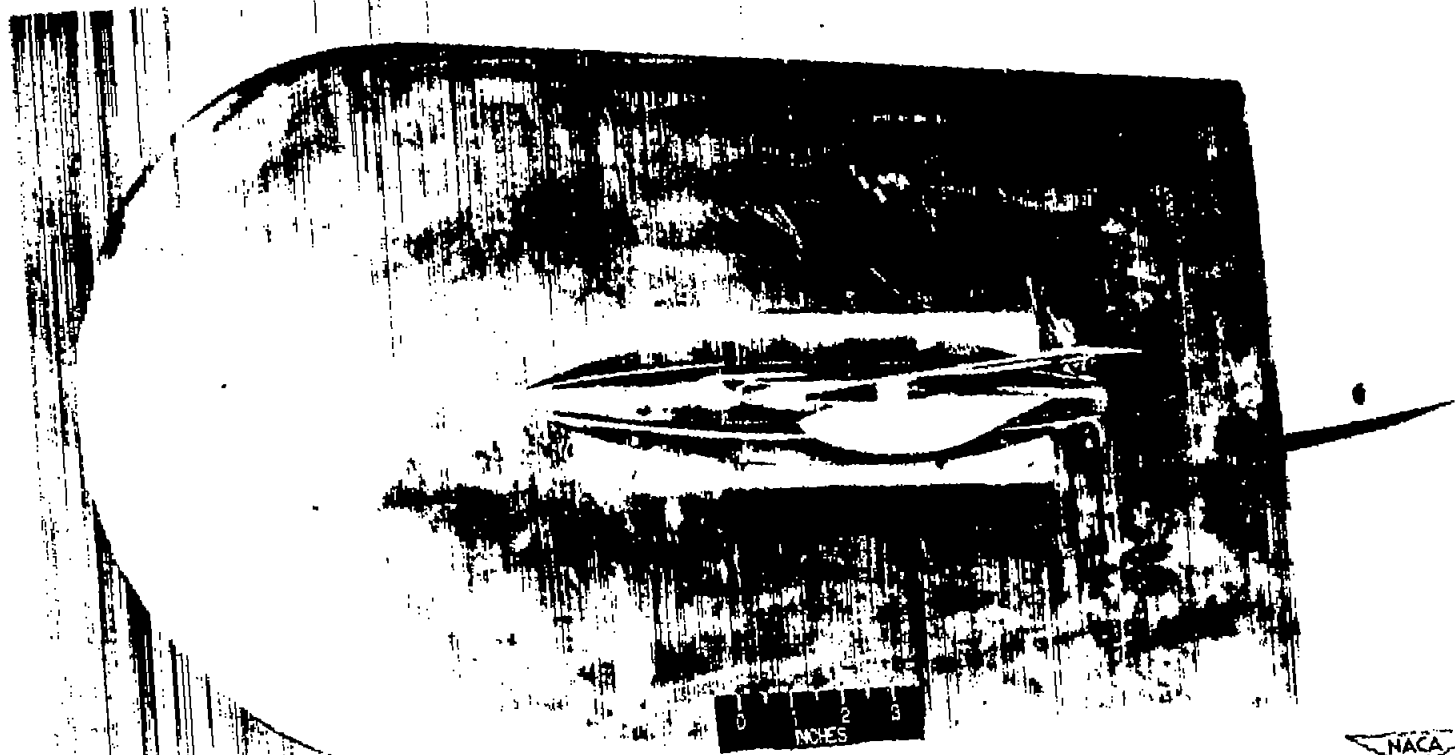




(a) Model with fineness-ratio-4 external store mounted with a pylon of $\frac{t}{c_p} = 10$ percent, $\frac{l_p}{c} = 9.45$ percent, $c_p = 1.5$ inches, and $\Lambda = 0^\circ$.

Figure 3.- Photographs of model and several typical external-store installations.

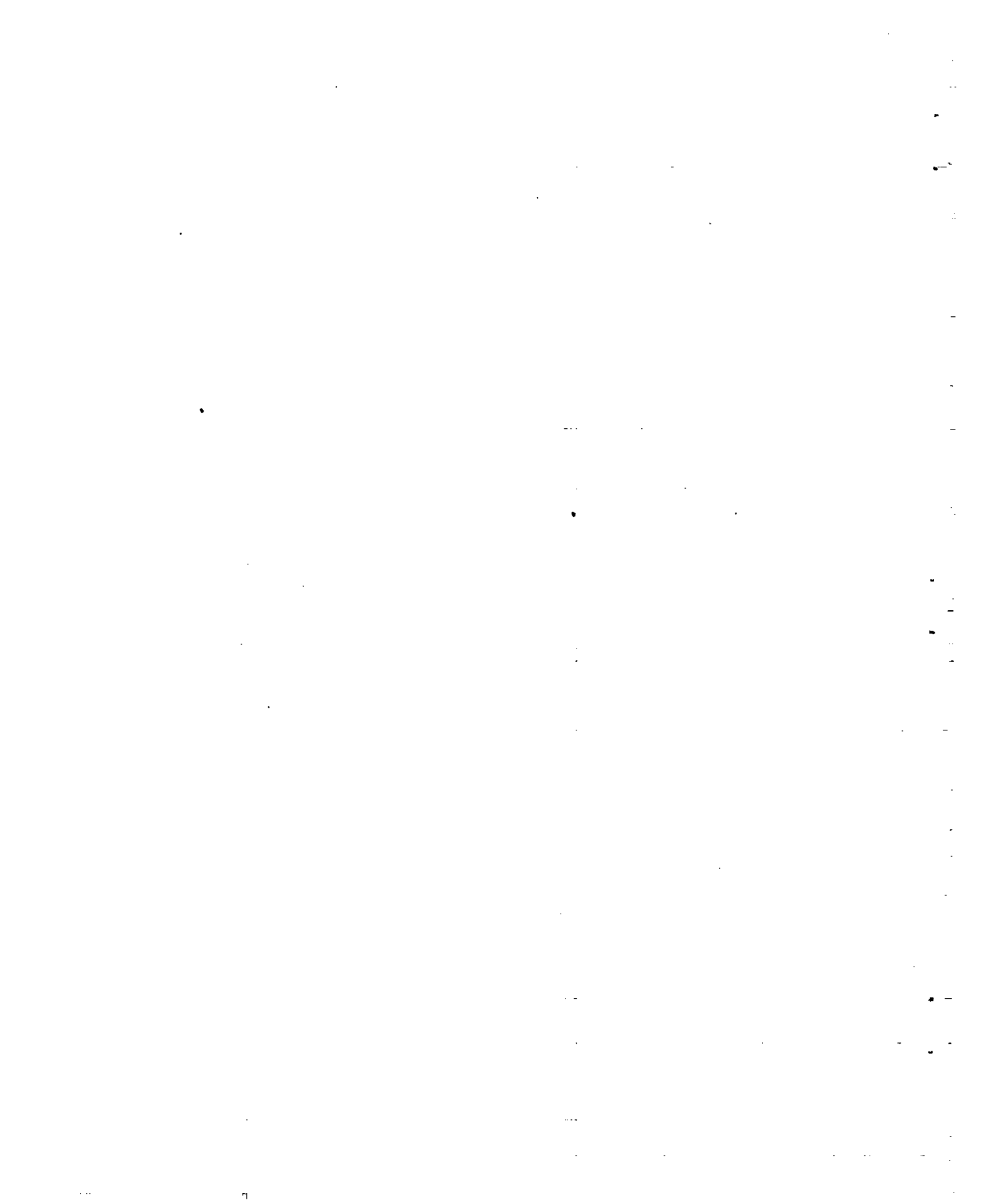


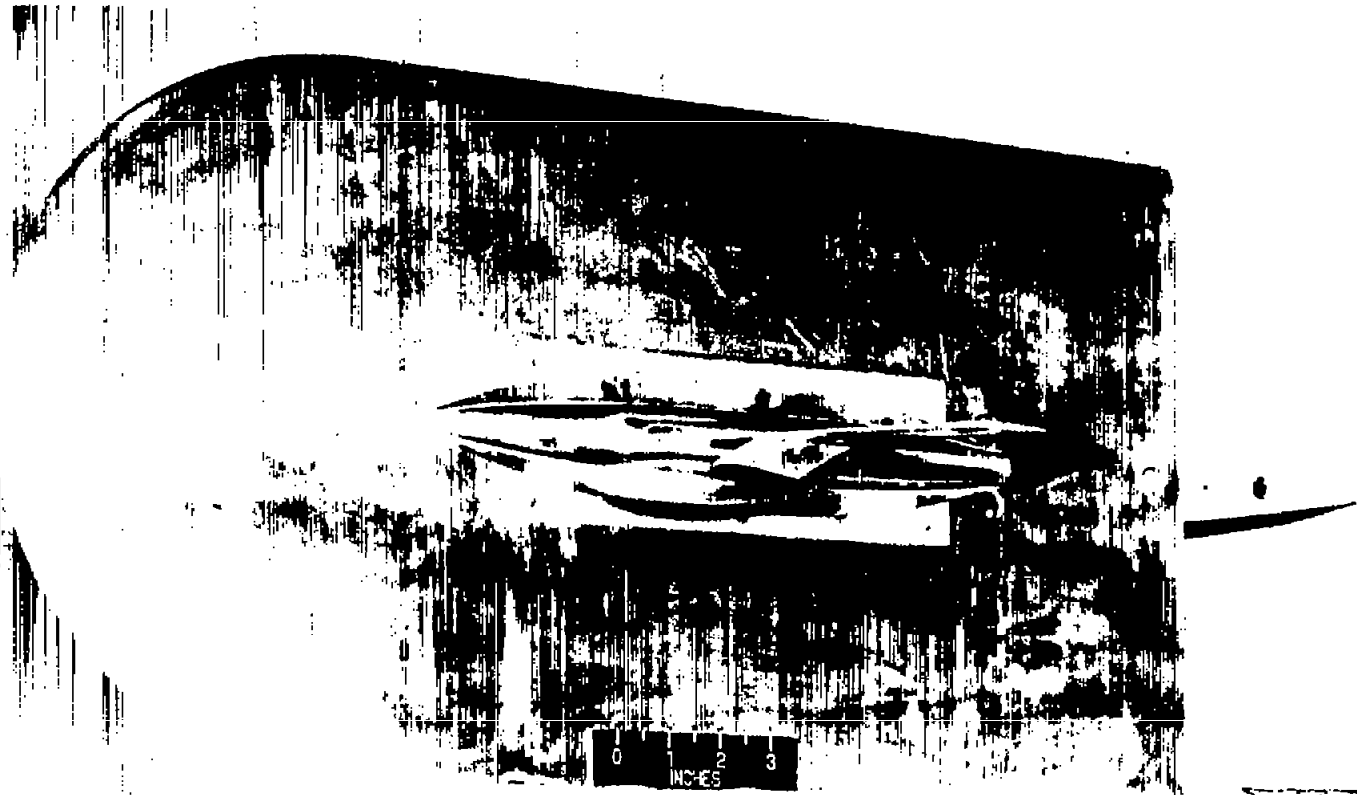
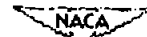


NACA
L-65638.1

(b) Model with fantail external store mounted with a pylon of
 $\frac{t}{c_p} = 20$ percent, $\frac{l_p}{c} = 9.45$ percent, $c_p = 1.0$ inch, and $\Lambda = 0^\circ$.

Figure 3.- Continued.

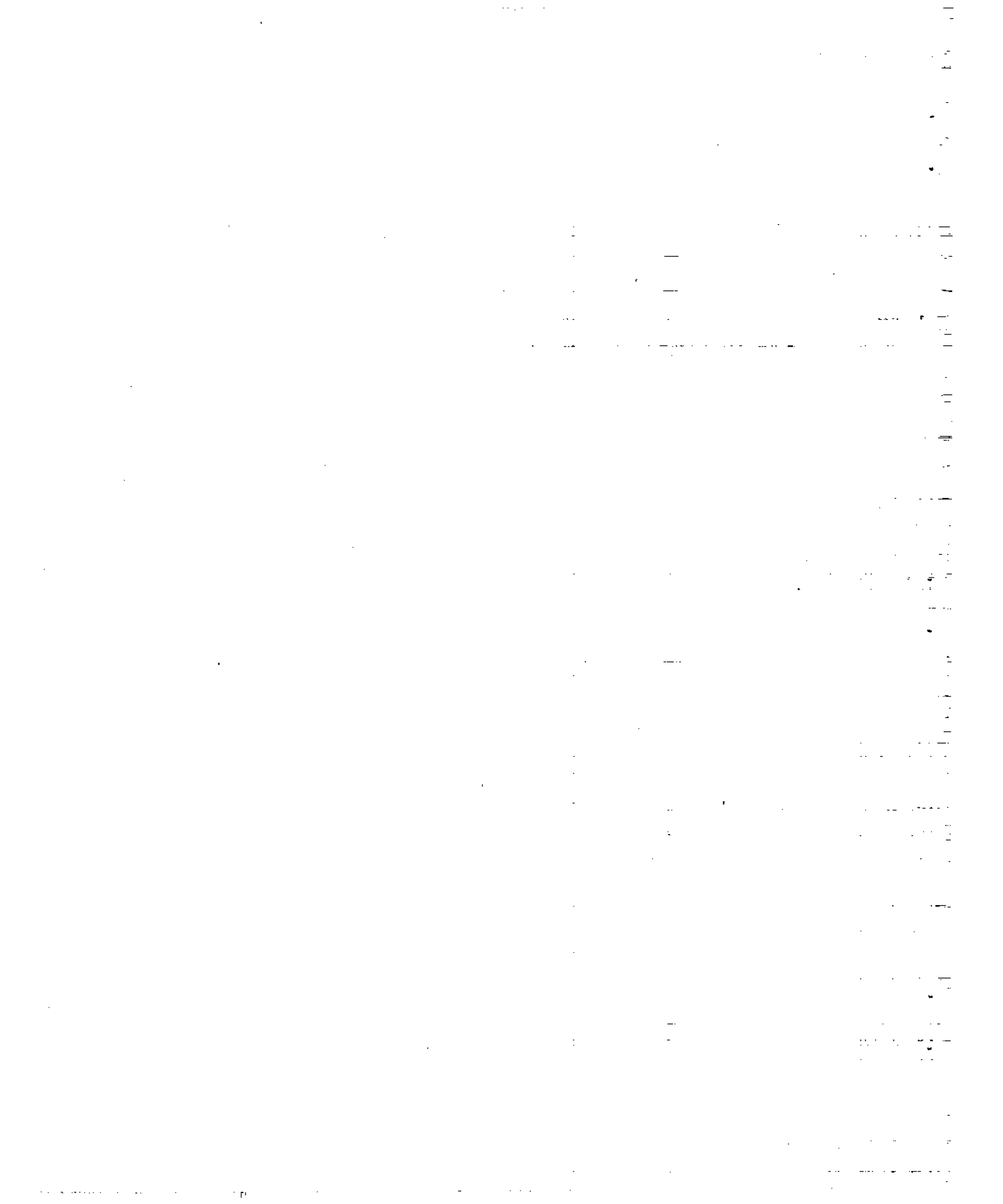


L-65637.1

(c) Model with fineness-ratio-6 external store mounted with a pylon of $\frac{t}{c_p} = 20$ percent, $\frac{l_p}{c} = 18.9$ percent, $c_p = 1.0$ inch, and a store chordwise position of $\frac{x}{c} = -141.3$ percent.

Figure 3.- Concluded.



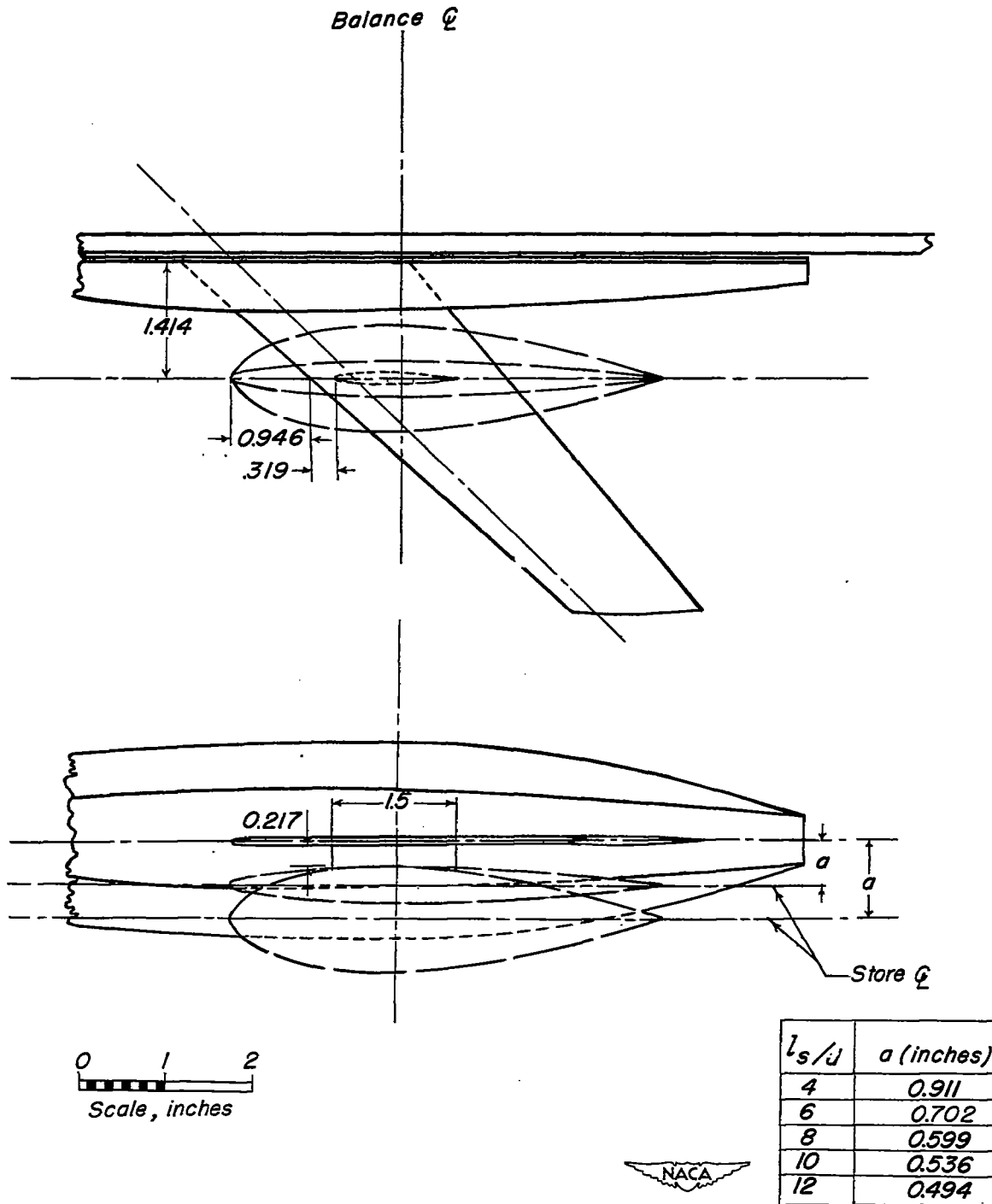


Figure 4.- Drawing of fineness-ratio external stores tested on model using a pylon of $\frac{t}{c_p} = 10$ percent and $\frac{l_p}{c} = 9.45$ percent.

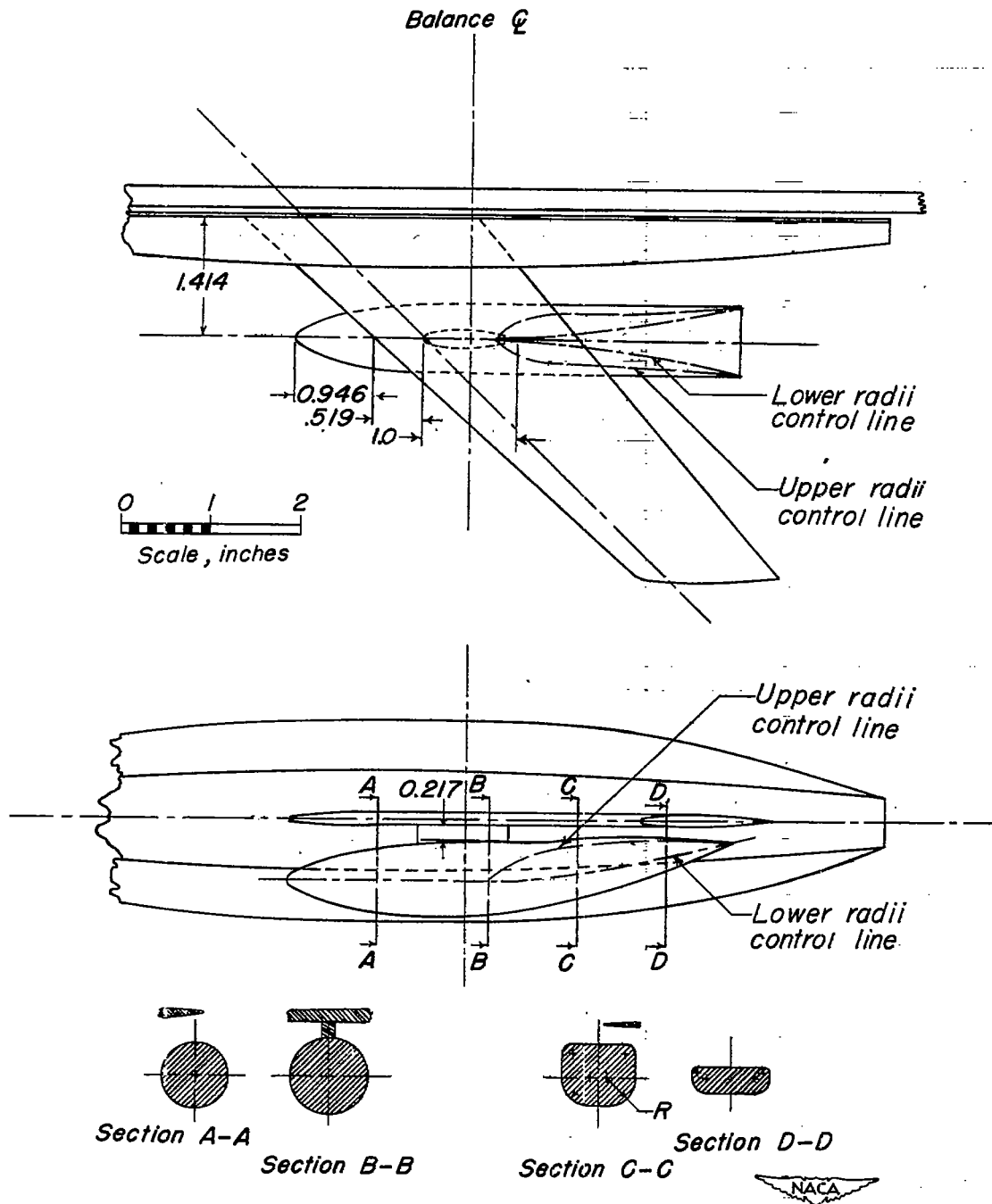


Figure 5.- Drawing of fantail external store tested on model using a pylon of $\frac{t}{c_p} = 20$ percent and $\frac{l_p}{c} = 9.45$ percent.

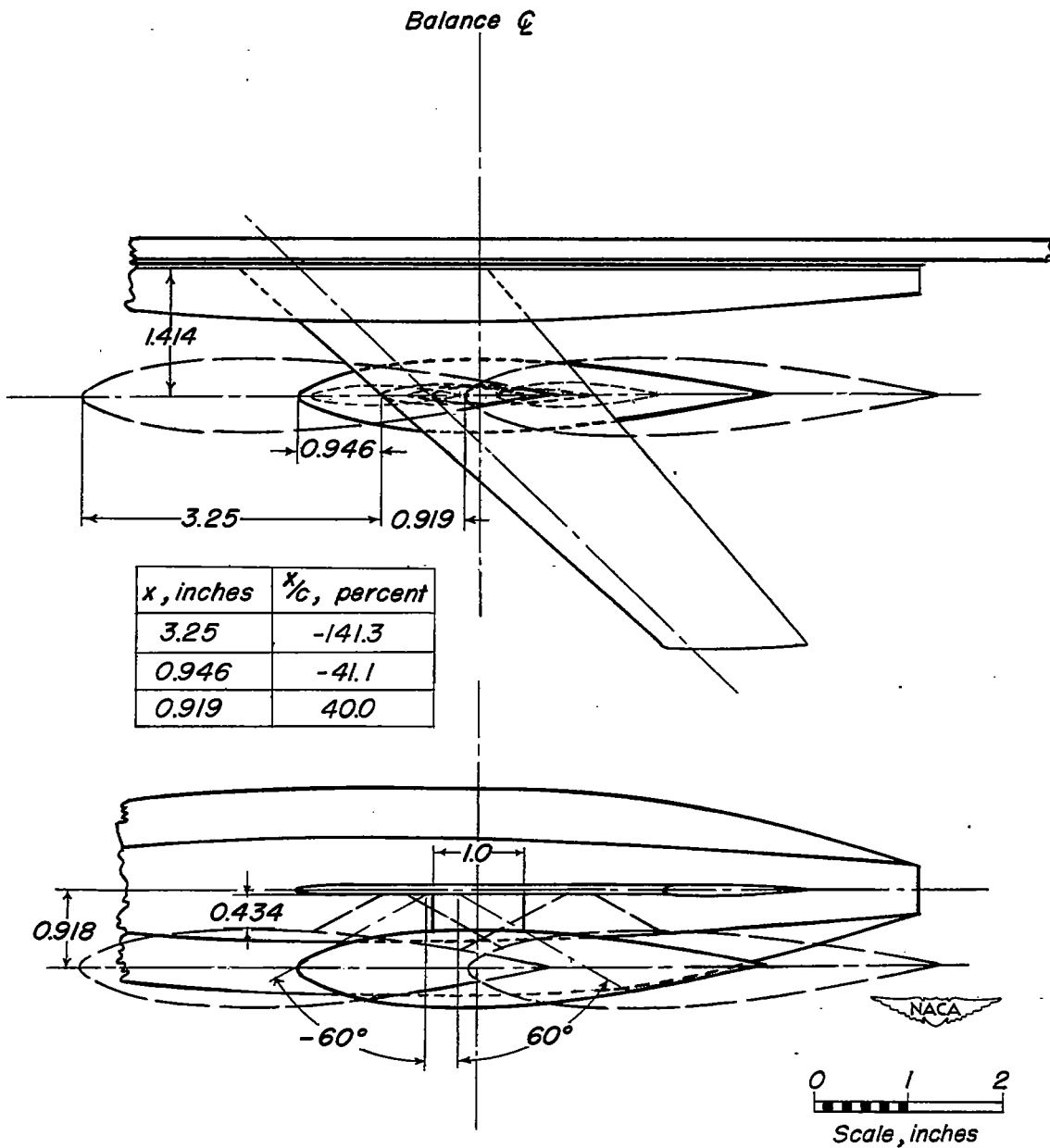
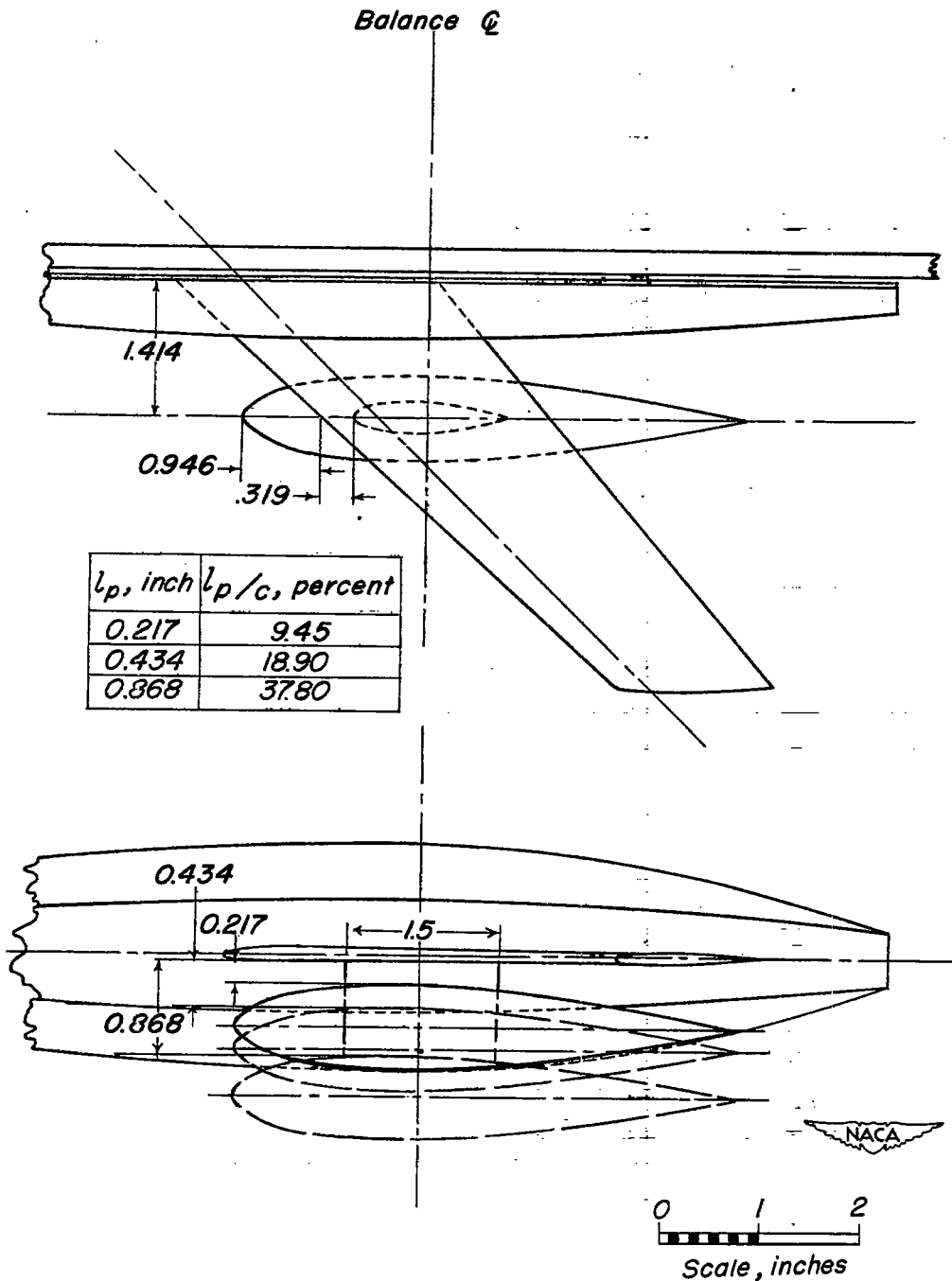
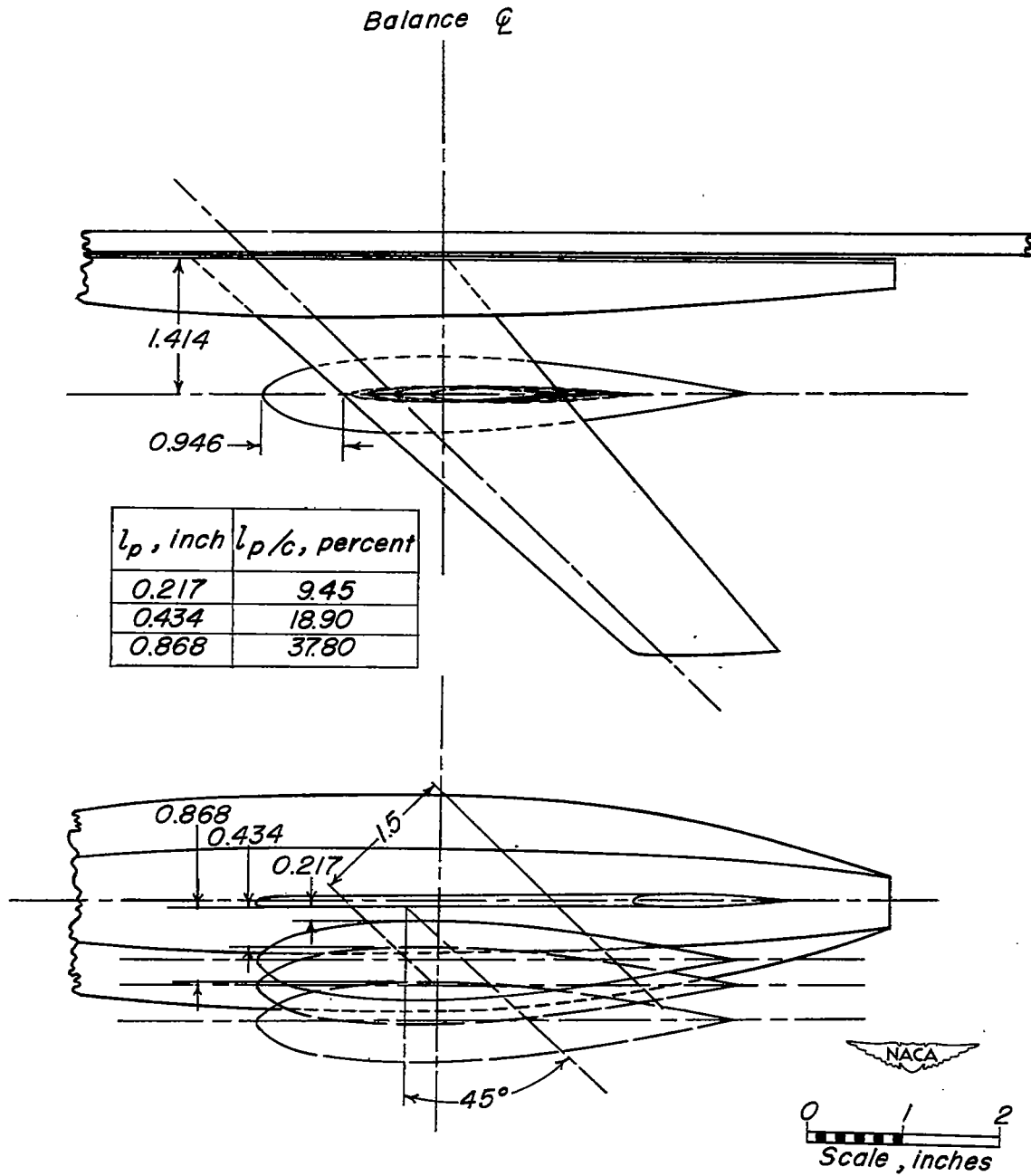


Figure 6.- Drawing of three external-store chordwise positions tested on model using a fineness-ratio-6 store and a pylon of $\frac{t}{c_p} = 20$ percent and $\frac{l_p}{c} = 18.9$ percent.



(a) $\frac{t}{c_p} = 10$ percent, $\Lambda = 0^\circ$.

Figure 7.- Drawing of pylon lengths tested on model employing a fineness-ratio-6 external store.



(b) $\frac{t}{c_p} = 10$ percent, $\Lambda = 45^\circ$.

Figure 7.- Concluded.

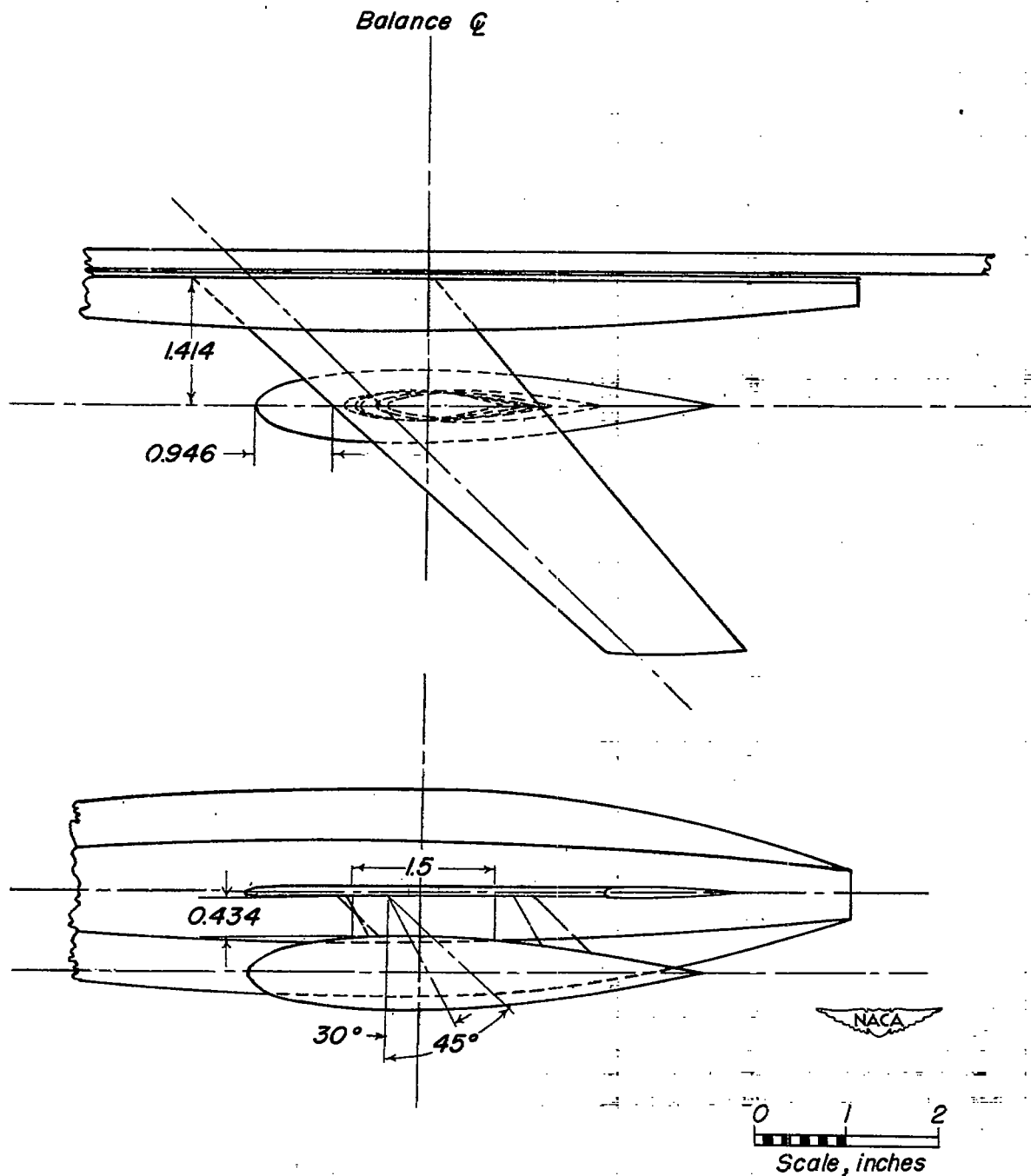


Figure 8.- Drawing of pylon sweep angles tested on model employing a fineness-ratio-6 external store and a pylon of $\frac{t}{c_p} = 10$ percent and $\frac{l_p}{c} = 18.9$ percent.

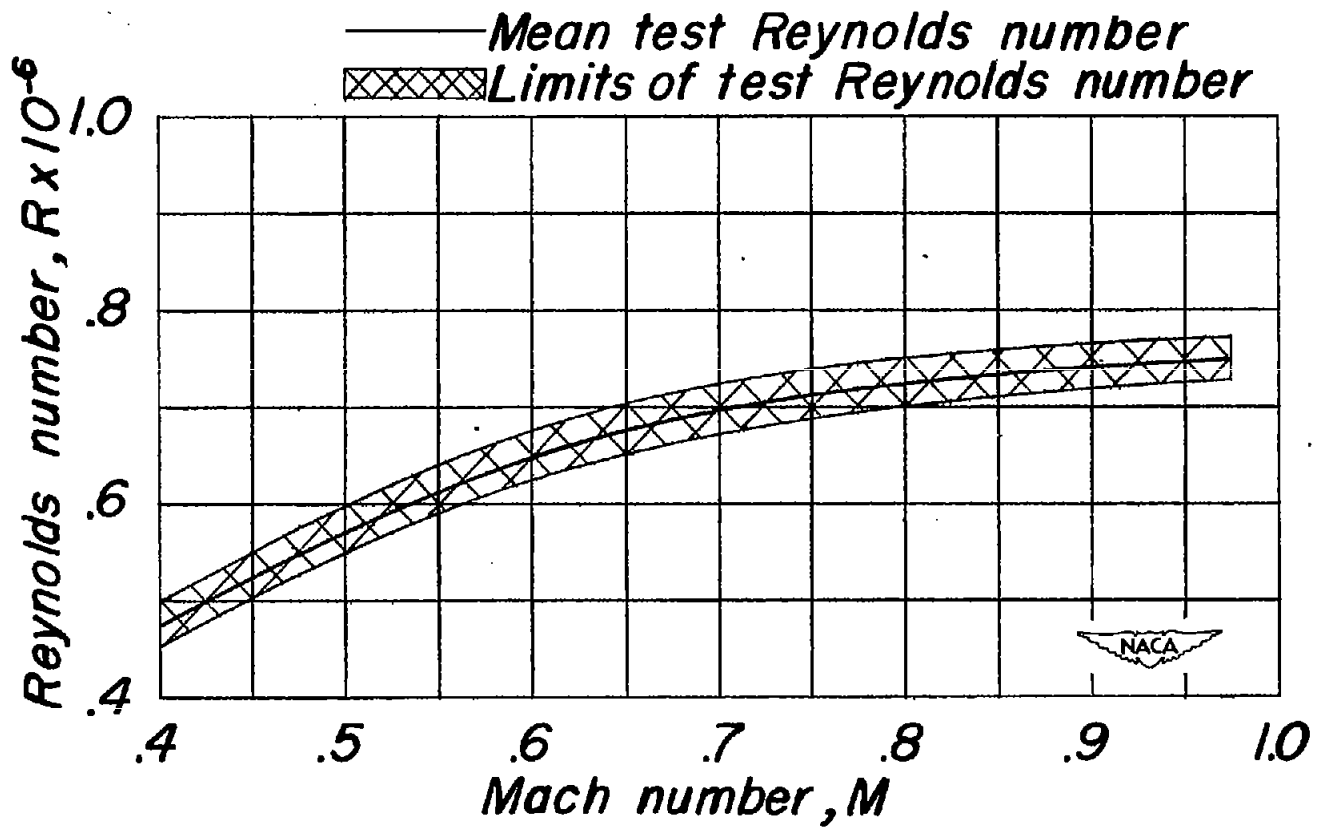


Figure 9.- Variation of Reynolds number with Mach number for the basic model in the Langley high-speed 7- by 10-foot tunnel.

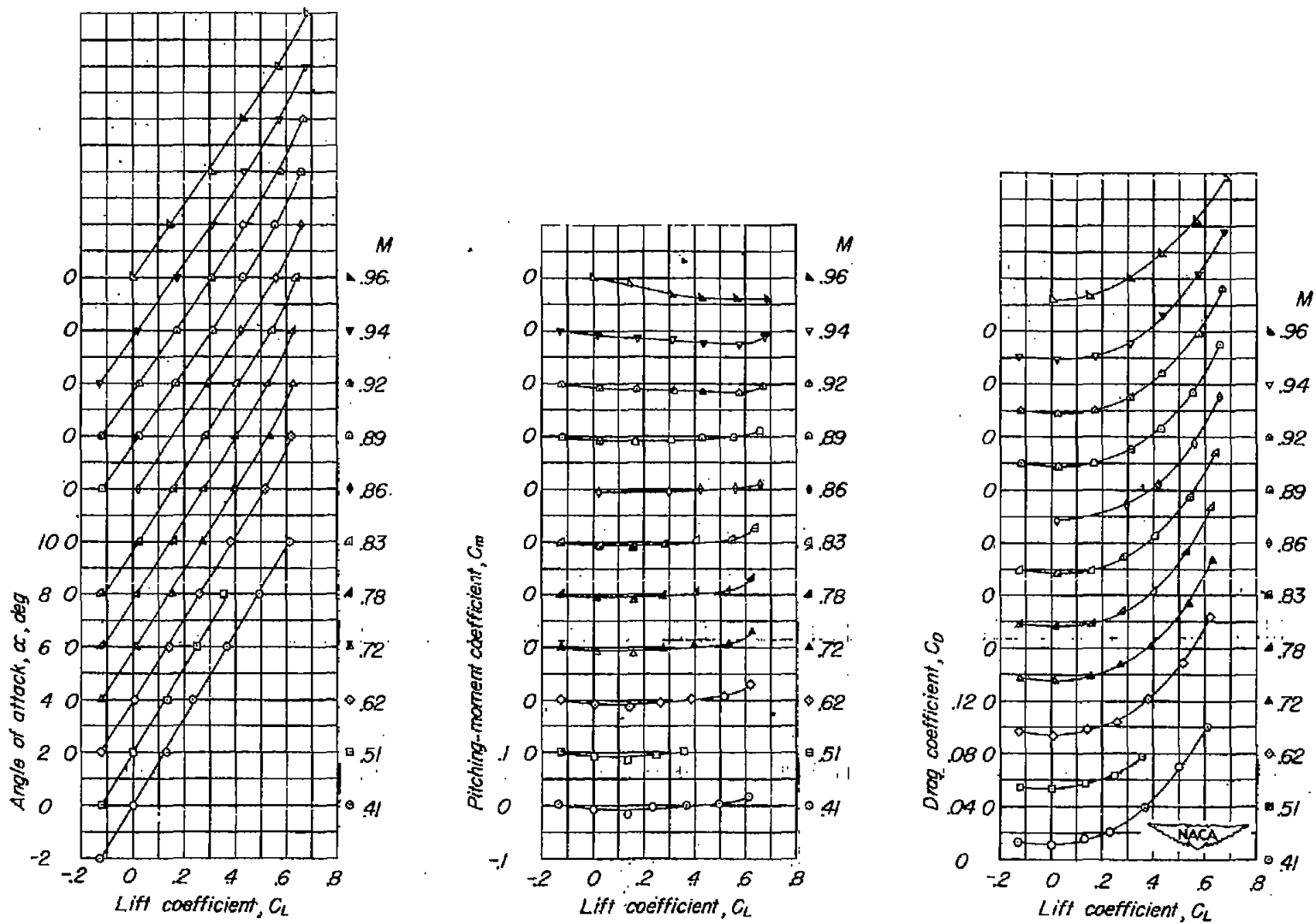


Figure 10.- Aerodynamic characteristics of the basic model.

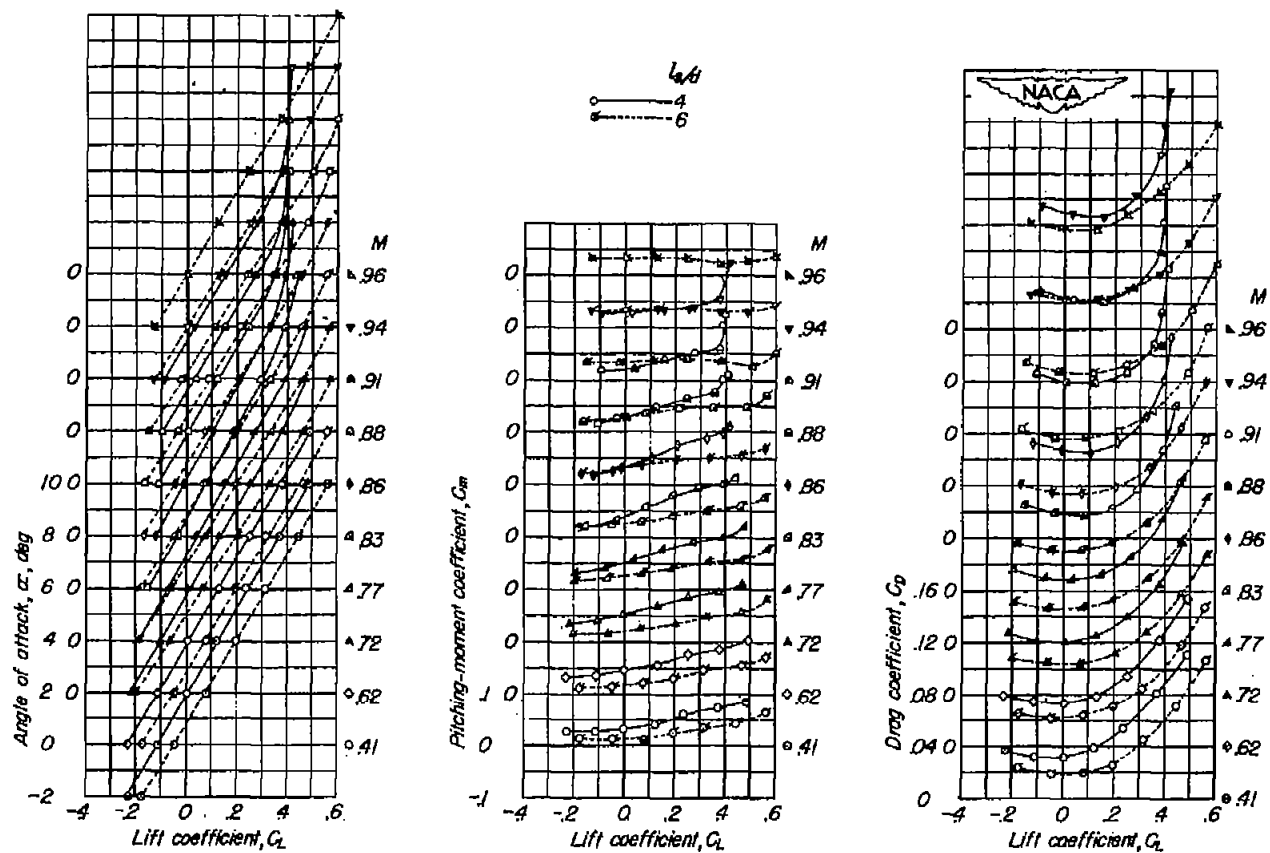
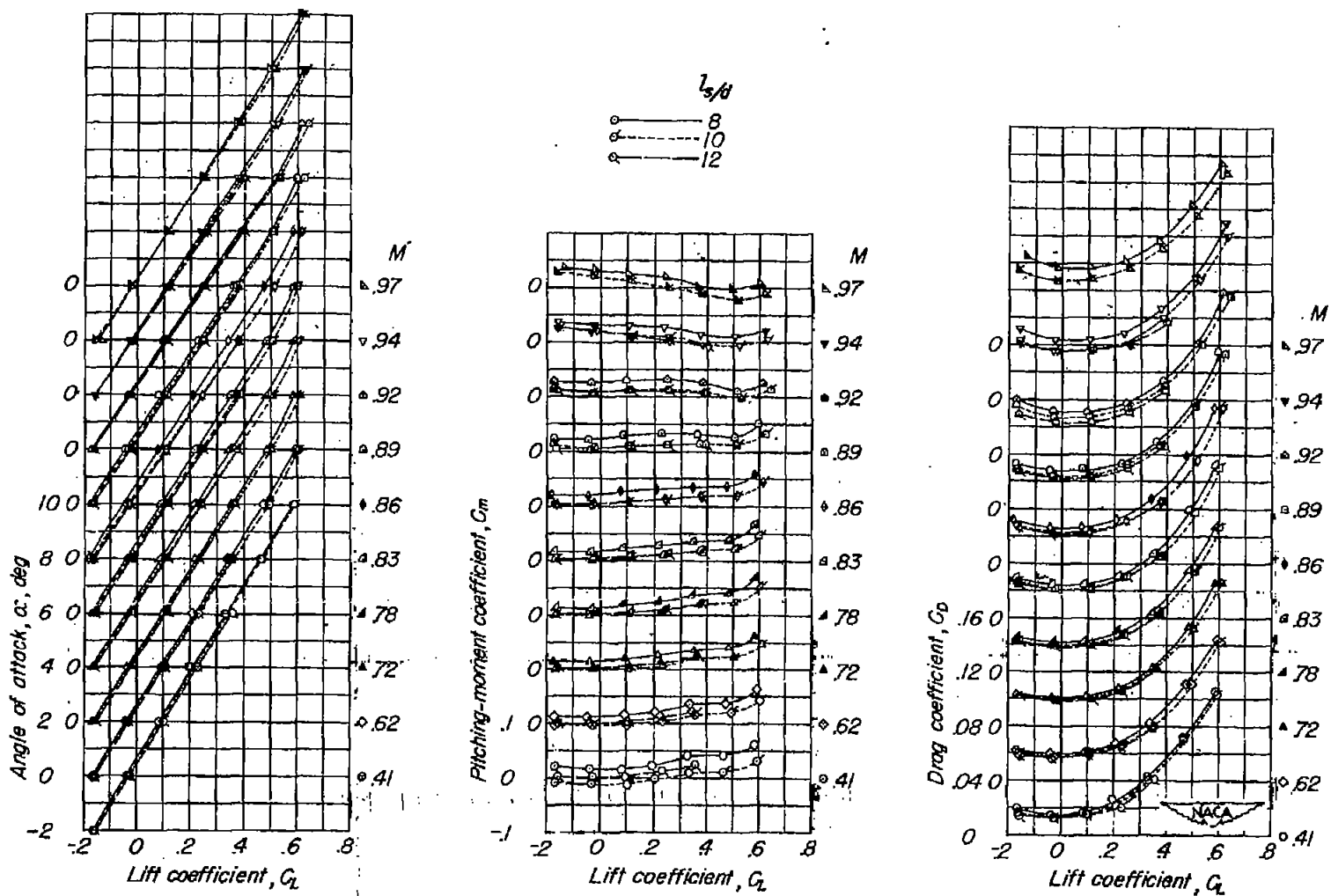
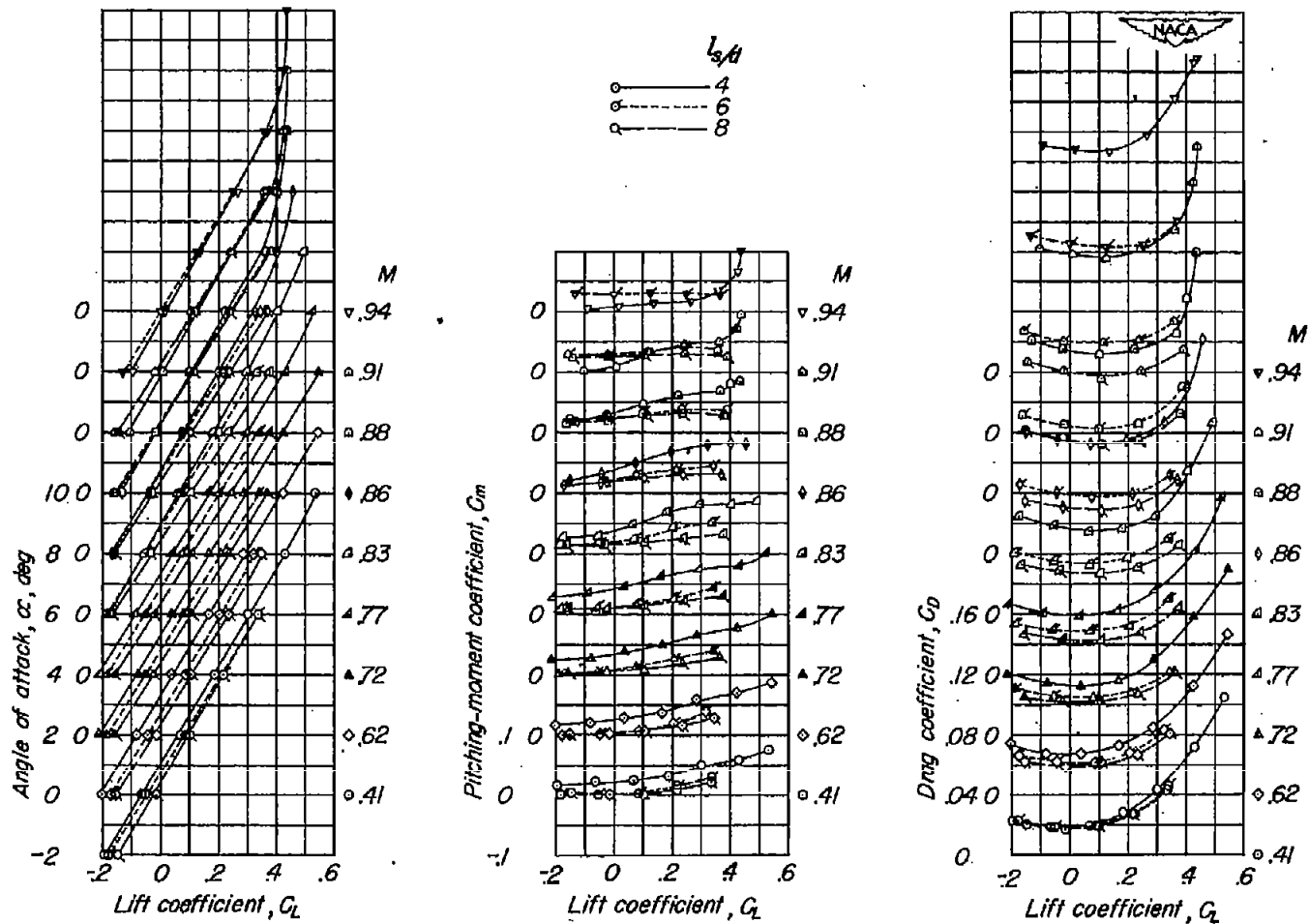


Figure 11.- Aerodynamic characteristics of the basic model with an external-store installation showing the effects of variations in external-store fineness ratio; $\frac{t}{c_p} = 10$ percent; $c_p = 1.5$ inches; $\Lambda = 0^\circ$.



(a) Concluded.

Figure 11.- Continued.



(b) $\frac{l_p}{c} = 37.8$ percent.

Figure 11.- Concluded.

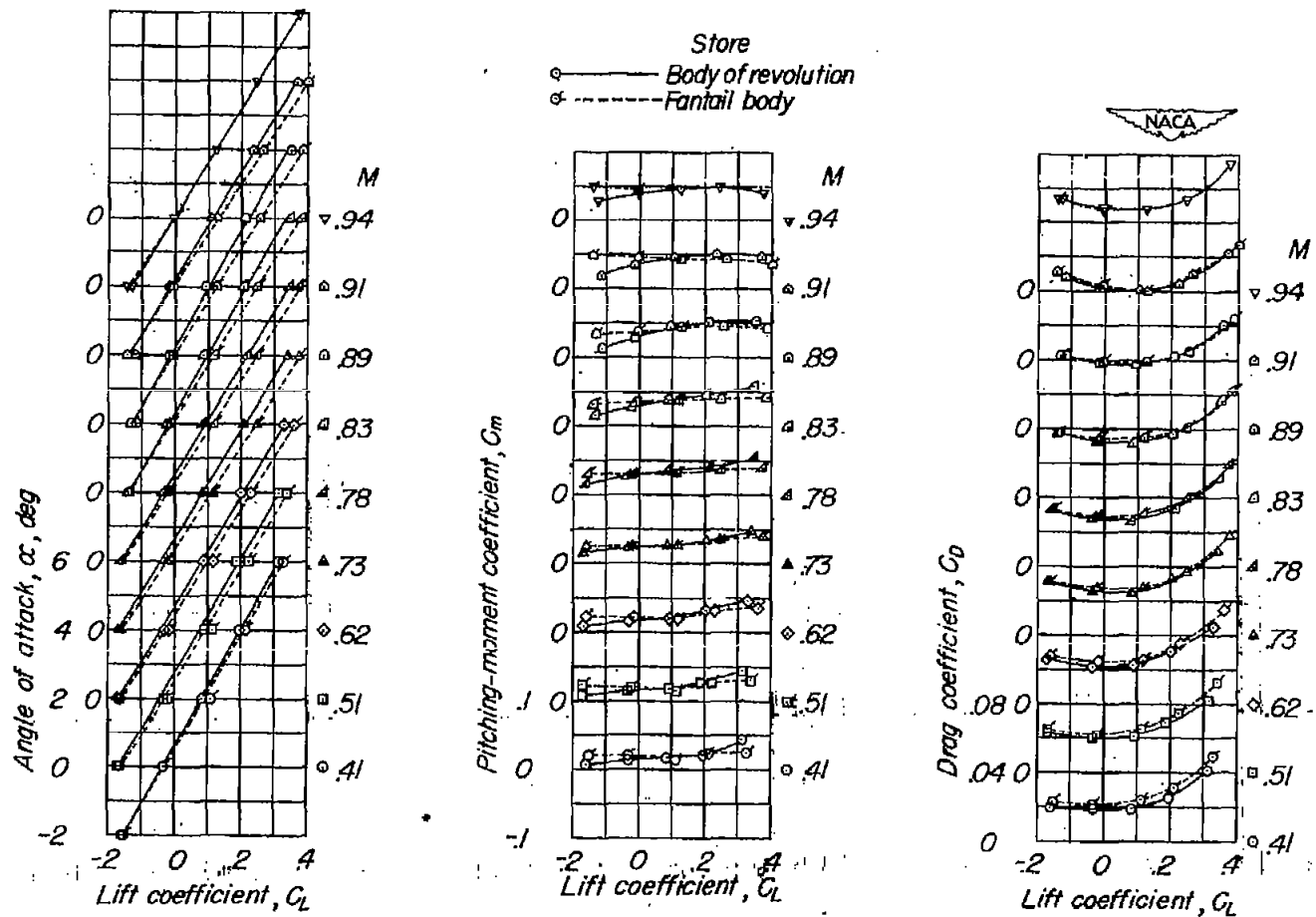


Figure 12.- Aerodynamic characteristics of the basic model with an external-store installation showing the effects of variations in external-store shape; $\frac{l_s}{d} = 6$; $\frac{t}{c_p} = 20$ percent; $\frac{l_p}{c} = 9.45$ percent; $c_p = 1.0$ inch; $\Lambda = 0^\circ$.

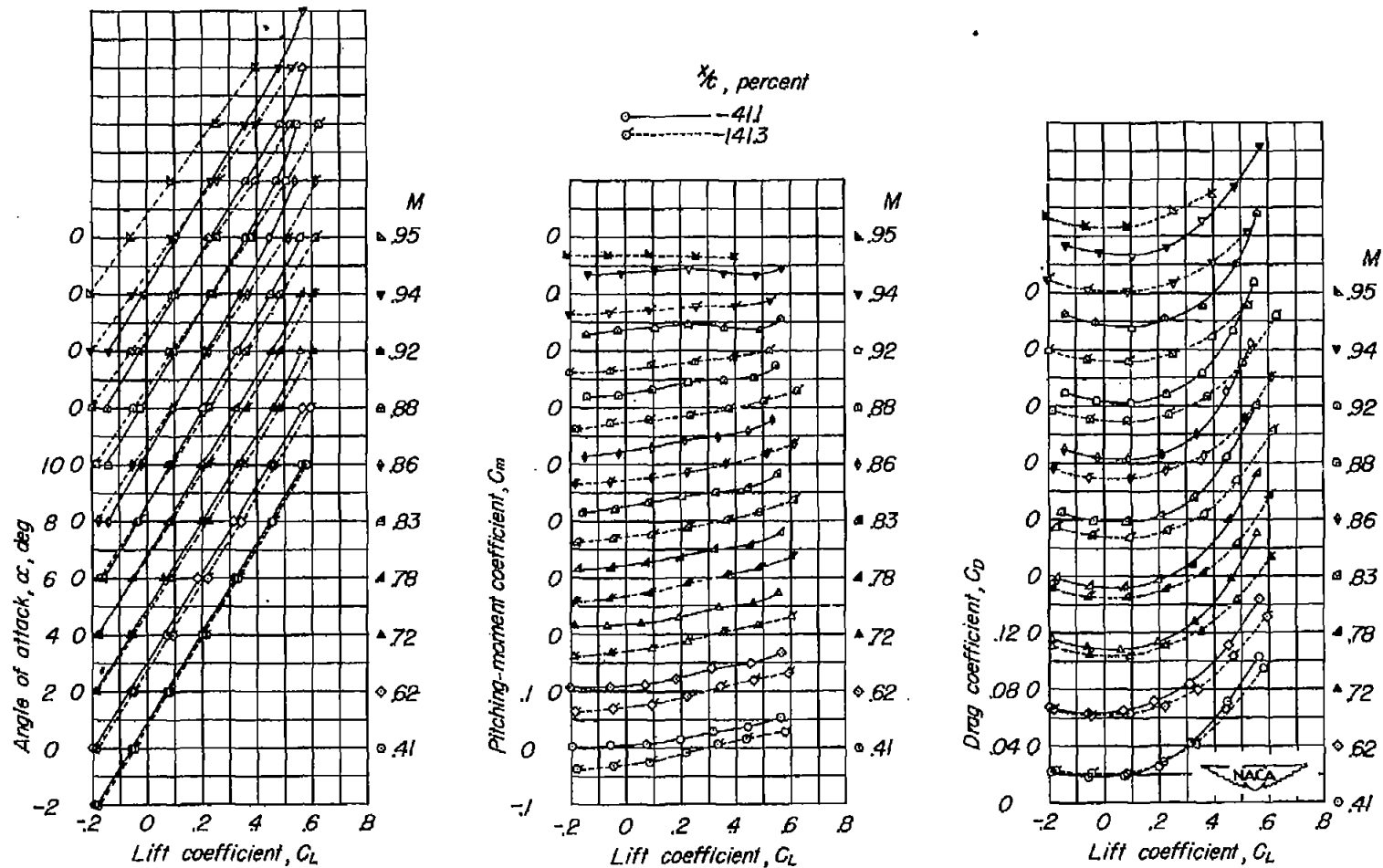


Figure 13.- Aerodynamic characteristics of the basic model with an external-store installation showing the effects of variations of external-store chordwise positions; $\frac{l_s}{d} = 6$, $\frac{t}{c_p} = 20$ percent; $\frac{l_p}{c} = 18.9$ percent; $c_p = 1.0$ inch.

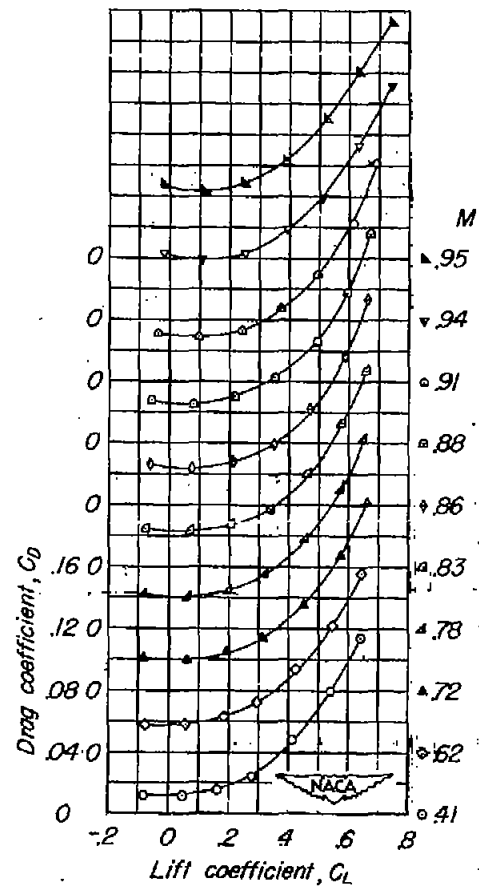
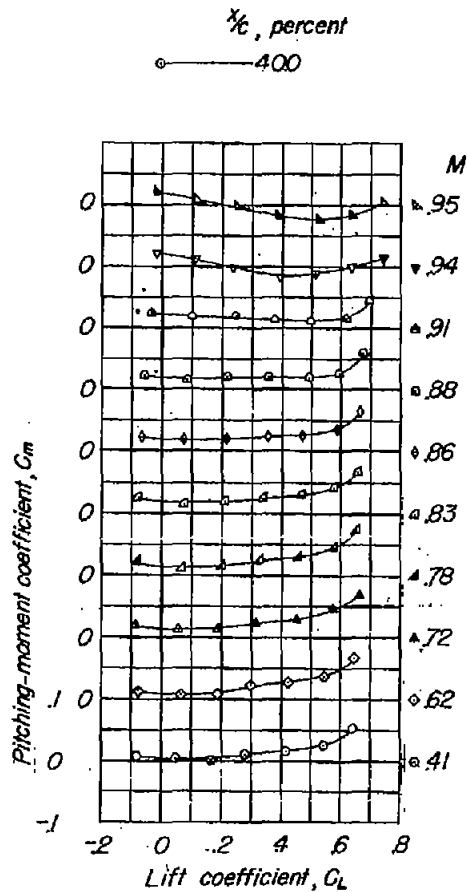
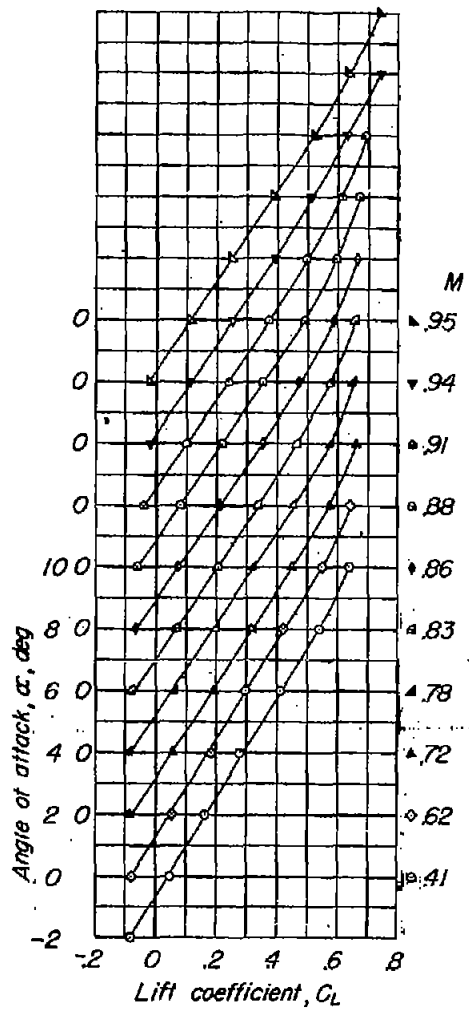
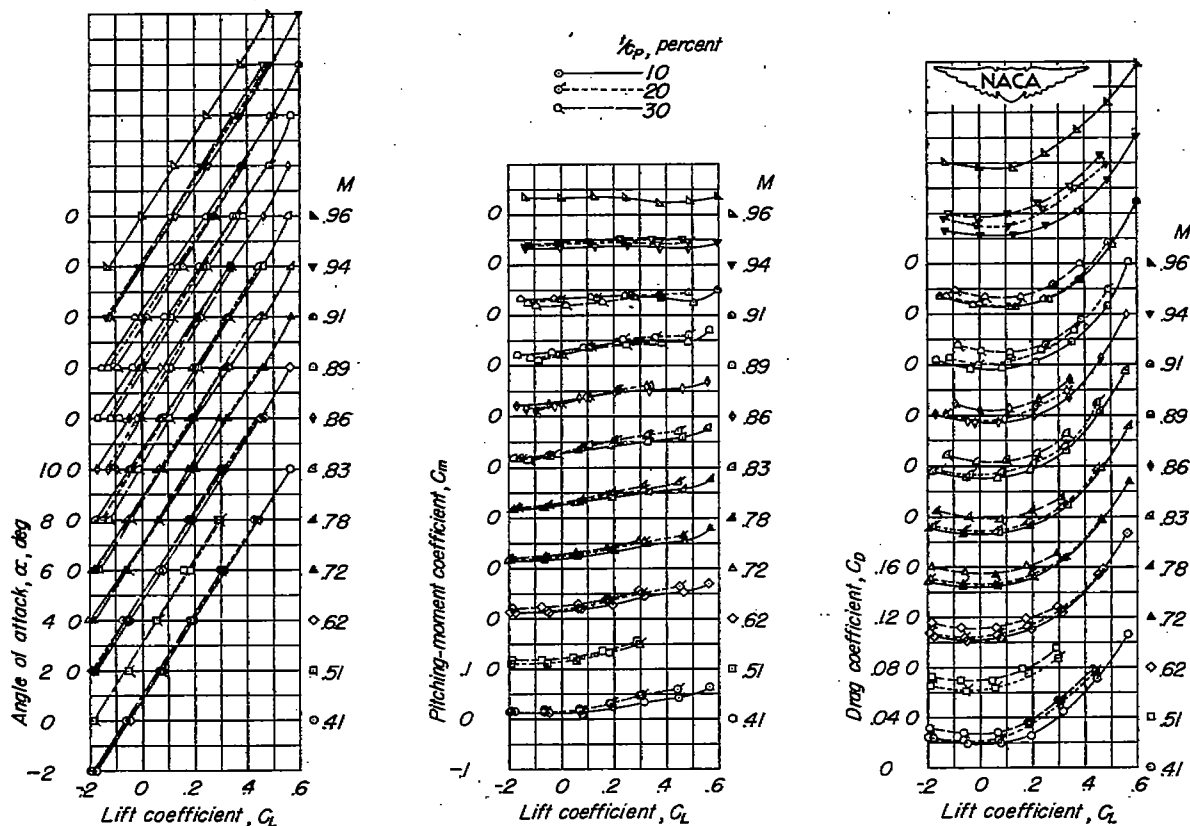
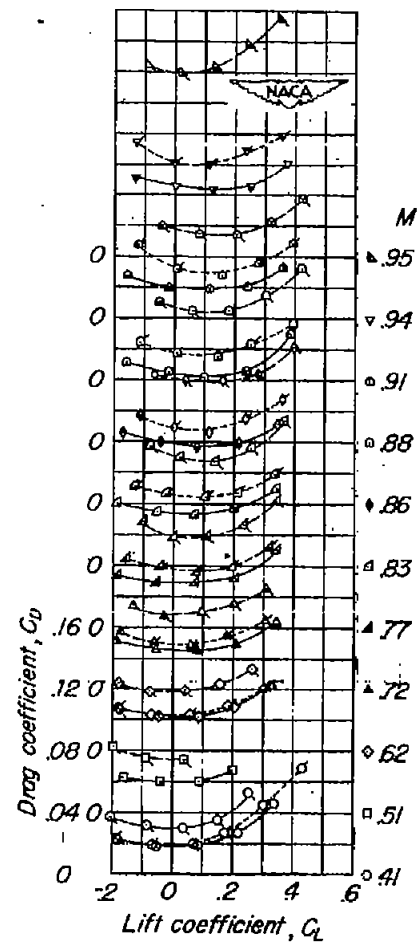
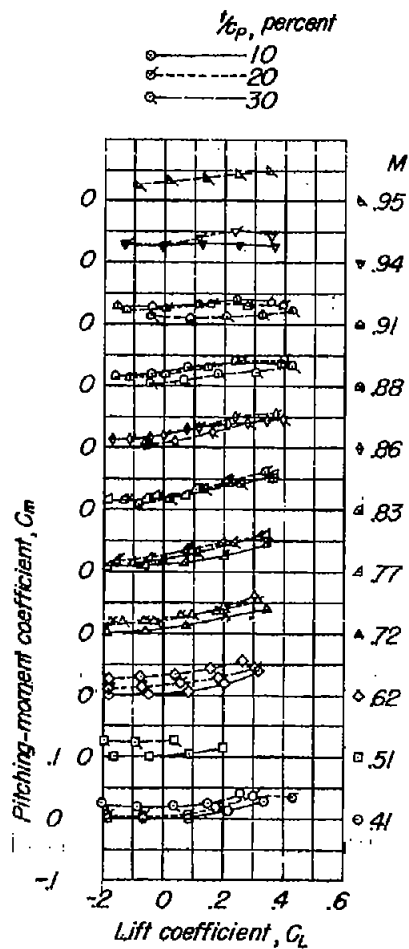
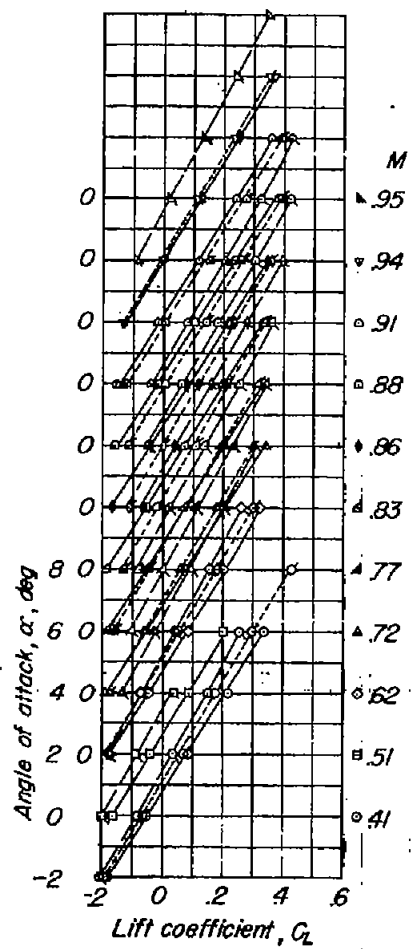


Figure 13.- Concluded.



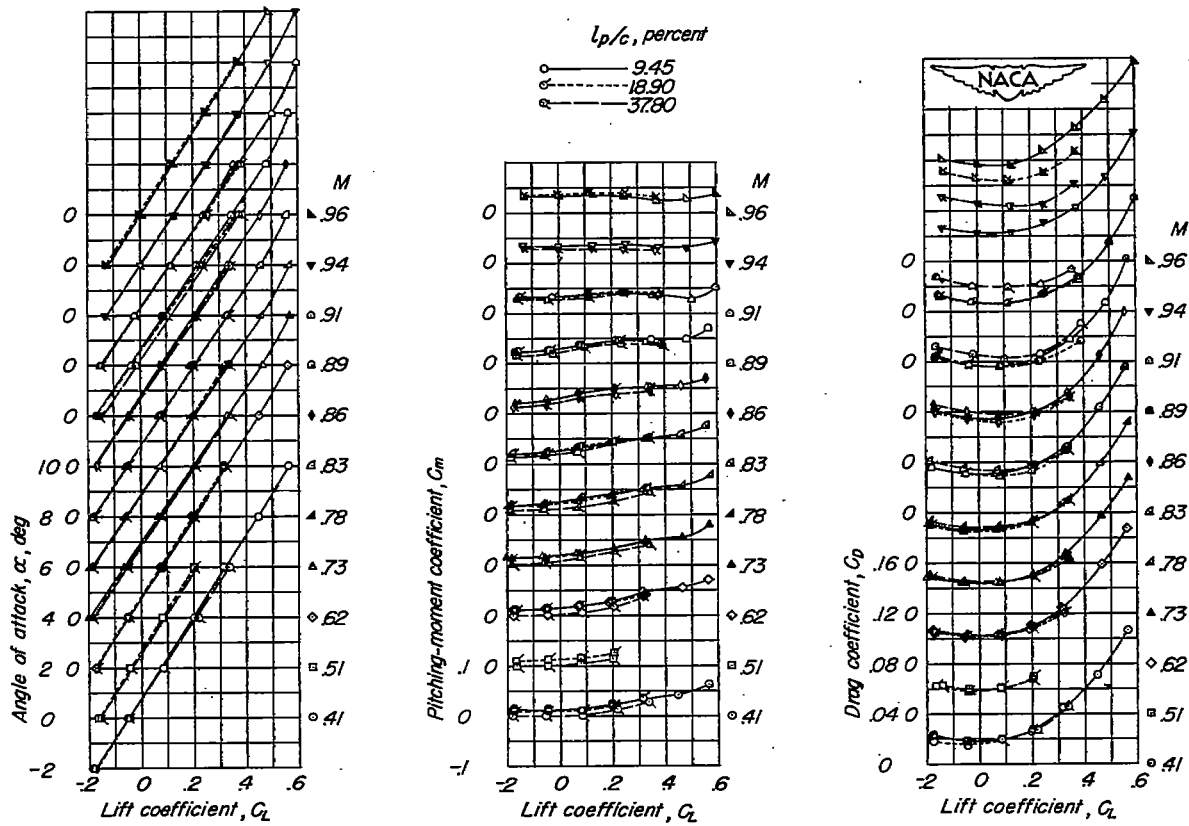
(a) $\frac{l_p}{c} = 9.45$ percent.

Figure 14.- Aerodynamic characteristics of the basic model with an external-store installation showing the effects of variations in pylon thickness; $\frac{l_s}{d} = 6$; $c_p = 1.5$ inches; $\Lambda = 0^\circ$.



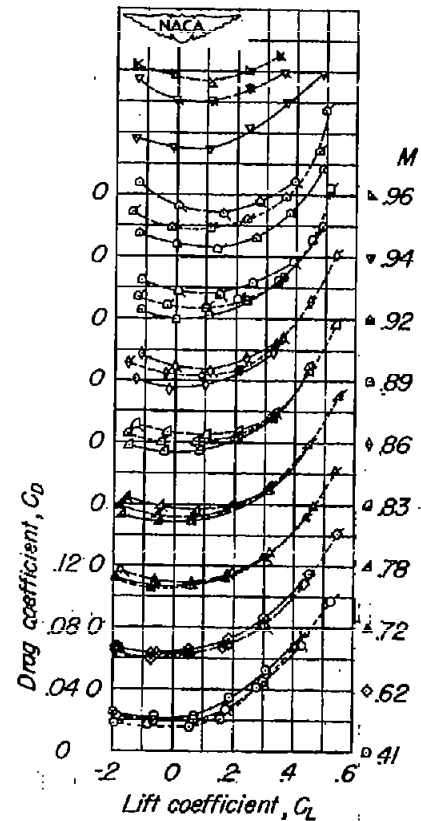
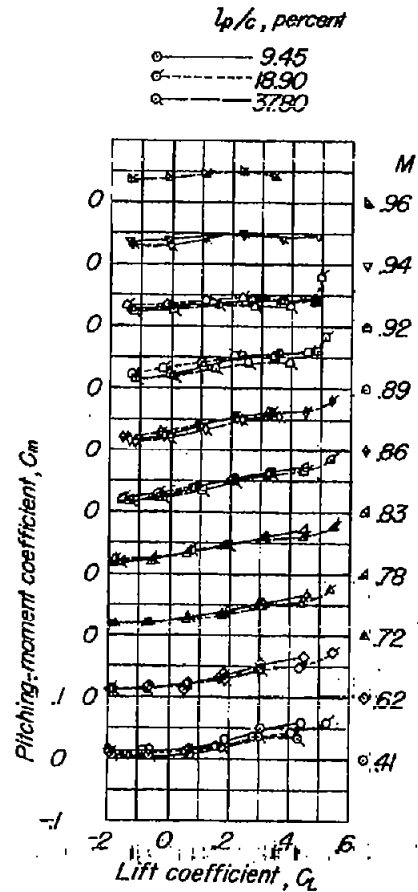
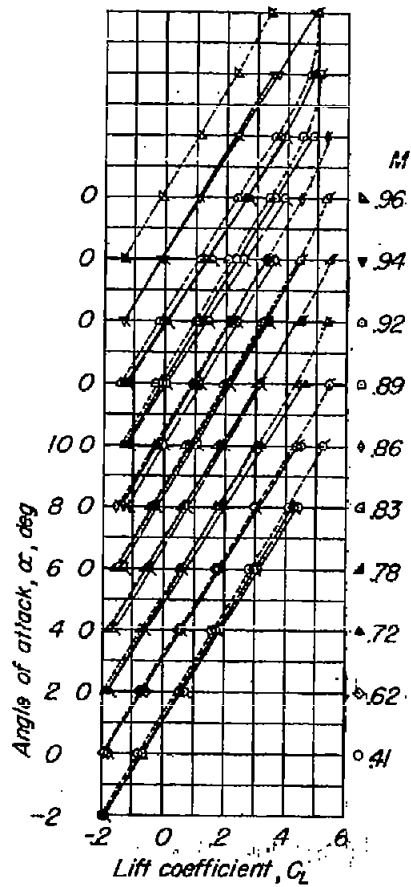
(b) $\frac{z_p}{c} = 37.8$ percent.

Figure 14.- Concluded.



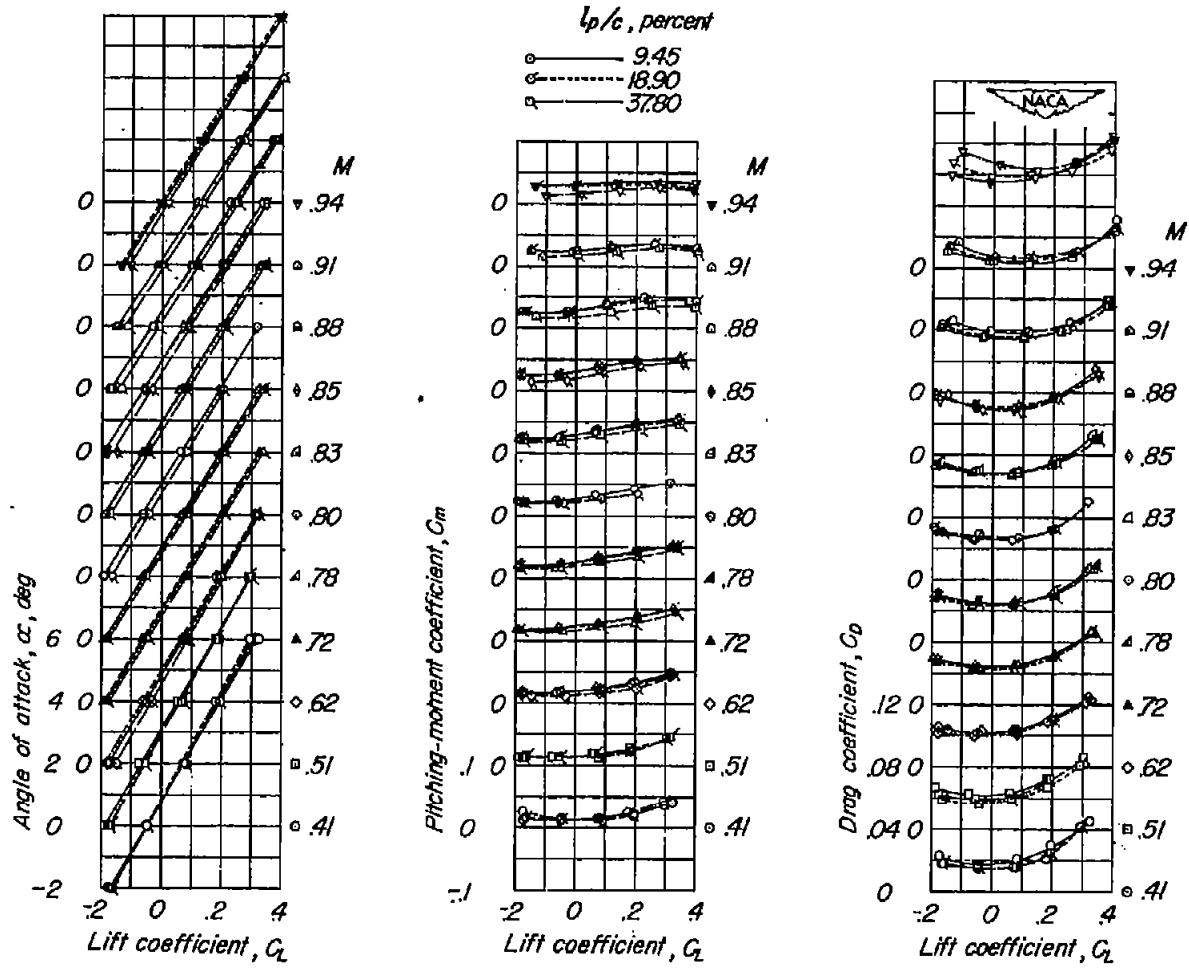
(a) $\frac{t}{c_p} = 10$ percent, $\Lambda = 0^\circ$.

Figure 15.- Aerodynamic characteristics of the basic model with an external-store installation showing the effects of variations in pylon length; $\frac{l_s}{d} = 6$; $c_p = 1.5$ inches.



(b) $\frac{t}{c_p} = 20$ percent; $\Lambda = 0^\circ$.

Figure 15.- Continued.



(c) $\frac{t}{c_p} = 10$ percent; $\Lambda = 45^\circ$.

Figure 15.- Concluded.

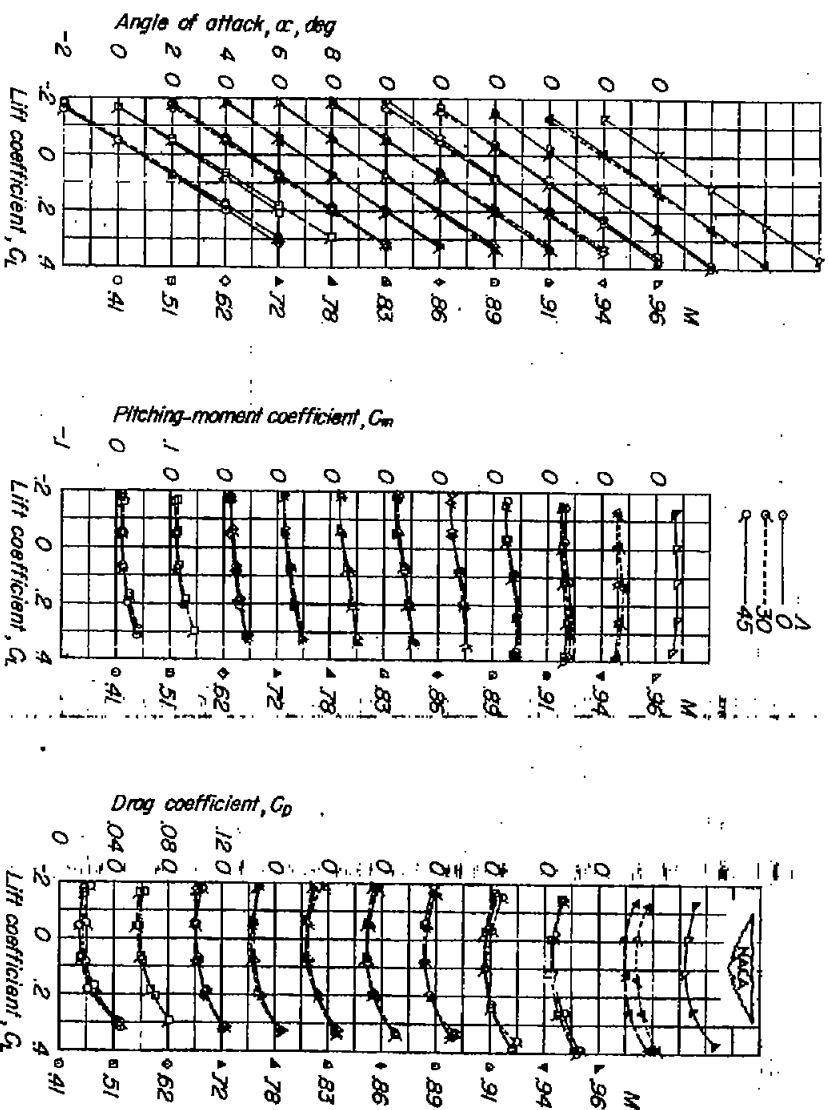
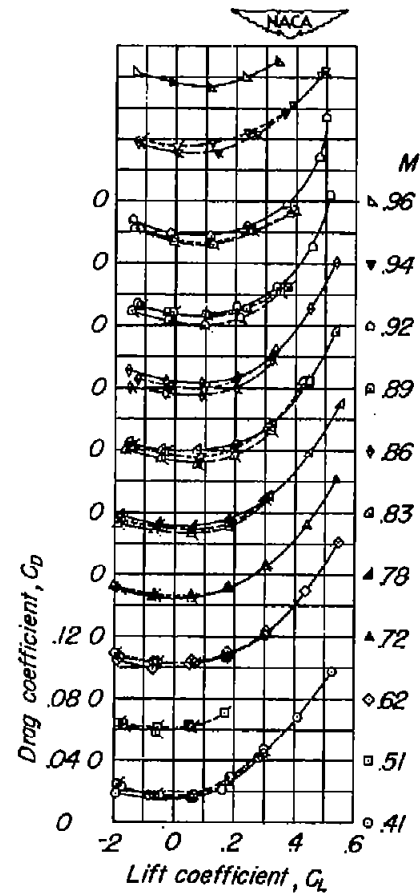
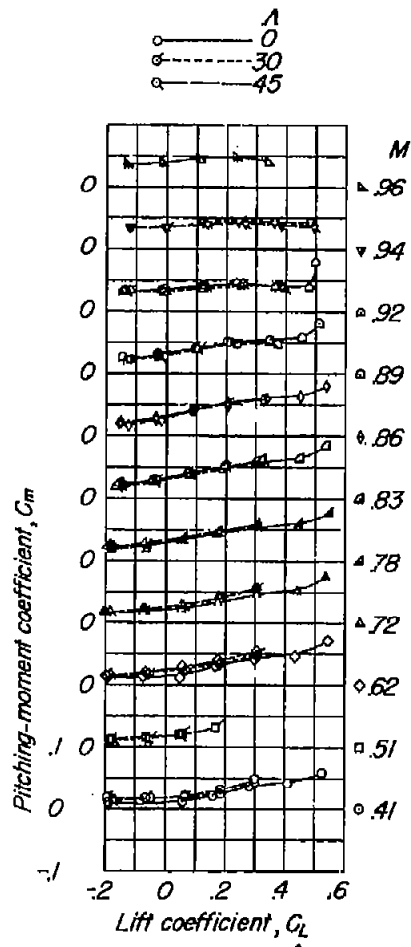
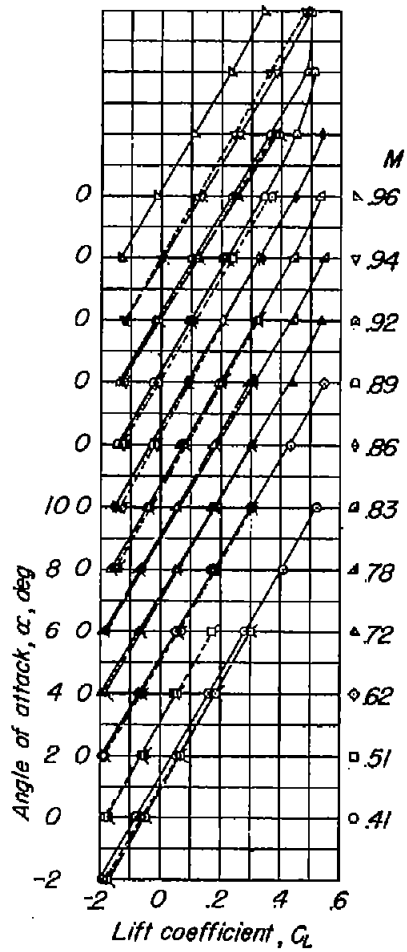


Figure 16.- Aerodynamic characteristics of the basic model with an external-store installation showing the effects of variations in pylon sweep angle; $\frac{l_s}{d} = 6$; $\frac{l_p}{c} = 18.9$ percent; $c_p = 1.5$ inches.



(b) $\frac{t}{c_p} = 20$ percent.

Figure 16.- Concluded.

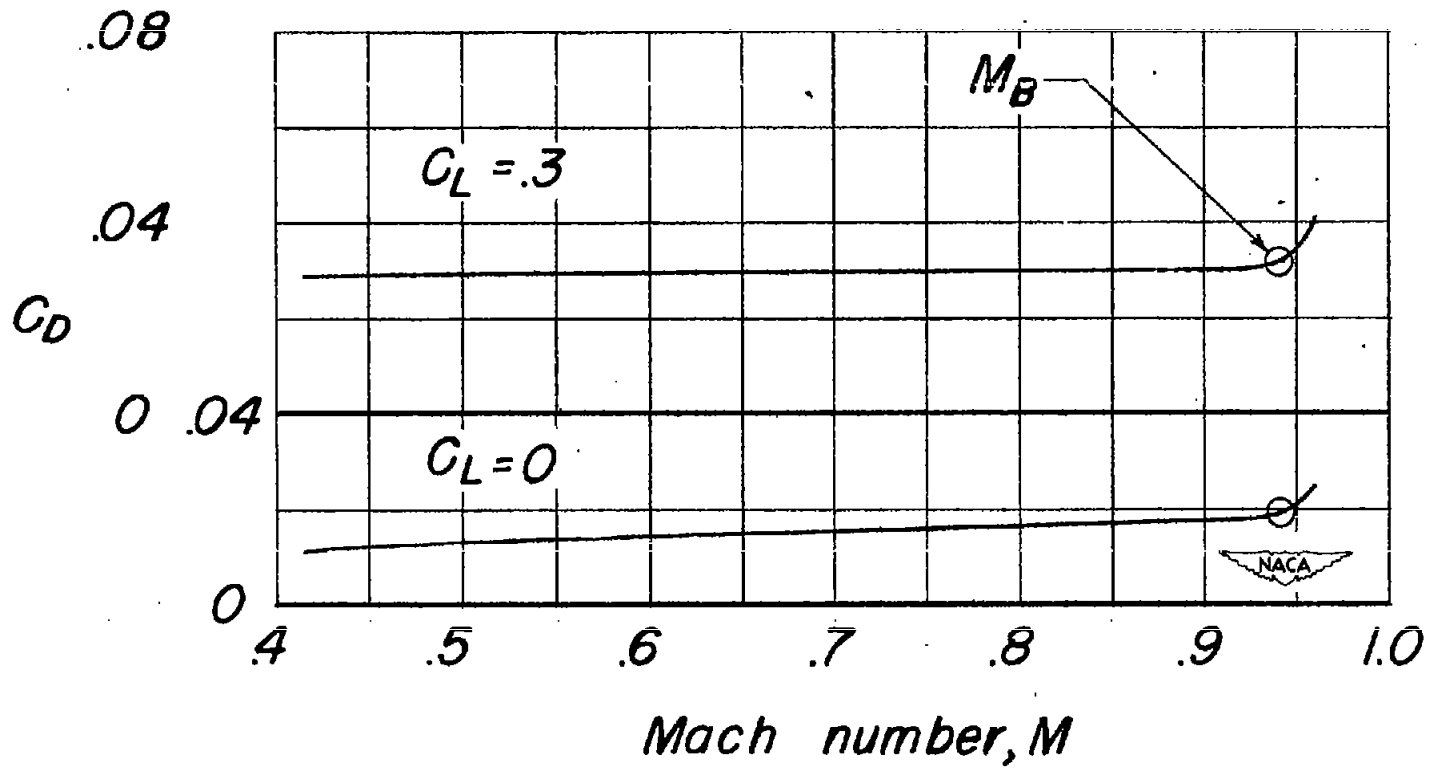


Figure 17.- Effect of Mach number on the drag characteristics of the basic model.

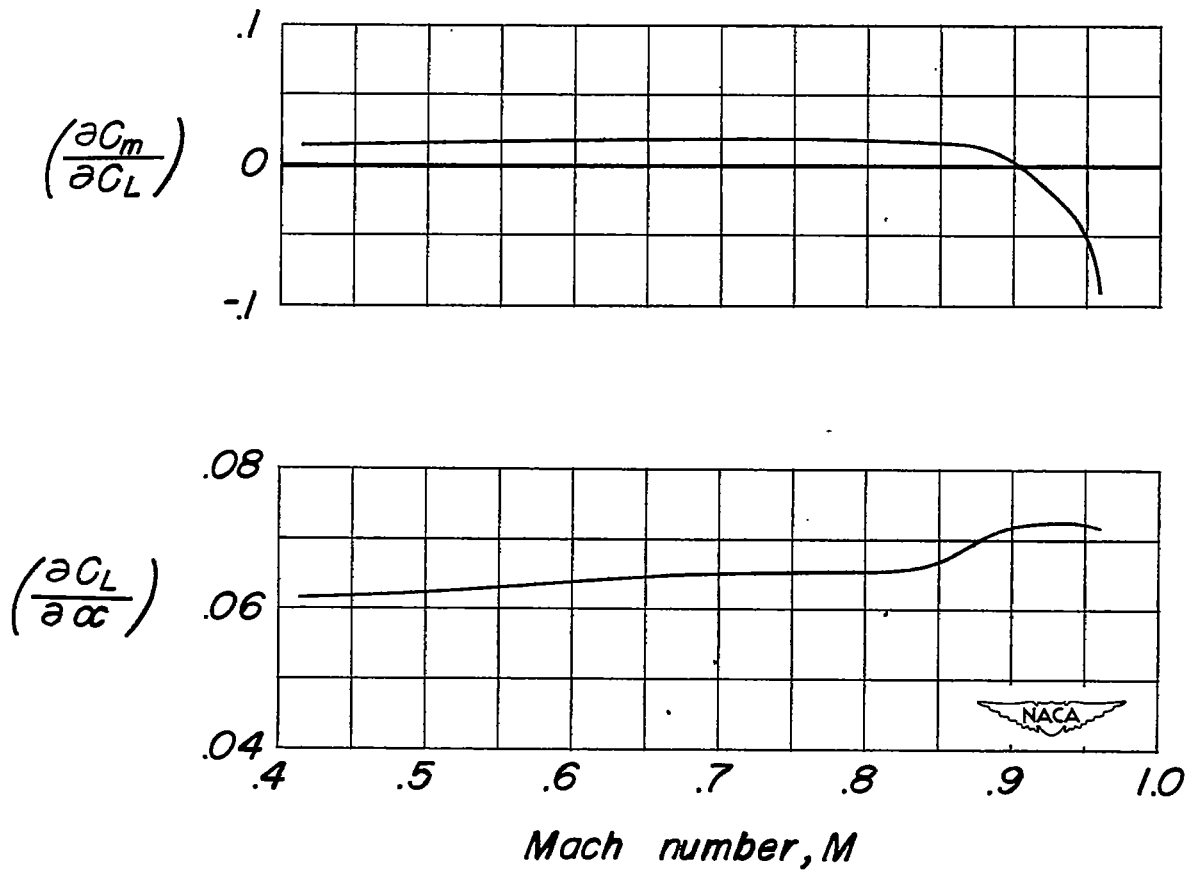
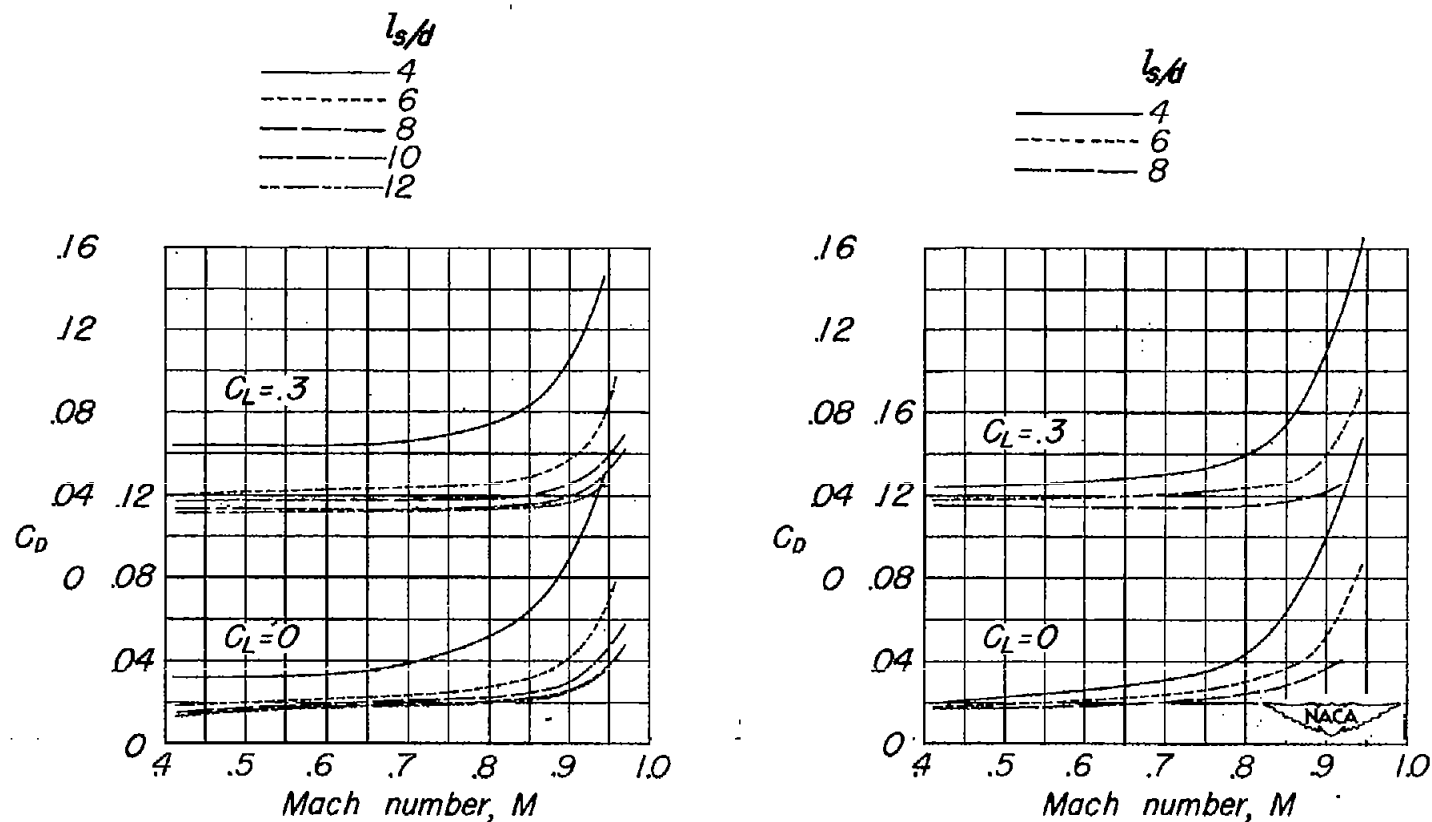


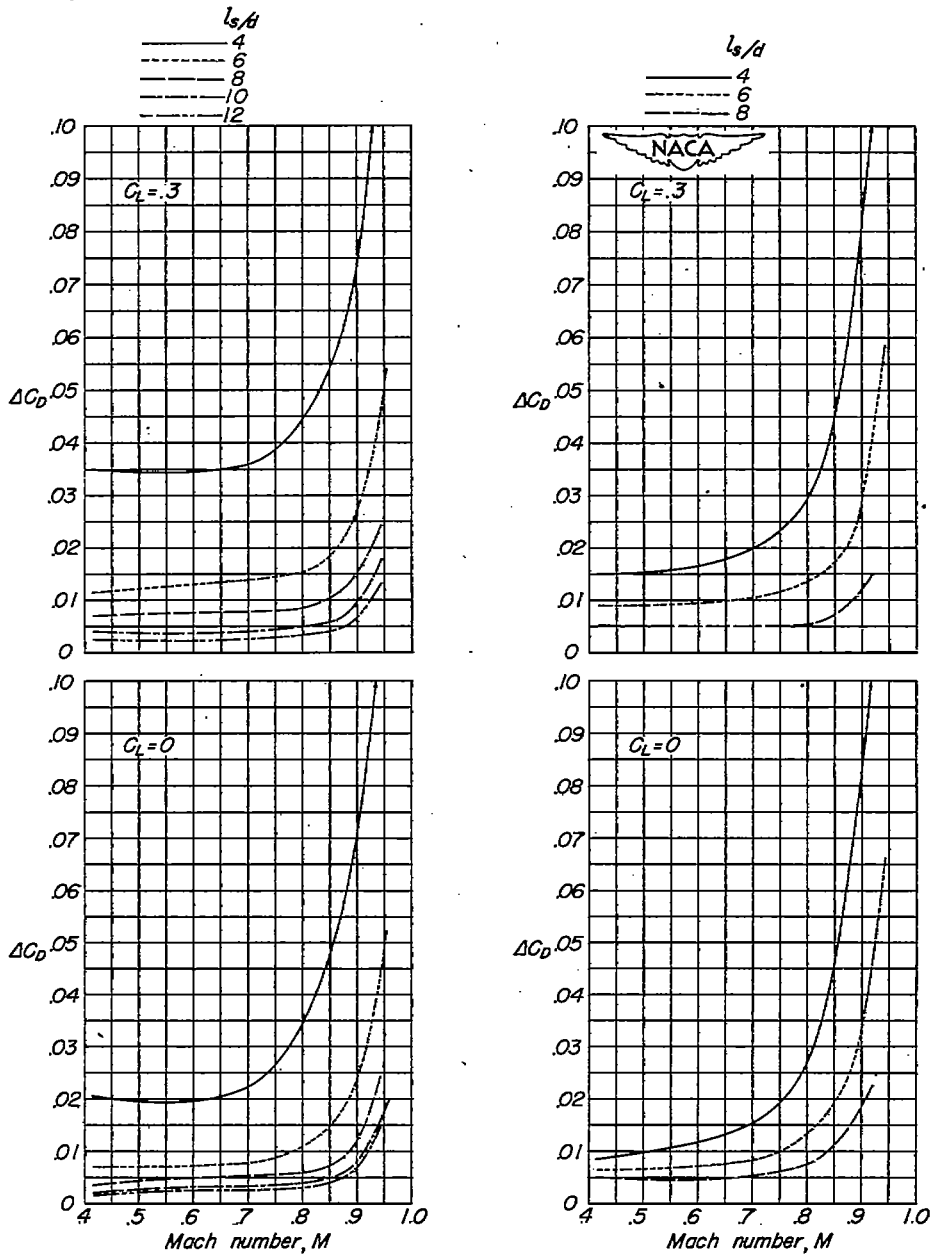
Figure 18.- Effect of Mach number on the aerodynamic-center location and lift-curve slope of the basic model.



(a) $\frac{l_p}{c} = 9.45$ percent.

(b) $\frac{l_p}{c} = 37.8$ percent.

Figure 19.- Effect of Mach number on the drag characteristics of the basic model with an external-store installation showing the effects of variations in external-store fineness ratio; $\frac{t}{c_p} = 10$ percent; $c_p = 1.5$ inches; $\Lambda = 0^\circ$.

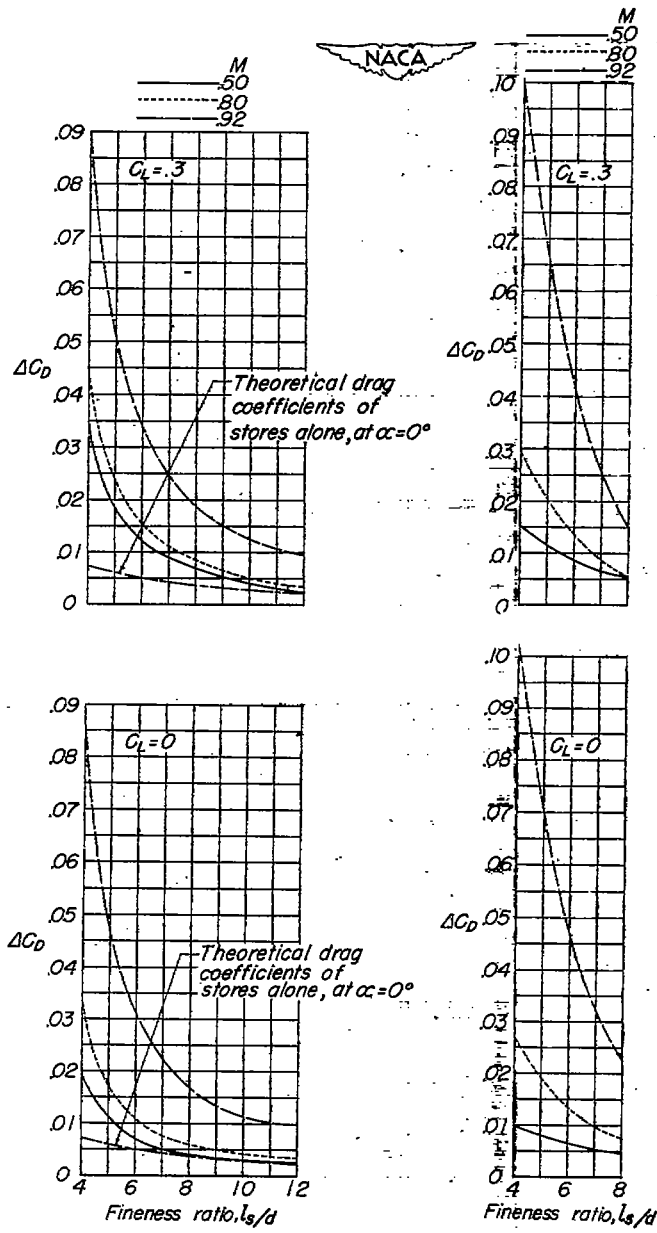


$$\frac{l_p}{c} = 9.45 \text{ percent}$$

$$\frac{l_p}{c} = 37.8 \text{ percent.}$$

(a) ΔC_D against M .

Figure 20.- Effect of variations in external-store fineness ratio on the drag characteristics of the basic model; $\frac{t}{c_p} = 10$ percent; $c_p = 1.5$ inches; $\Lambda = 0^\circ$.

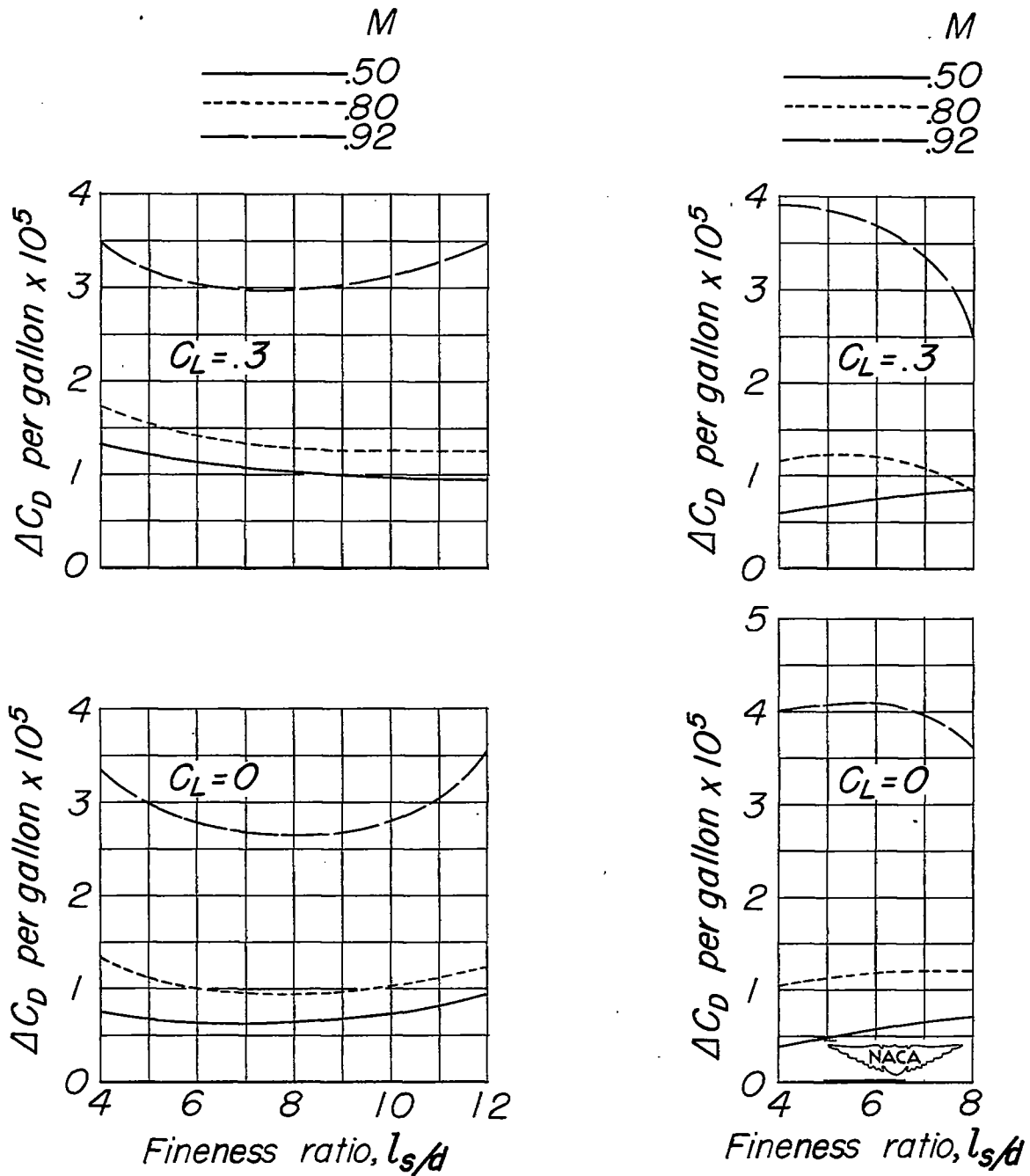


$$\frac{l_p}{c} = 9.45 \text{ percent}$$

$$\frac{l_p}{c} = 37.8 \text{ percent}$$

(b) ΔC_D against $\frac{l_s}{d}$.

Figure 20.- Continued.

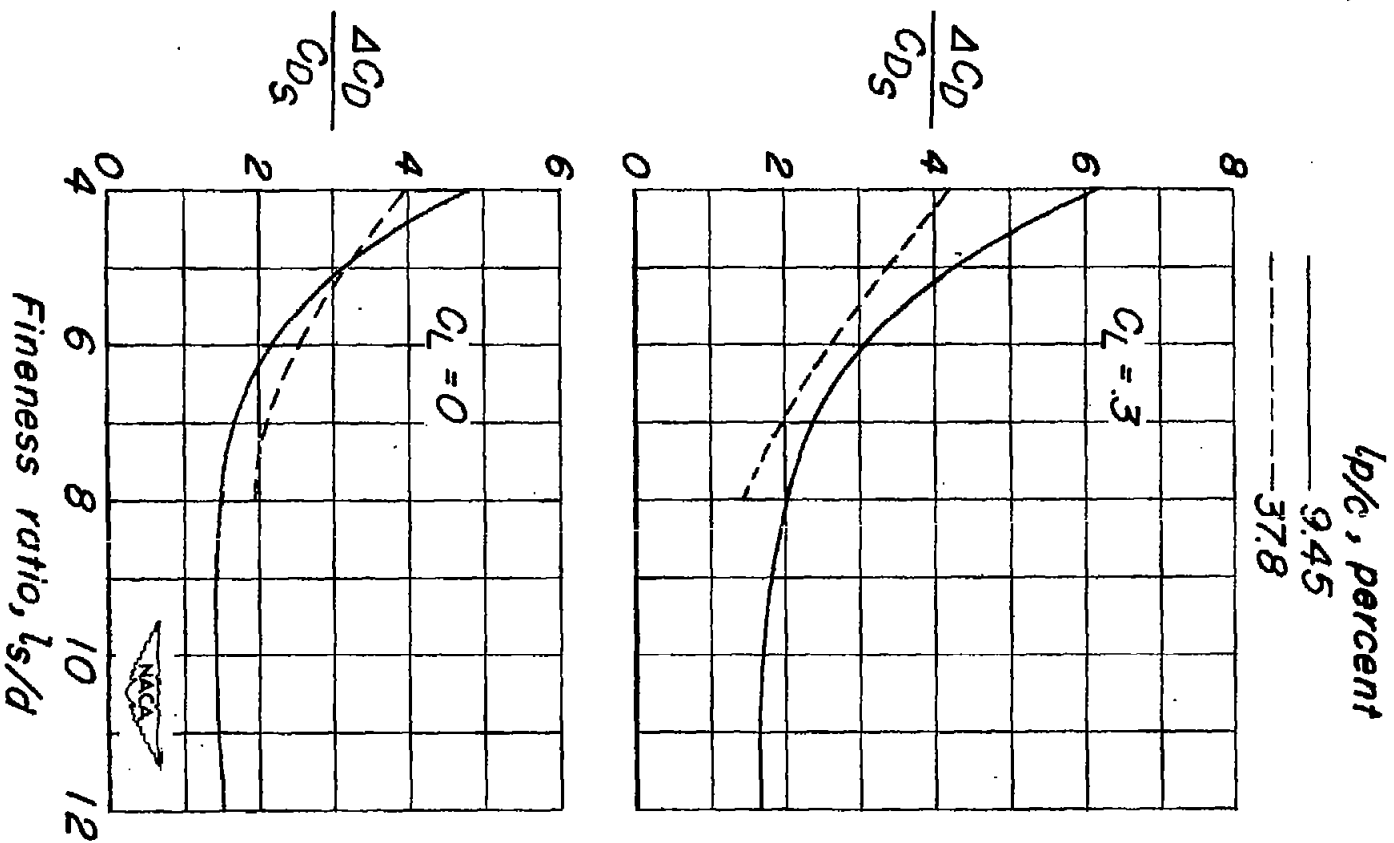


$\frac{l_p}{c} = 9.45$ percent

$\frac{l_p}{c} = 37.8$ percent

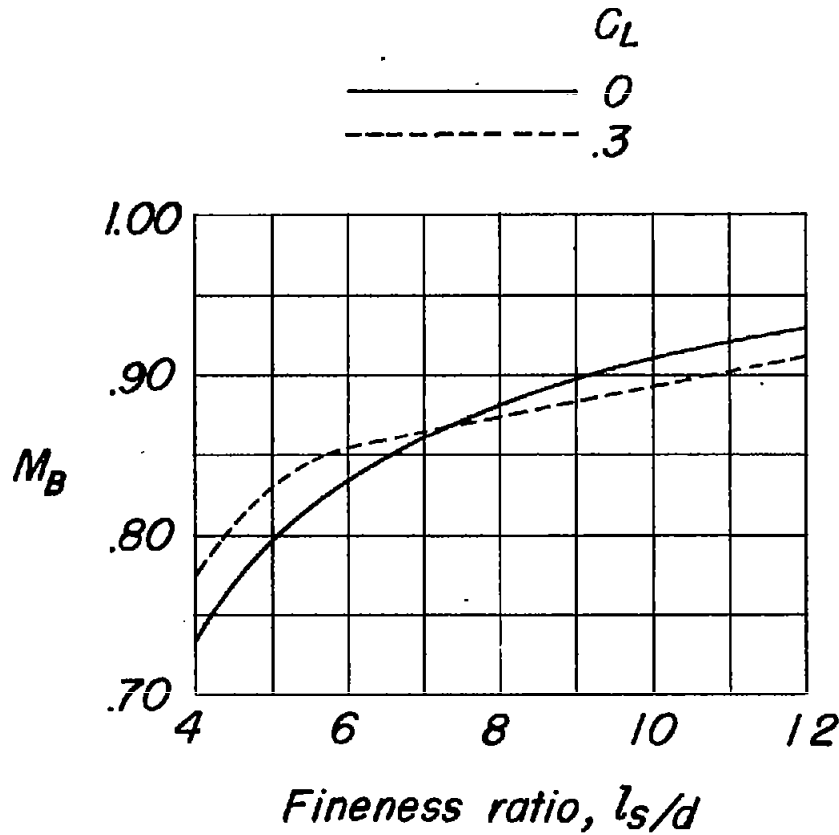
(c) ΔC_D per gallon $\times 10^5$ against $\frac{l_s}{d}$.

Figure 20.- Continued.

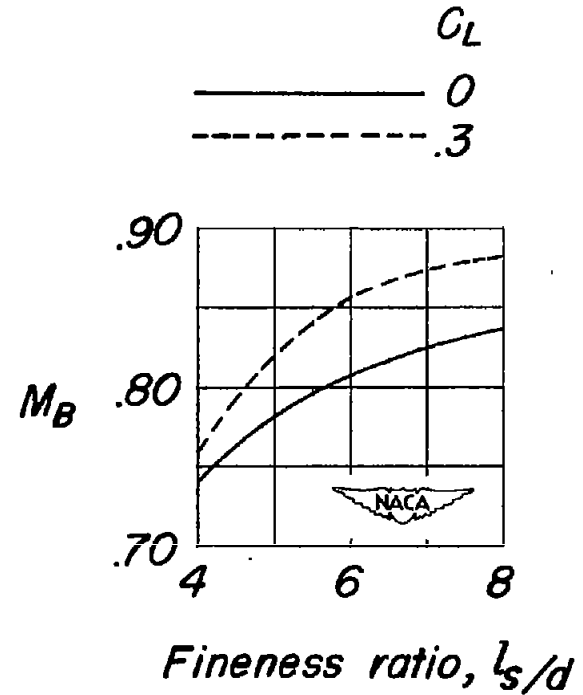


(a) $\frac{\Delta C_D}{C_{Dg}}$ against $\frac{l_s}{d}$ at a Mach number of 0.80.

Figure 20. - Concluded.

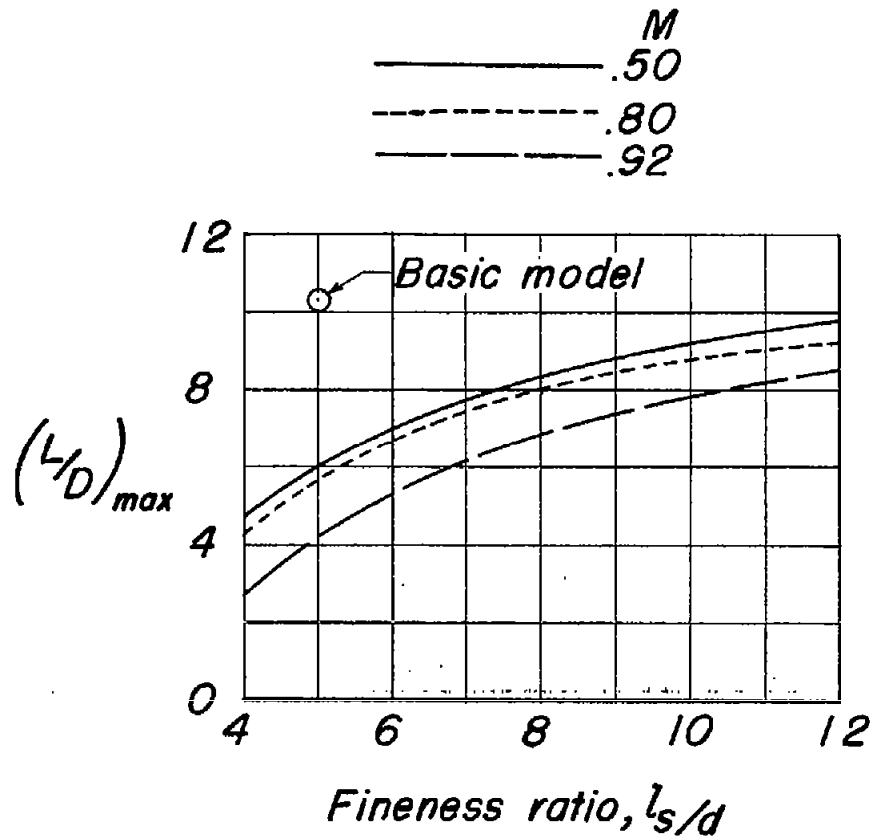


(a) $\frac{l_p}{c} = 9.45$ percent.

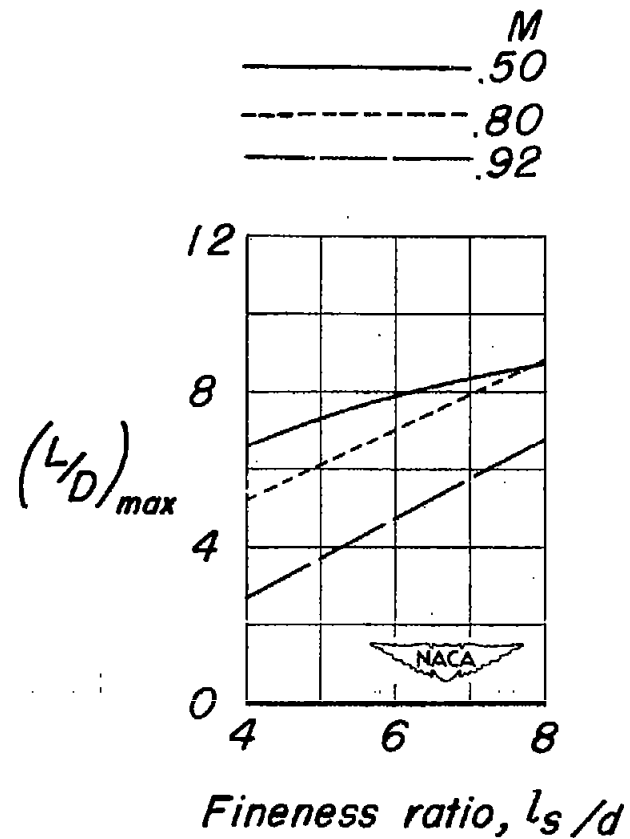


(b) $\frac{l_p}{c} = 37.8$ percent.

Figure 21.- Effect of variations in external-store fineness ratio on the drag-break Mach numbers of the basic model; $\frac{t}{c_p} = 10$ percent; $c_p = 1.5$ inches; $\Lambda = 0^\circ$.

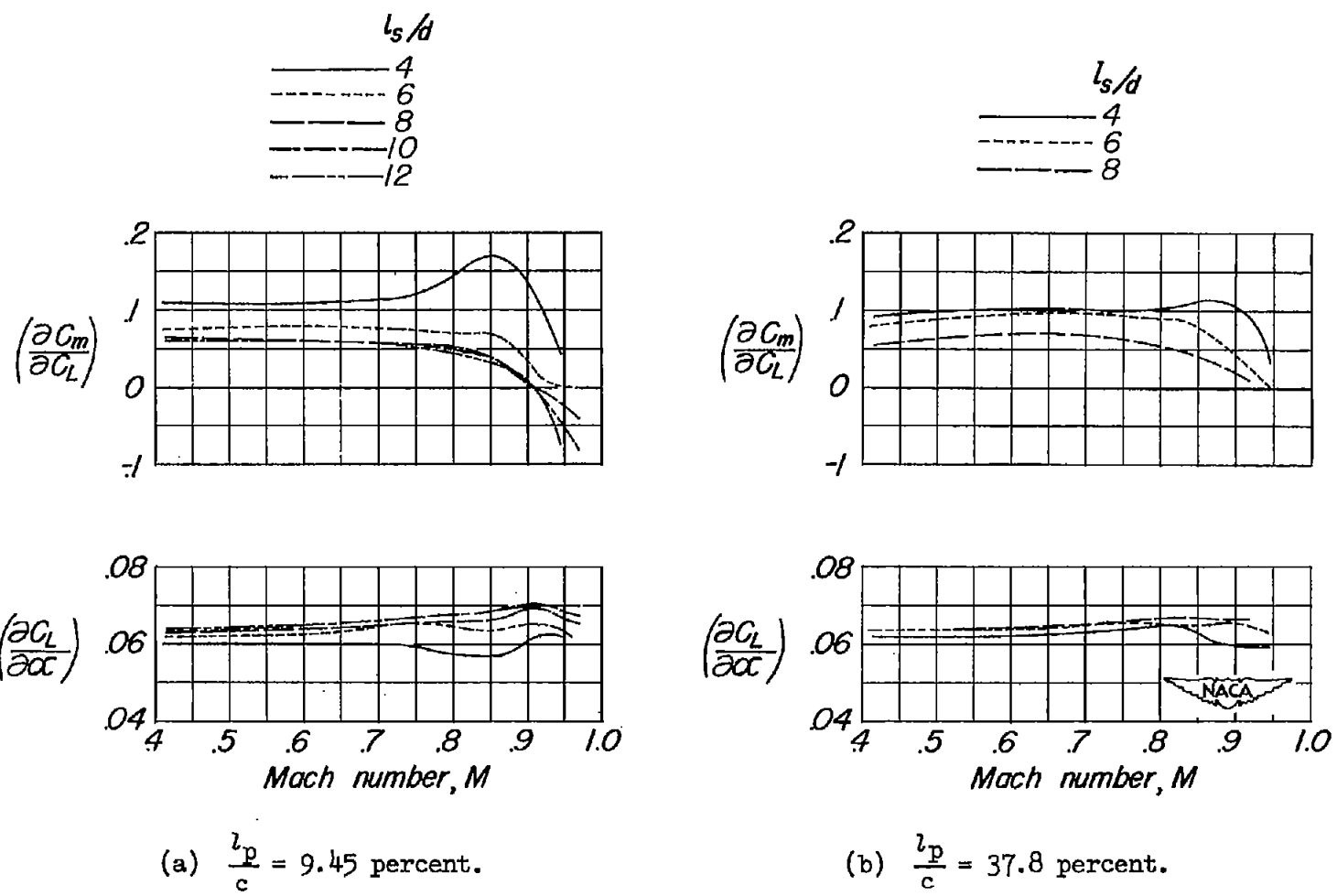


(a) $\frac{l_p}{c} = 9.45$ percent.



(b) $\frac{l_p}{c} = 37.8$ percent.

Figure 22.- Effect of variations in external-store fineness ratio on the maximum lift-drag ratios of the basic model; $\frac{t}{c_p} = 10$ percent; $c_p = 1.5$ inches; $\Lambda = 0^\circ$.



(a) $\frac{l_p}{c} = 9.45$ percent.

(b) $\frac{l_p}{c} = 37.8$ percent.

Figure 23.- Effect of Mach number on the aerodynamic-center location and lift-curve slope of the basic model with an external-store installation showing the effects of variations in external-store fineness ratio; $\frac{t}{c_p} = 10$ percent; $c_p = 1.5$ inches; $\Lambda = 0^\circ$.

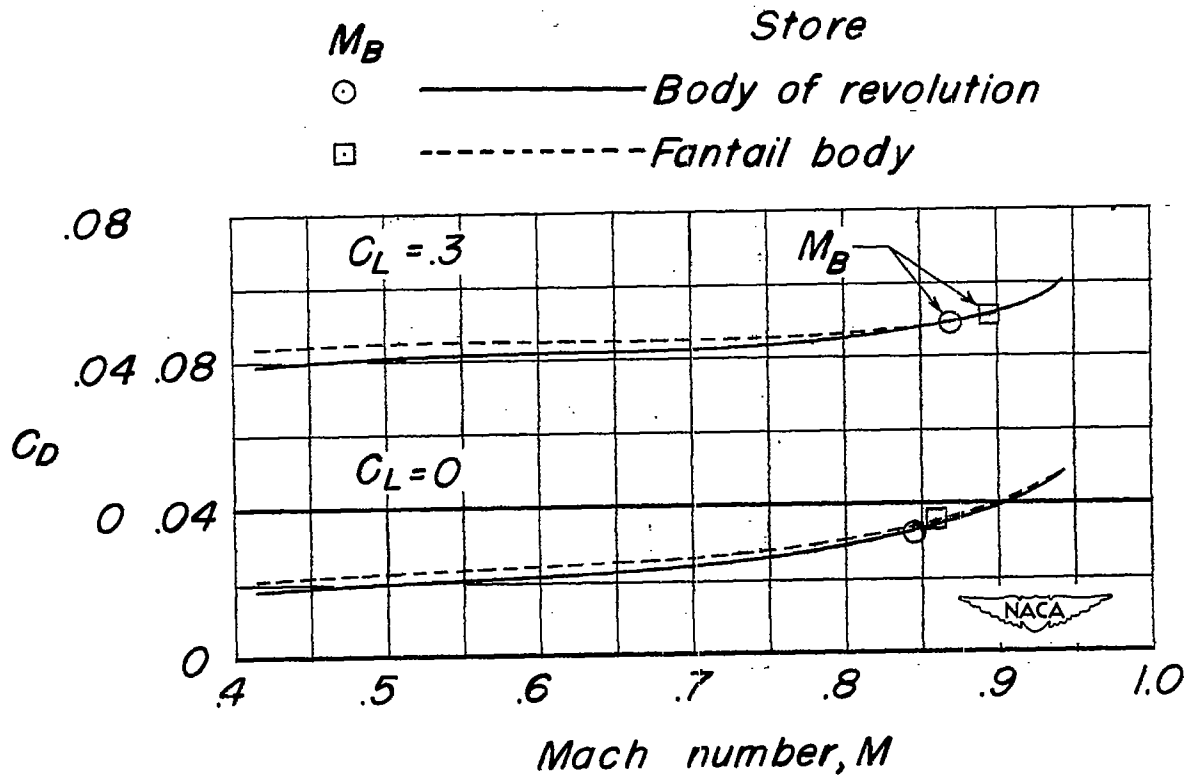
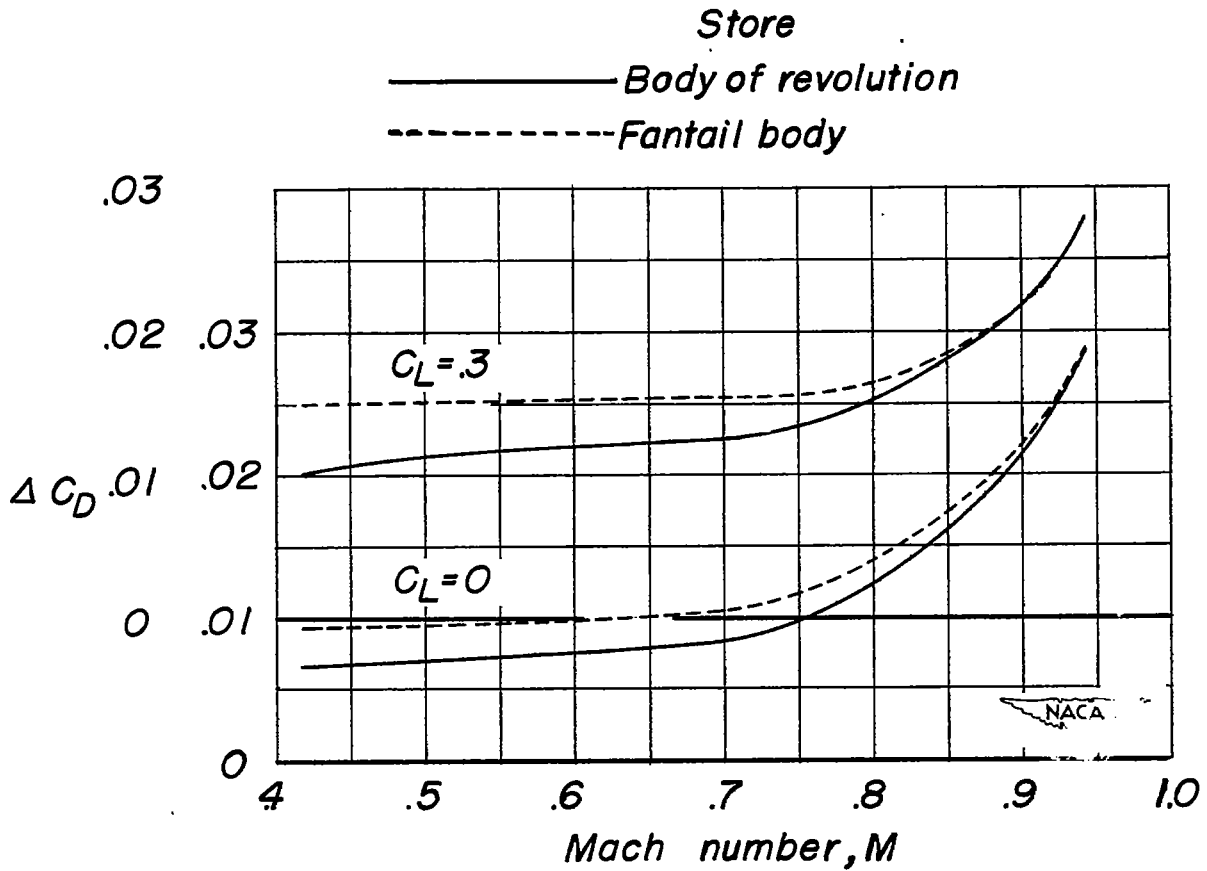
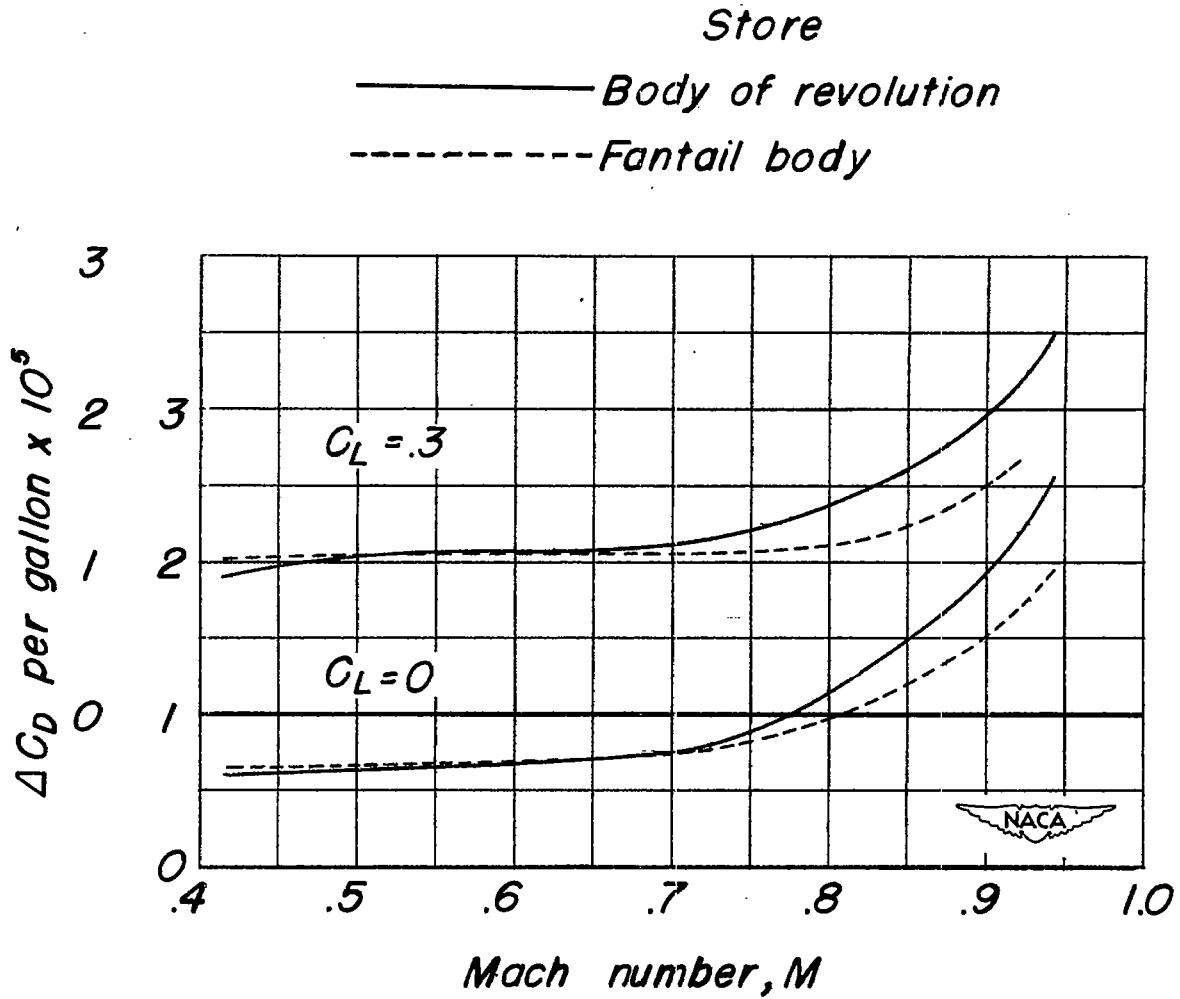


Figure 24.- Effect of Mach number on the drag characteristics of the basic model with an external-store installation showing the effects of variations in external-store shape; $\frac{l_s}{d} = 6$; $\frac{t}{c_p} = 20$ percent; $\frac{l_p}{c} = 9.45$ percent; $c_p = 1.0$ inch; $\Lambda = 0^\circ$.



(a) ΔC_D against M.

Figure 25.- Effect of variations in external-store shape on the drag characteristics of the basic model; $\frac{l_s}{d} = 6$; $\frac{t}{c_p} = 20$ percent; $\frac{l_p}{c} = 9.45$ percent; $c_p = 1.0$ inch; $\Lambda = 0^\circ$.



(b) ΔC_D per gallon $\times 10^5$ against M .

Figure 25.- Concluded.

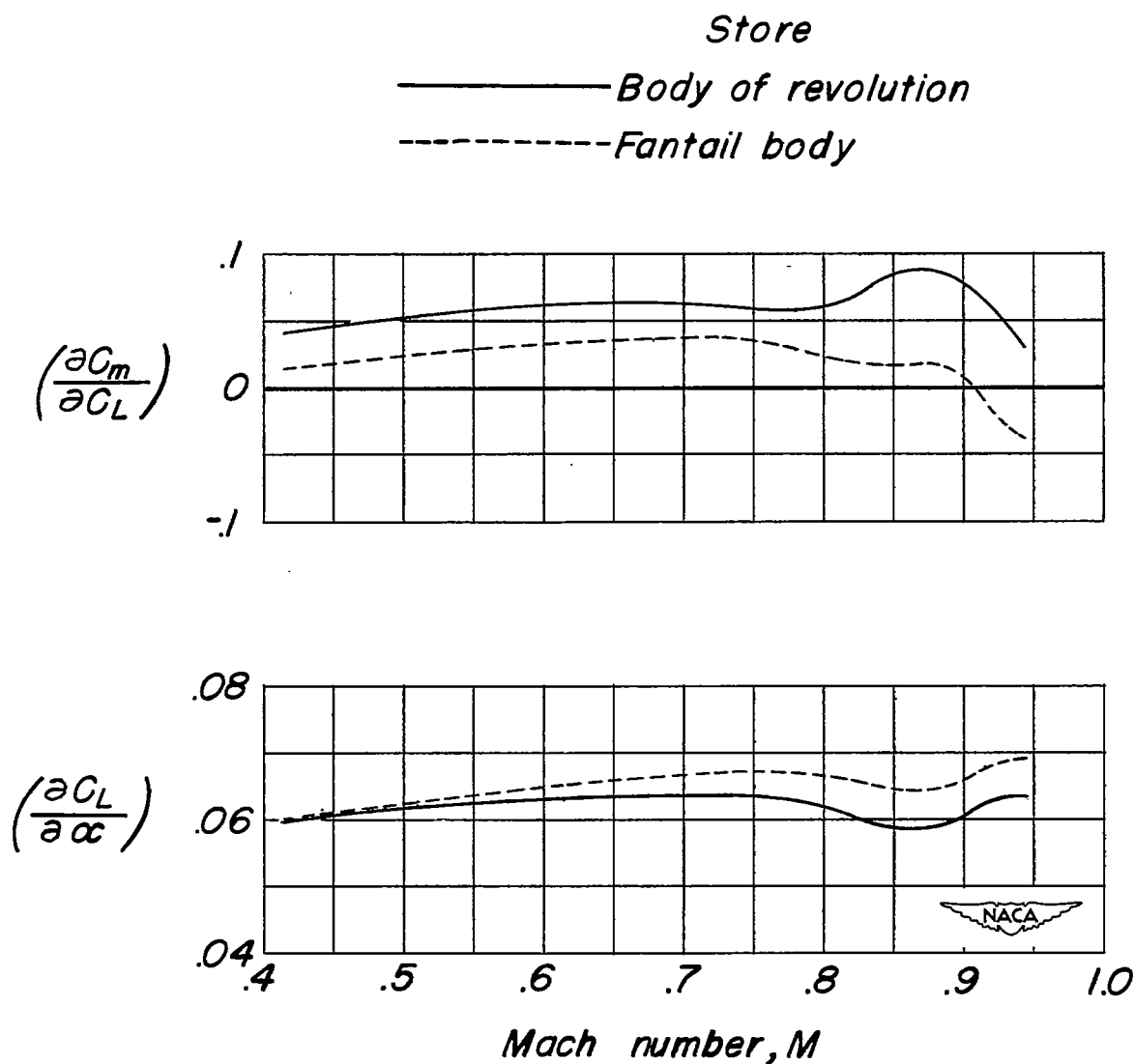


Figure 26.- Effect of Mach number on the aerodynamic-center location and lift-curve slope of the basic model with an external-store installation showing the effects of variations in external-store shape; $\frac{l_s}{d} = 6$; $\frac{t}{c_p} = 20$ percent; $\frac{l_p}{c} = 9.45$ percent; $c_p = 1.0$ inch; $\Lambda = 0^\circ$.

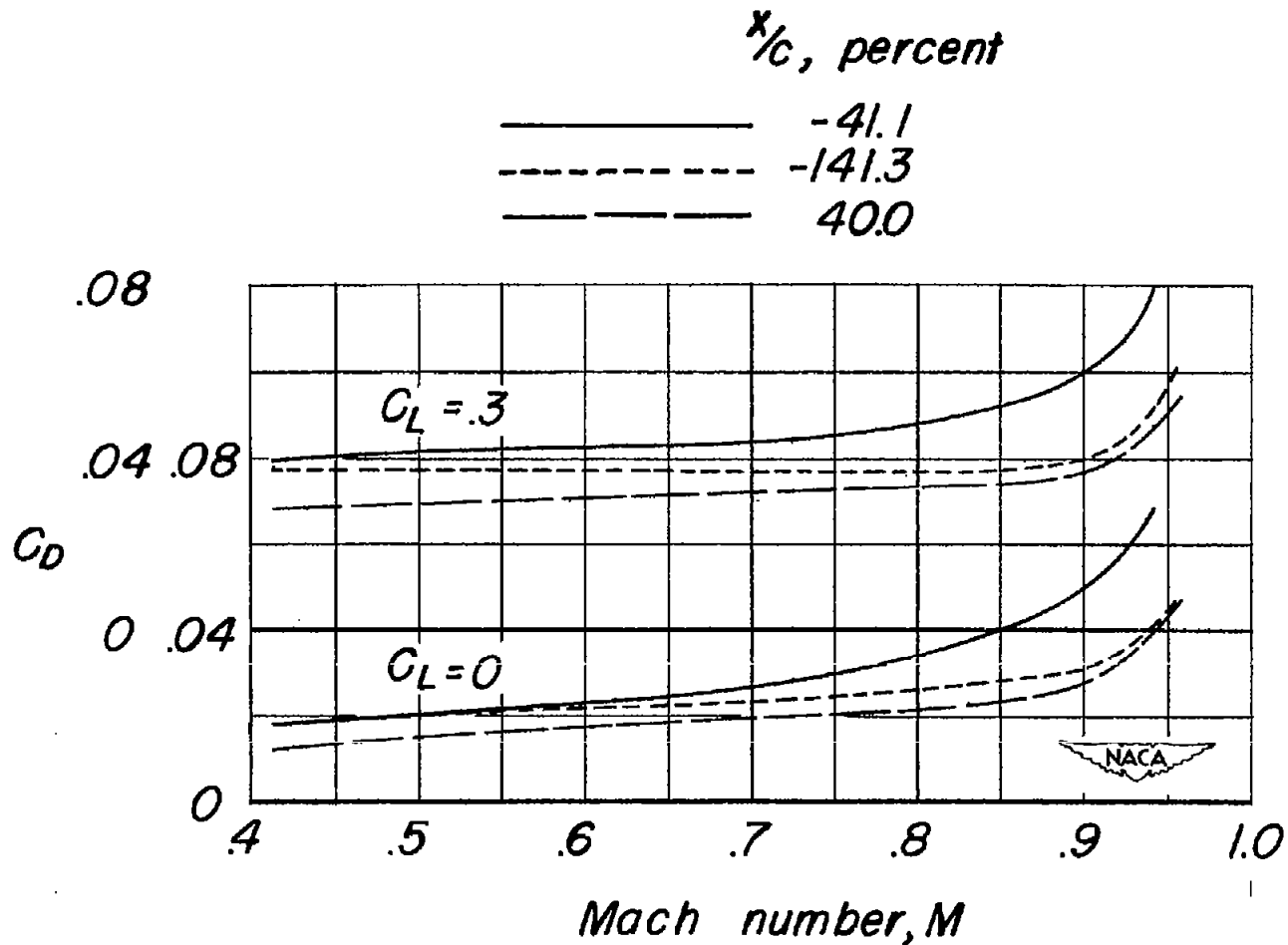
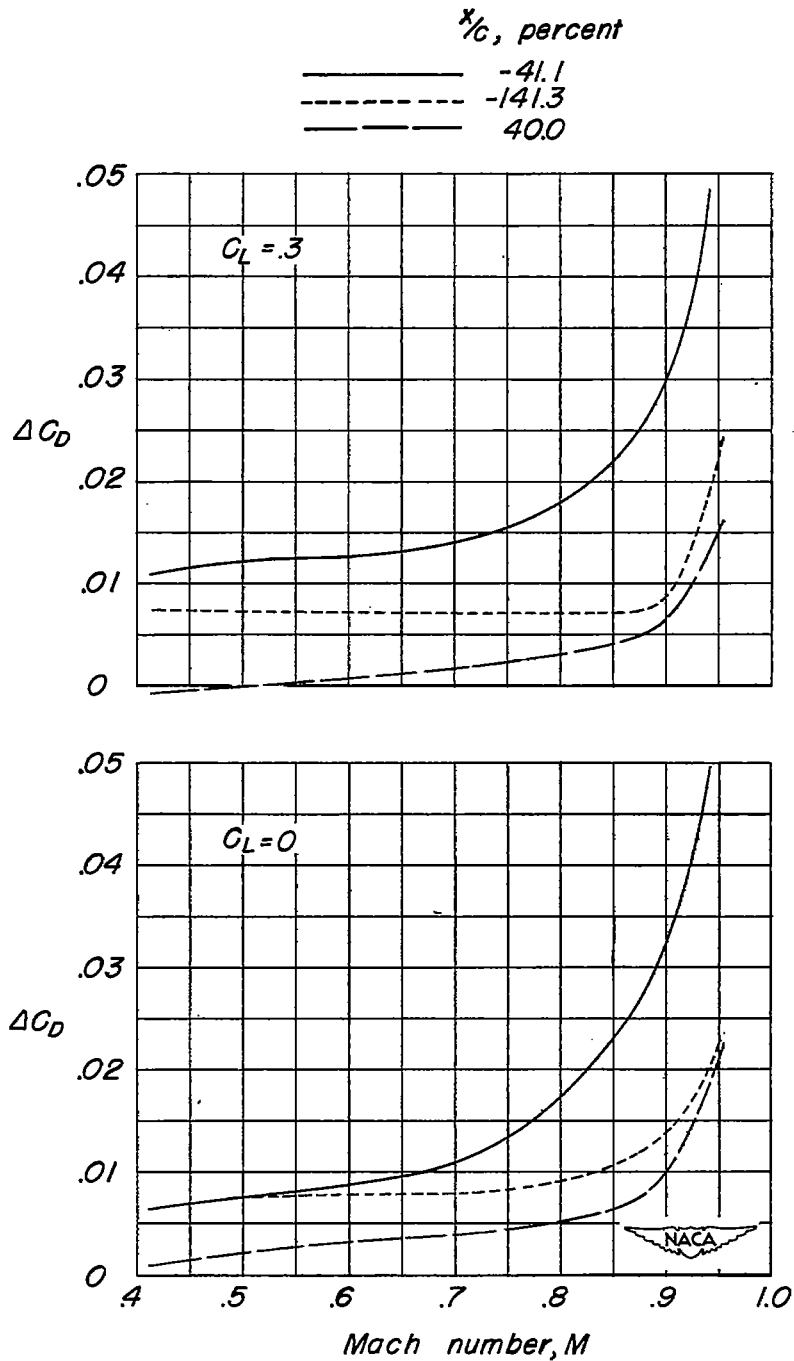
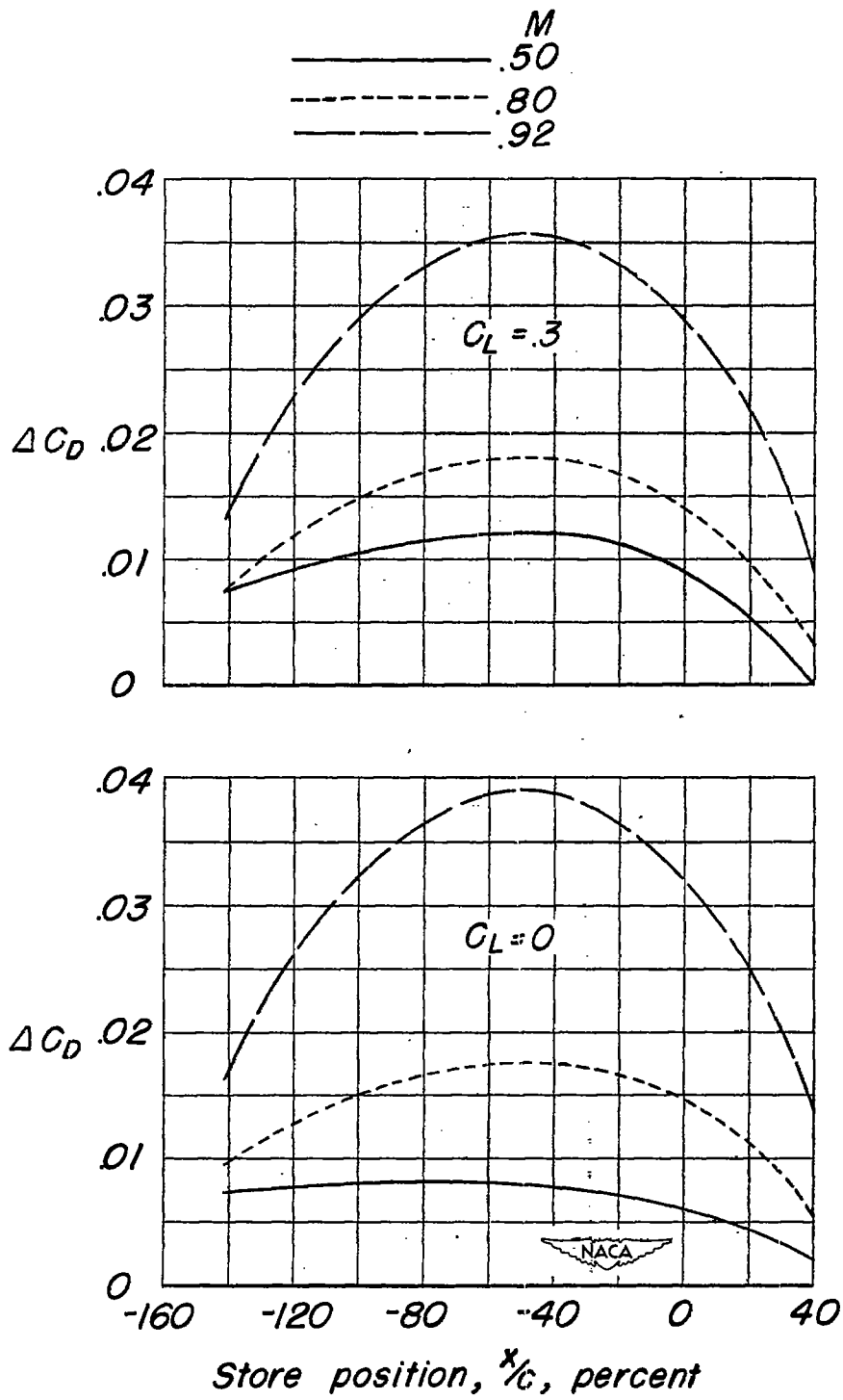


Figure 27.- Effect of Mach number on the drag characteristics of the basic model with an external-store installation showing the effects of variations in external-store chordwise position; $\frac{l_g}{d} = 6$; $\frac{t}{c_p} = 20$ percent; $\frac{l_p}{c} = 18.9$ percent; $c_p = 1.0$ inch.



(a) ΔC_D against M .

Figure 28.- Effect of variations in external-store chordwise position on the drag characteristics of the basic model; $\frac{l_s}{d} = 6$; $\frac{t}{c_p} = 20$ percent; $\frac{l_p}{c} = 18.9$ percent; $c_p = 1.0$ inch.



(b) ΔC_D against x/c .

Figure 28.- Concluded.

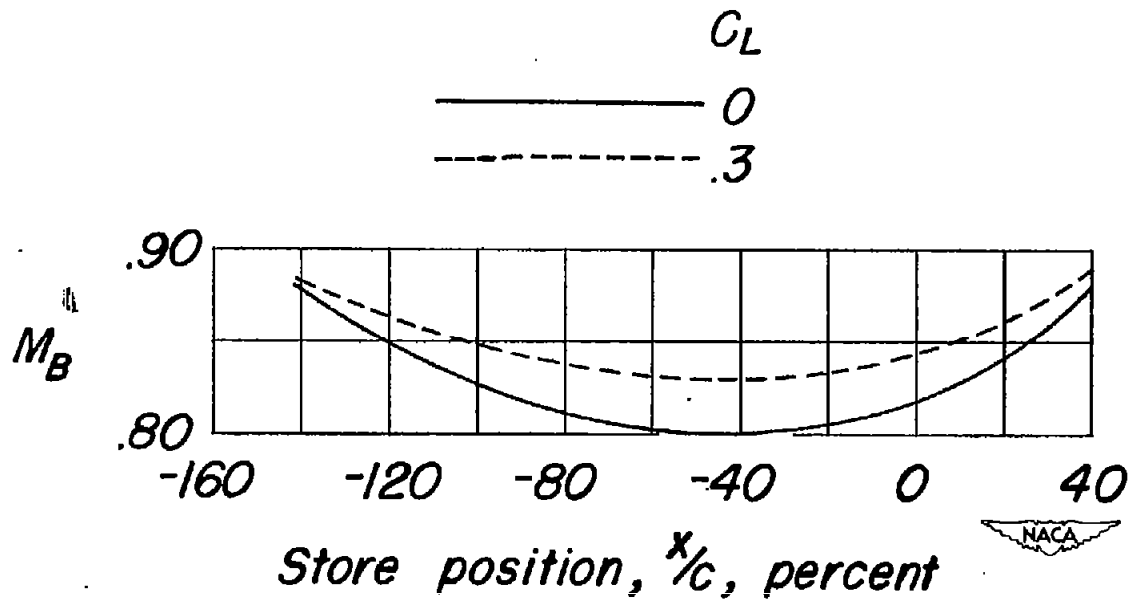


Figure 29.- Effect of variations in external-store chordwise position on the drag-break Mach numbers of the basic model; $\frac{l_B}{d} = 6$; $\frac{t}{c_p} = 20$ percent; $\frac{l_p}{c} = 18.9$ percent; $c_p = 1.0$ inch.

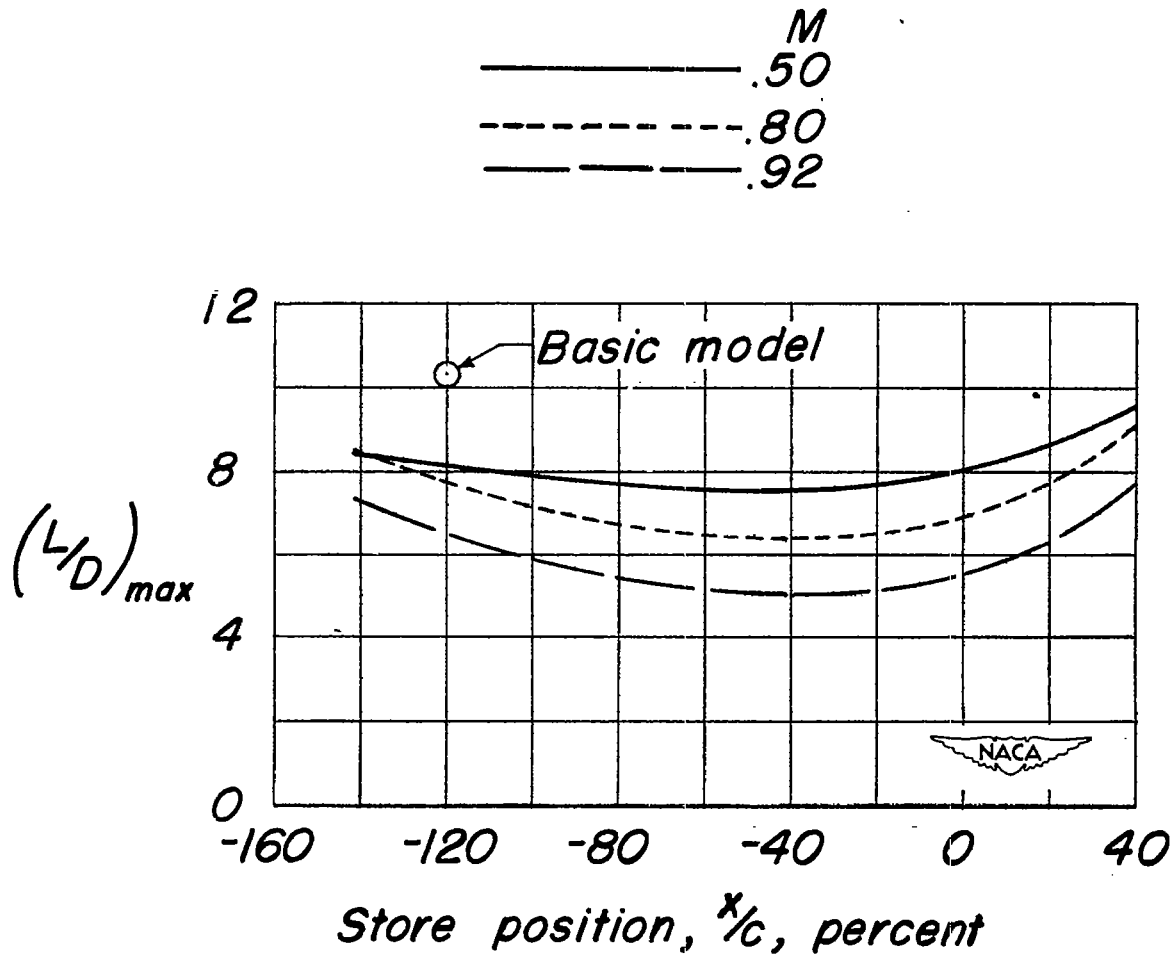


Figure 30.- Effect of variations in external-store chordwise position on the maximum lift-drag ratios of the basic model; $\frac{l_s}{d} = 6$; $\frac{t}{c_p} = 20$ percent; $\frac{l_p}{c} = 18.9$ percent; $c_p = 1.0$ inch.

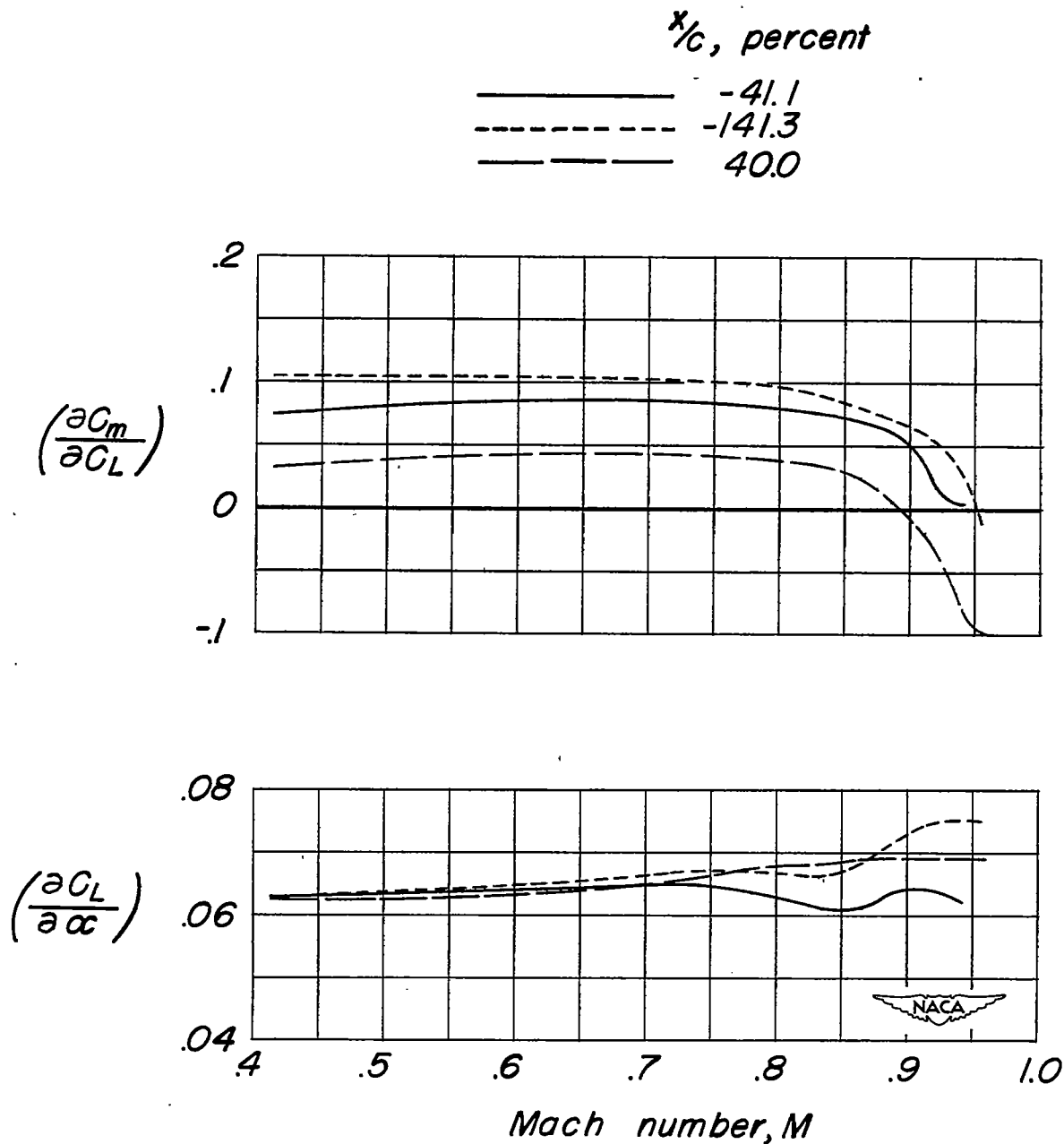


Figure 31.- Effect of Mach number on the aerodynamic-center location and lift-curve slope of the basic model with an external-store installation showing the effects of variations in external-store chordwise position;

$$\frac{l_s}{d} = 6; \quad \frac{t}{c_p} = 20 \text{ percent}; \quad \frac{l_p}{c} = 18.9 \text{ percent}; \quad c_p = 1.0 \text{ inch.}$$

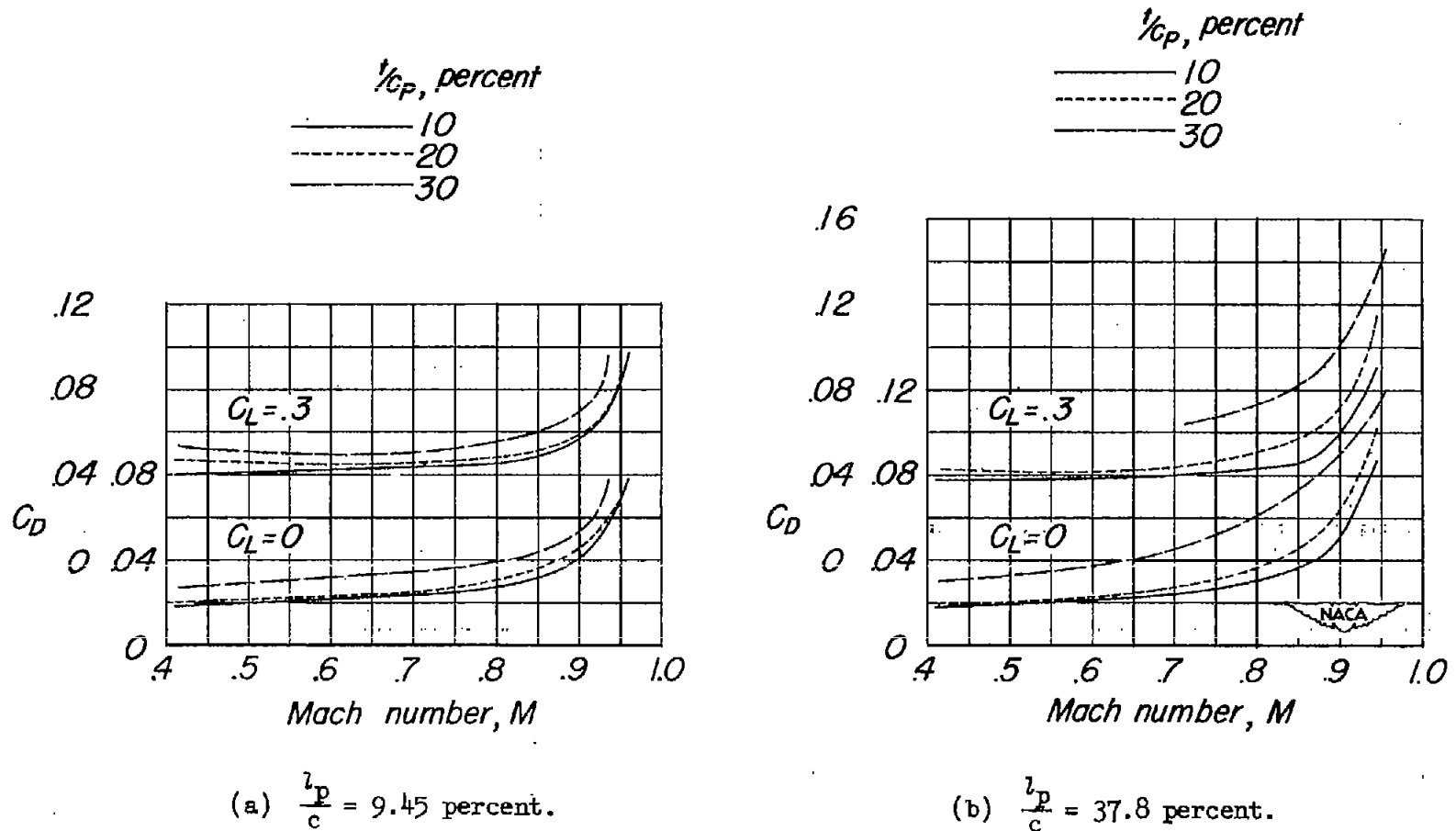
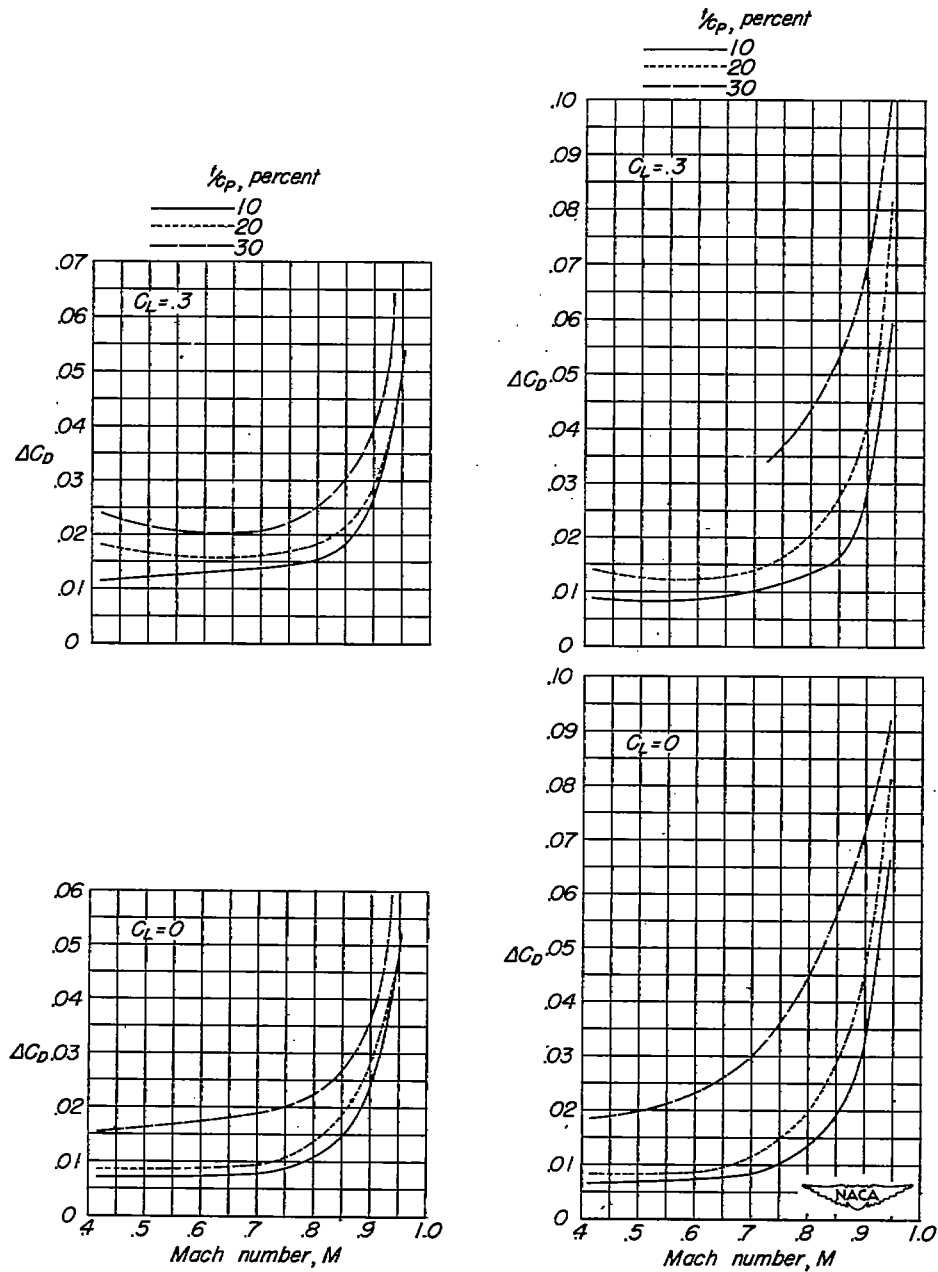
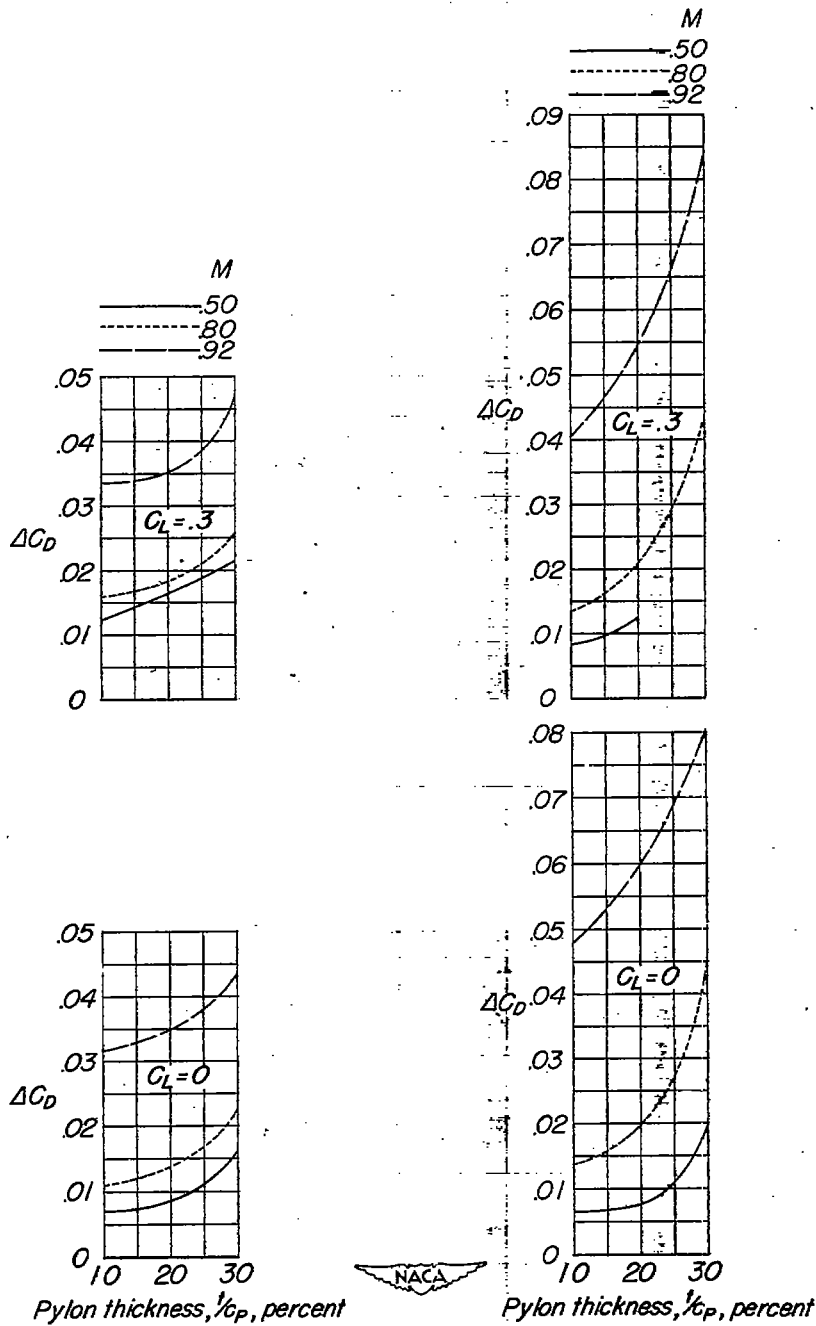


Figure 32.- Effect of Mach number on the drag characteristics of the basic model with an external-store installation showing the effects of variations in pylon thickness; $\frac{l_s}{d} = 6$; $c_p = 1.5$ inches; $\Lambda = 0^\circ$.



(a) ΔC_D against M .

Figure 33.- Effect of variations in pylon thickness on the drag characteristics of the basic model; $\frac{l_s}{d} = 6$; $c_p = 1.5$ inches; $\Lambda = 0^\circ$.

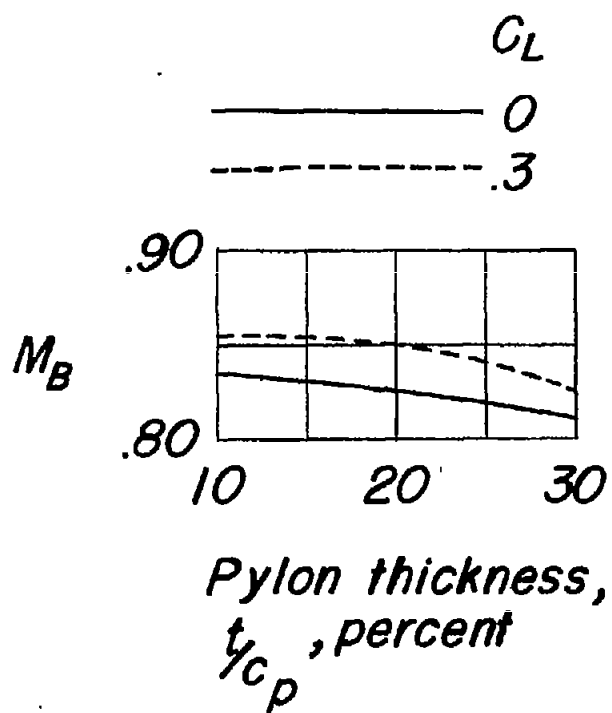


$\frac{l_p}{c} = 9.45$ percent

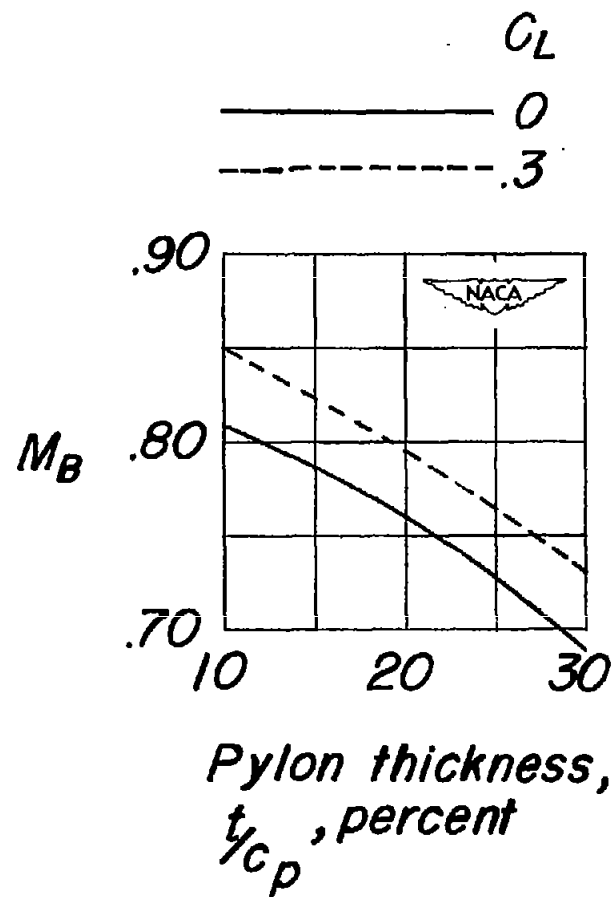
$\frac{l_p}{c} = 37.8$ percent

(b) ΔC_D against $\frac{t}{c_p}$.

Figure 33.- Concluded.

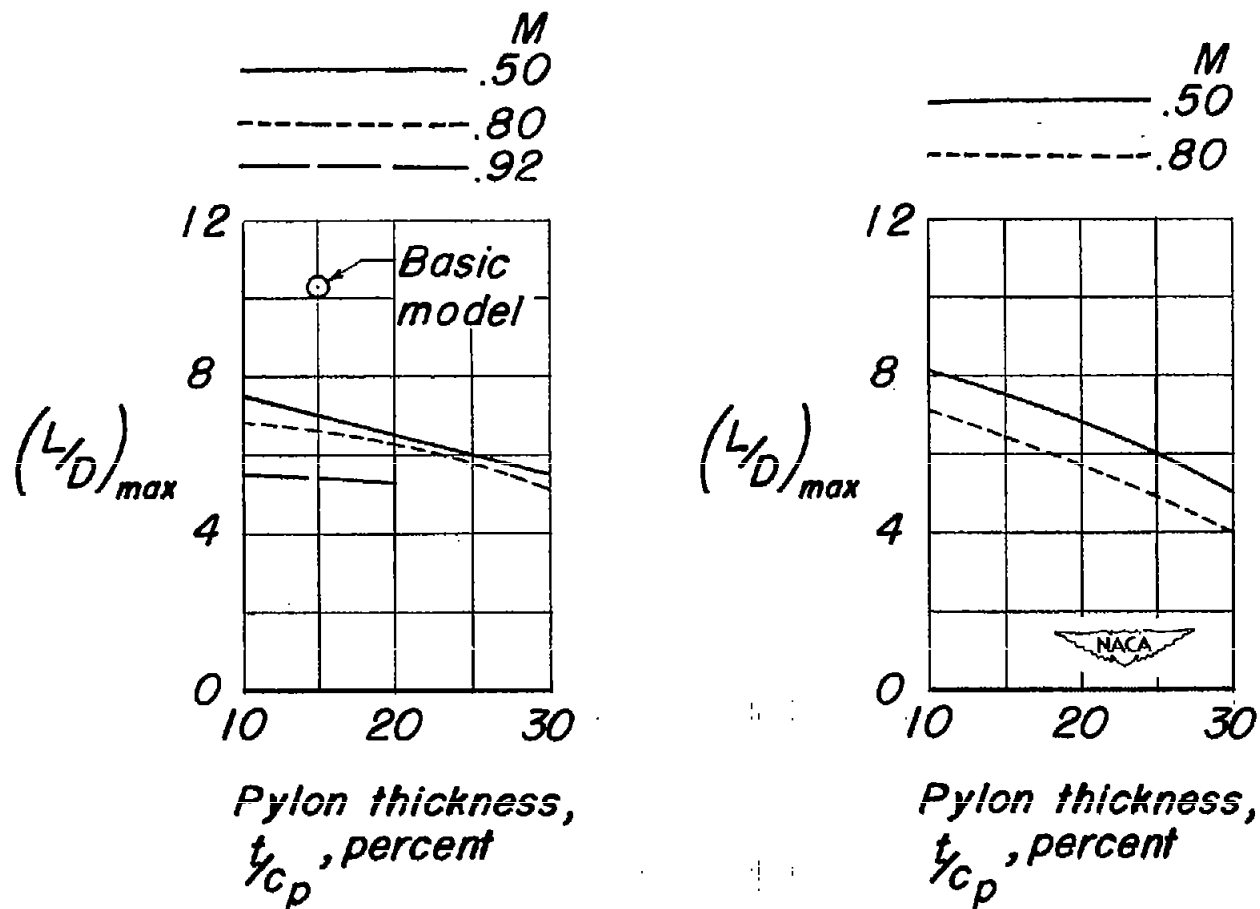


(a) $\frac{l_p}{c} = 9.45$ percent.



(b) $\frac{l_p}{c} = 37.8$ percent.

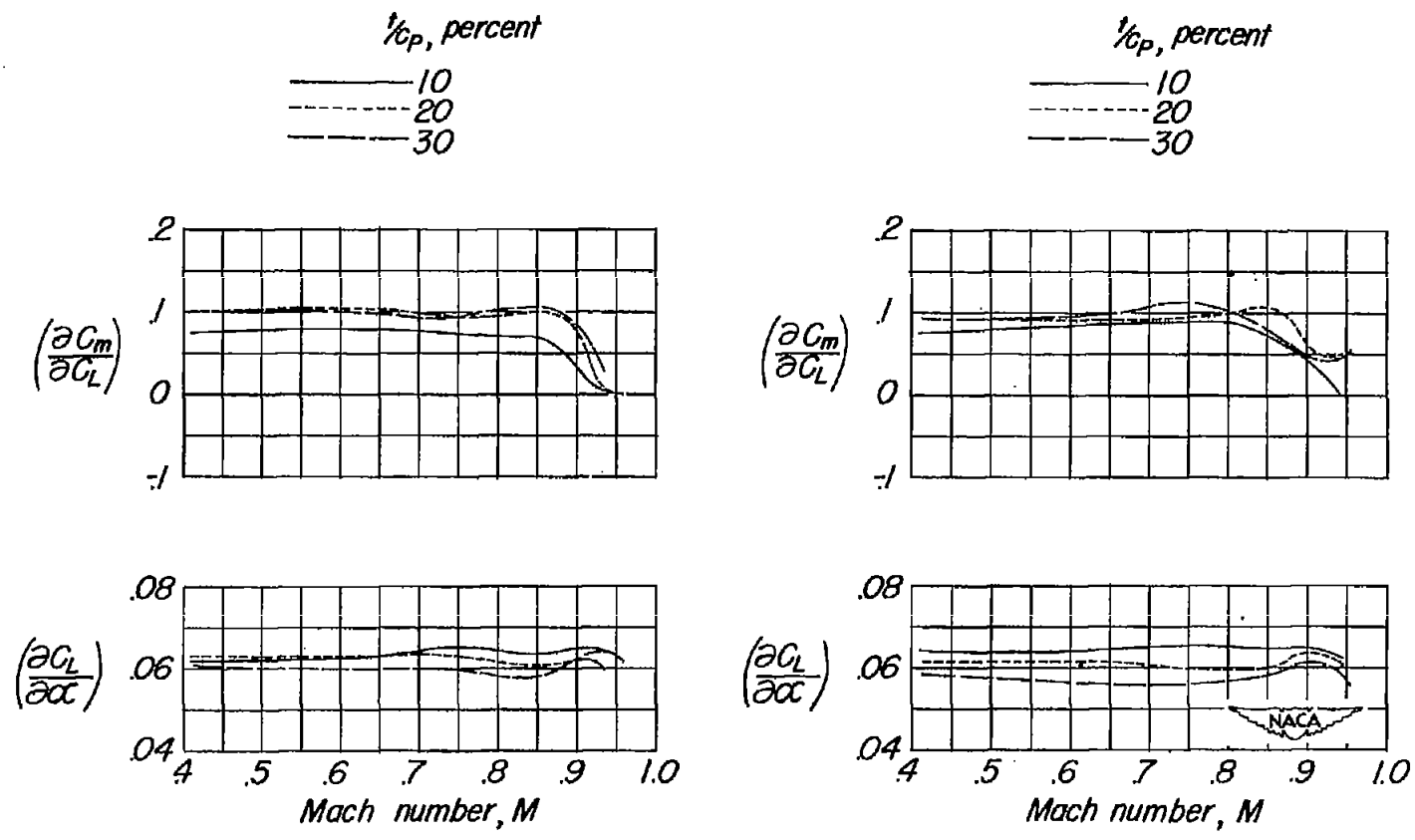
Figure 34.- Effect of variations in pylon thickness on the drag-break Mach numbers of the basic model; $\frac{l_B}{d} = 6$; $c_p = 1.5$ inches; $\Lambda = 0^\circ$.



(a) $\frac{l_p}{c} = 9.45$ percent.

(b) $\frac{l_p}{c} = 37.8$ percent.

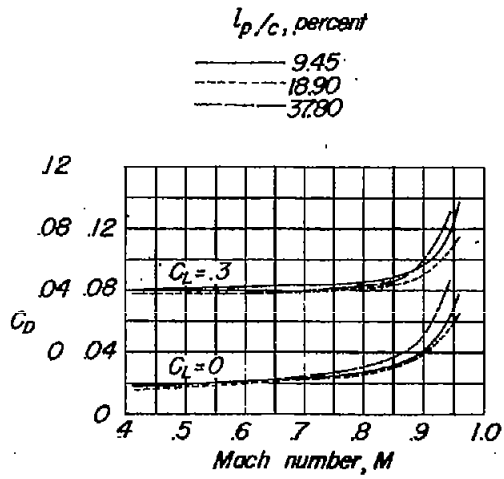
Figure 35.- Effect of variations in pylon thickness on the maximum lift-drag ratios of the basic model; $\frac{l_s}{d} = 6$; $c_p = 1.5$ inches; $\Lambda = 0^\circ$.



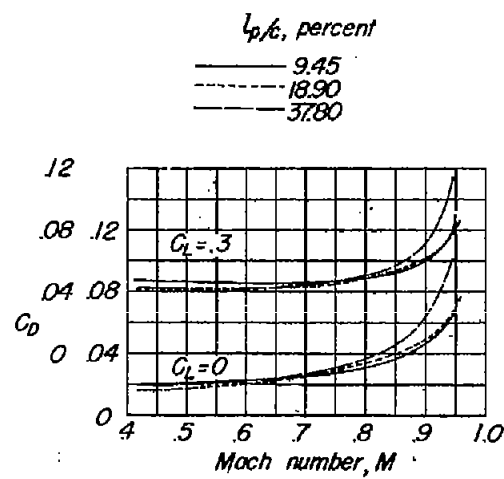
(a) $\frac{l_p}{c} = 9.45$ percent.

(b) $\frac{l_p}{c} = 37.8$ percent.

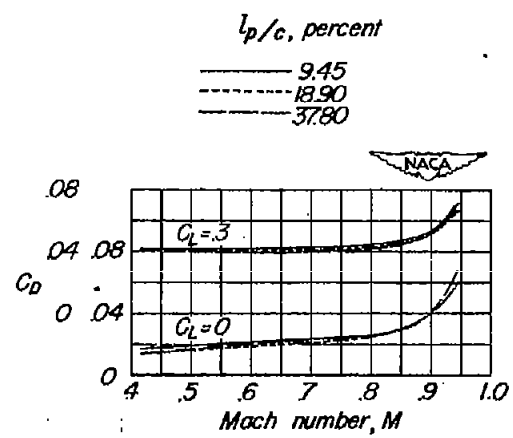
Figure 36.- Effect of Mach number on the aerodynamic-center location and lift-curve slope of the basic model with an external-store installation showing the effects of variations in pylon thickness; $\frac{l_g}{d} = 6$; $c_p = 1.5$ inches; $\Lambda = 0^\circ$.



(a) $\frac{t}{c_p} = 10$ percent;
 $A = 0^\circ$.

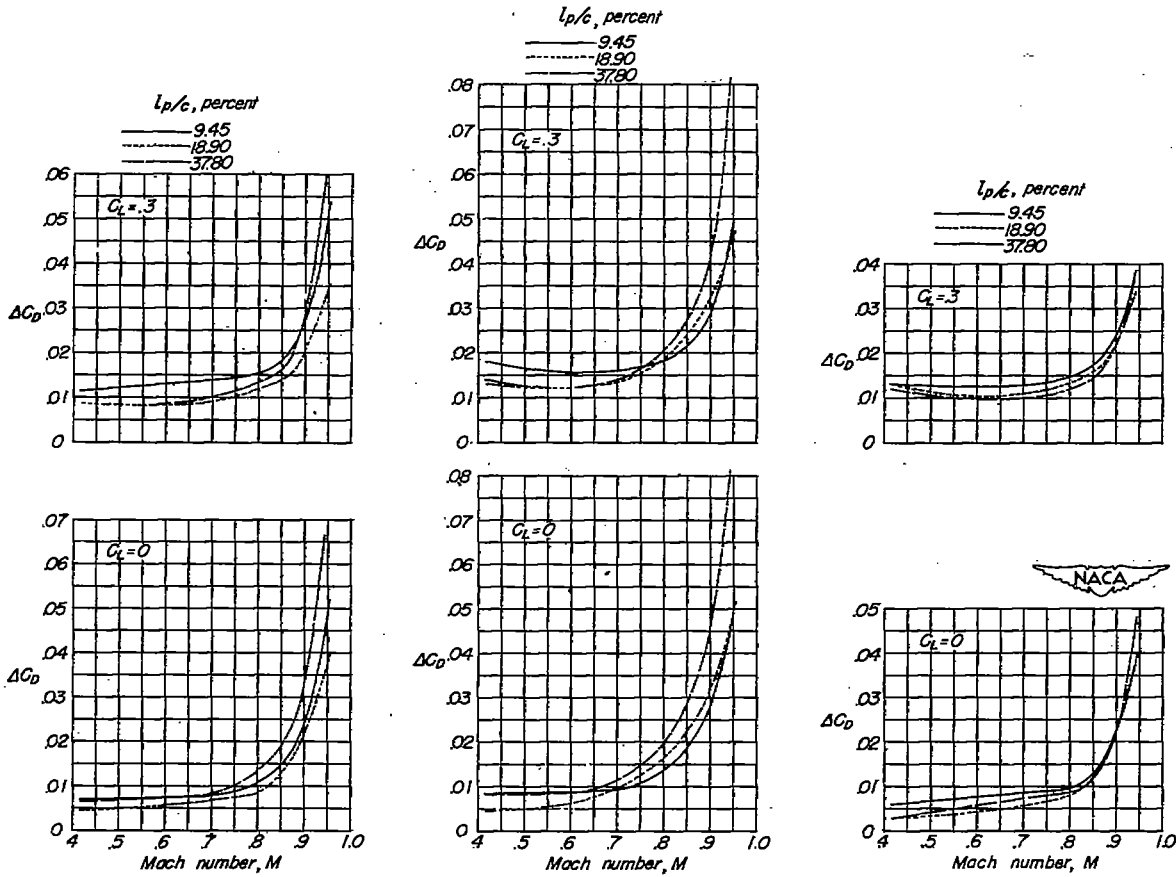


(b) $\frac{t}{c_p} = 20$ percent;
 $A = 0^\circ$.



(c) $\frac{t}{c_p} = 10$ percent;
 $A = 45^\circ$.

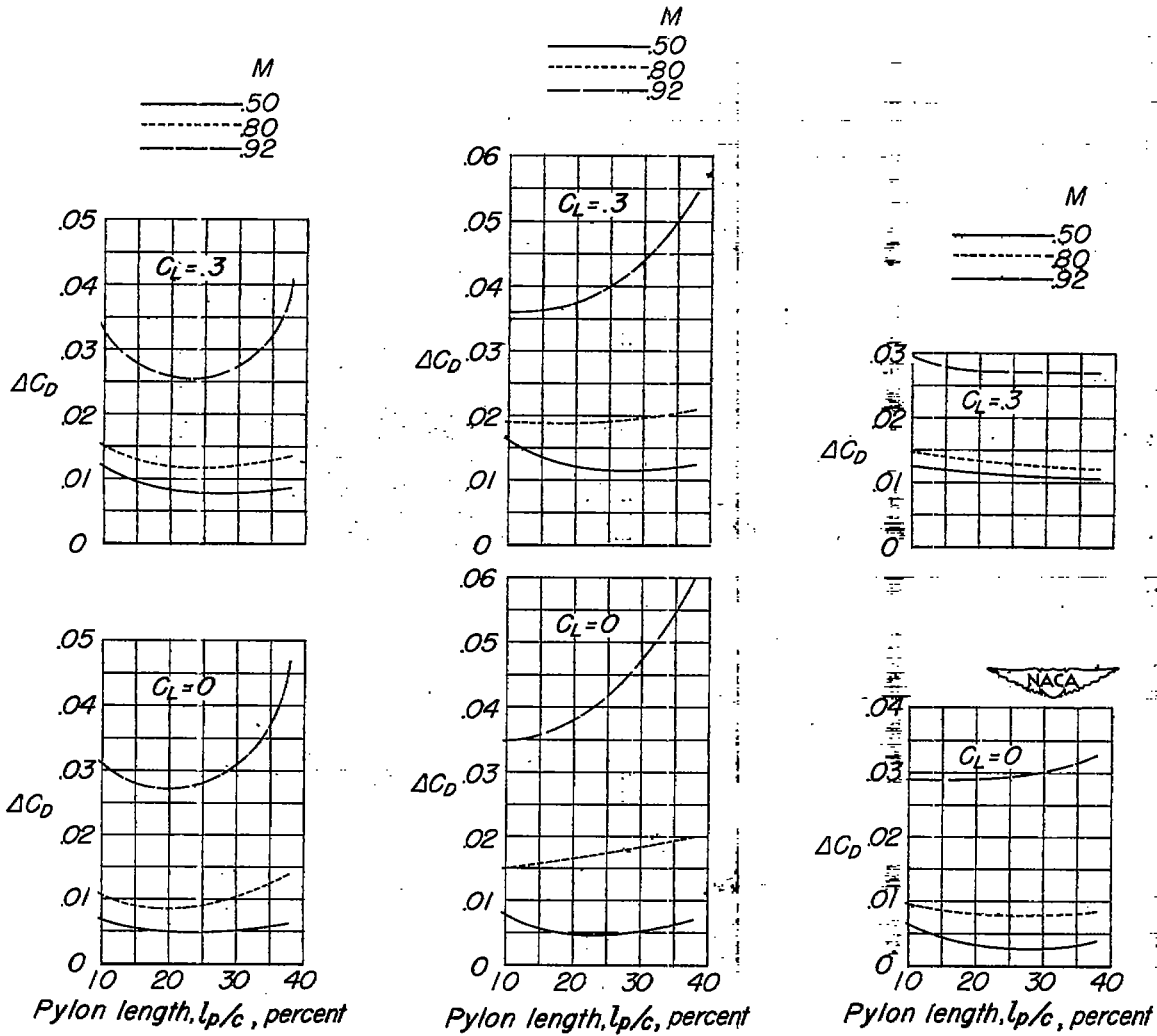
Figure 37.- Effect of Mach number on the drag characteristics of the basic model with an external-store installation showing the effects of variations in pylon length; $\frac{l_B}{d} = 6$; $c_p = 1.5$ inches.



$\frac{t}{c_p} = 10$ percent, $\Lambda = 0^\circ$ $\frac{t}{c_p} = 20$ percent, $\Lambda = 0^\circ$ $\frac{t}{c_p} = 10$ percent, $\Lambda = 45^\circ$

(a) ΔC_D against M.

Figure 38.- Effect of variations in pylon length on the drag characteristics of the basic model; $\frac{l_B}{d} = 6$; $c_p = 1.5$ inches.



$\frac{t}{c_p} = 10$ percent, $\Lambda = 0^\circ$

$\frac{t}{c_p} = 20$ percent, $\Lambda = 0^\circ$

$\frac{t}{c_p} = 10$ percent, $\Lambda = 45^\circ$

(b) ΔC_D against $\frac{l_p}{c}$.

Figure 38.- Concluded.

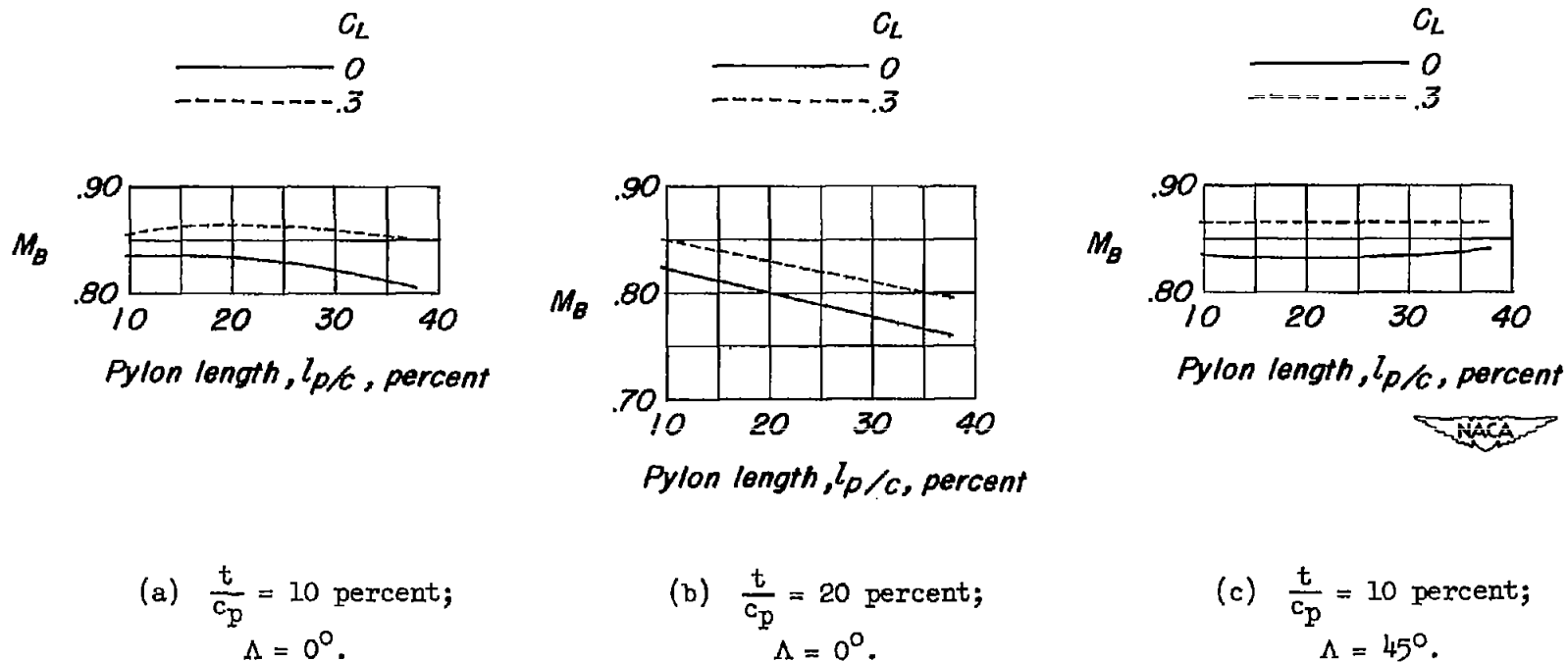


Figure 39.- Effect of variations in pylon length on the drag-break Mach numbers of the basic model;
 $\frac{l_B}{d} = 6$; $c_p = 1.5$ inches.

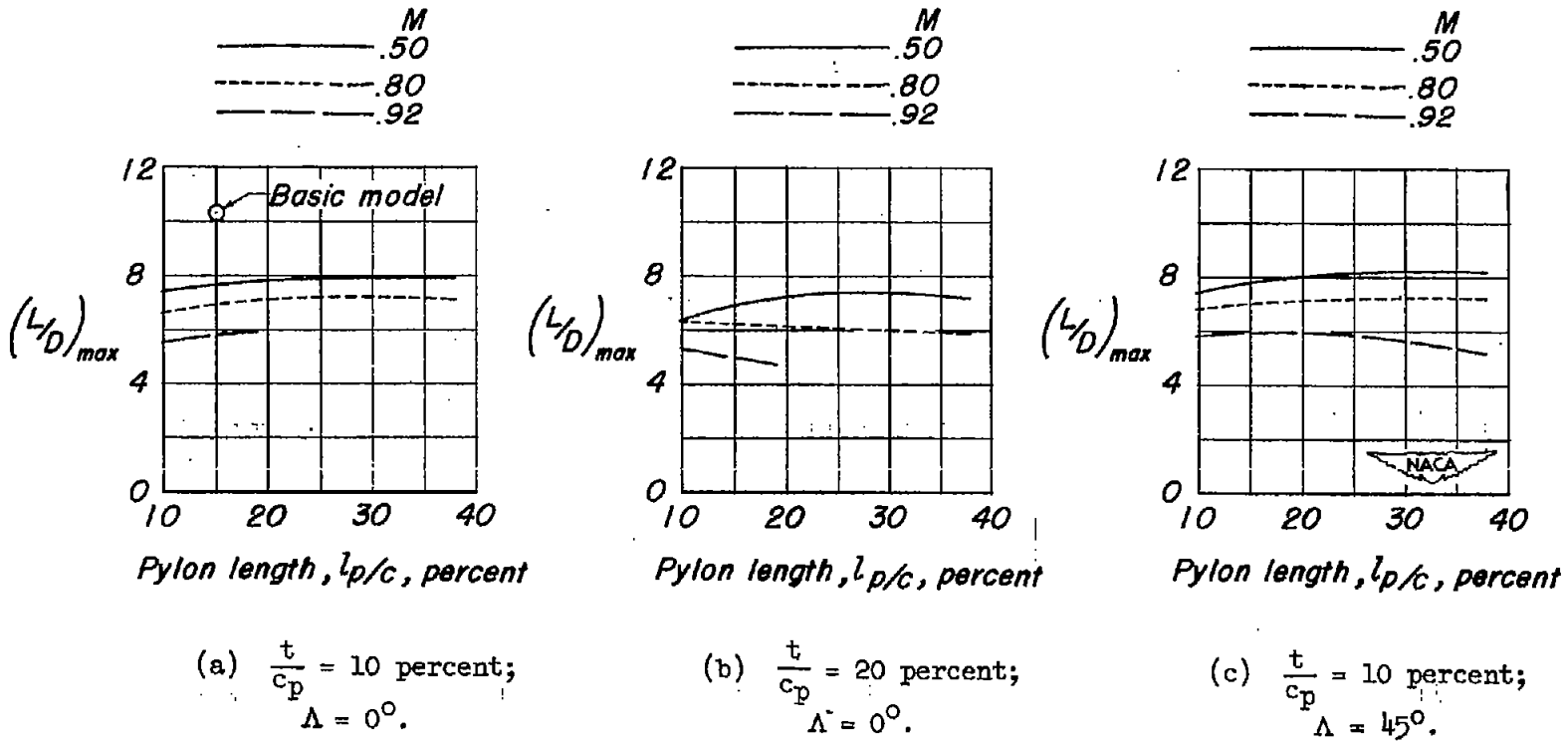


Figure 40.- Effect of variations in pylon length on the maximum lift-drag ratios of the basic model; $\frac{l_g}{d} = 6$; $c_p = 1.5$ inches.

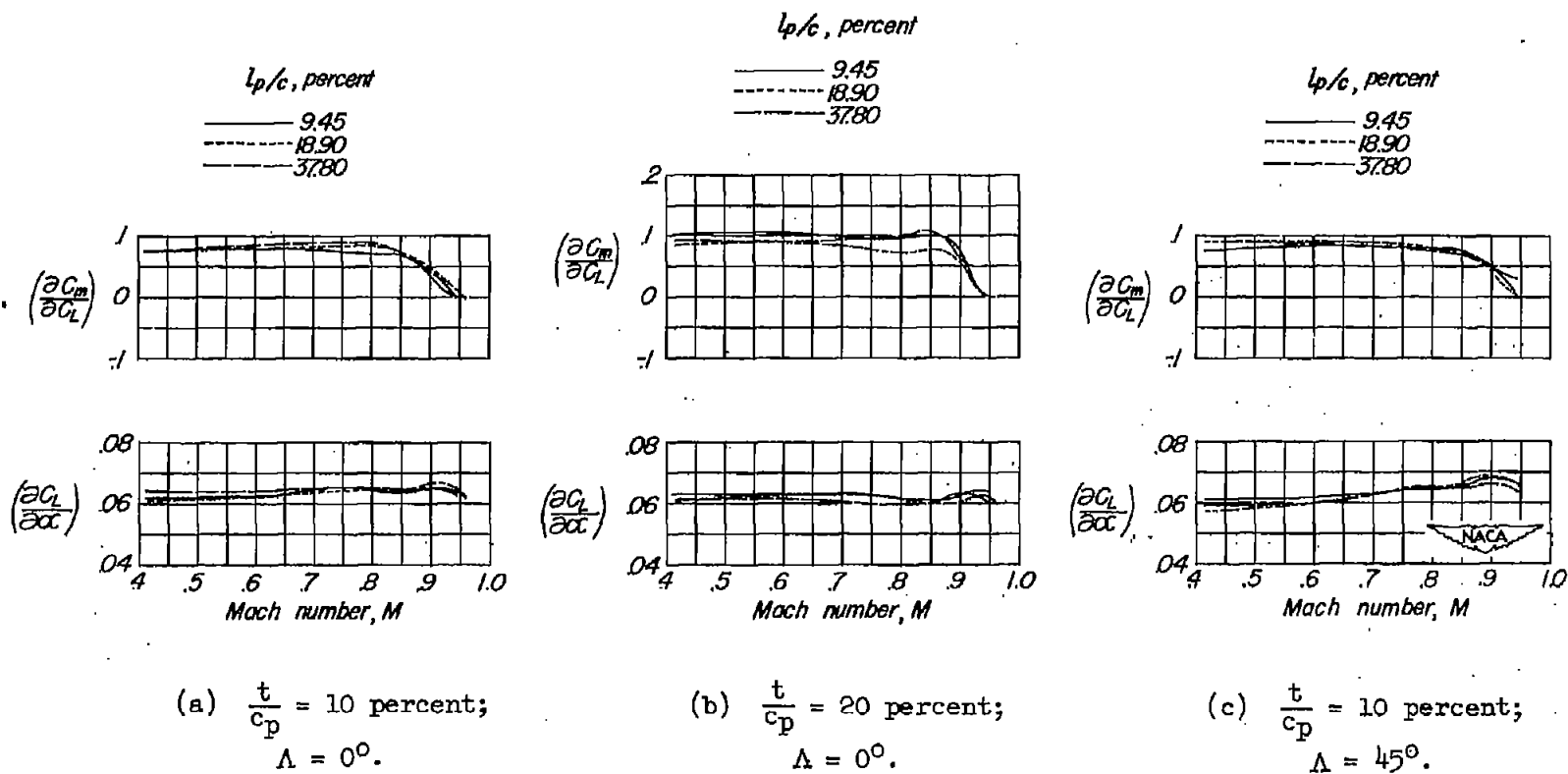


Figure 41.- Effect of Mach number on the aerodynamic-center location and lift-curve slope of the basic model with an external-store installation showing the effects of variations in pylon length; $\frac{z_B}{d} = 6$; $c_p = 1.5$ inches.

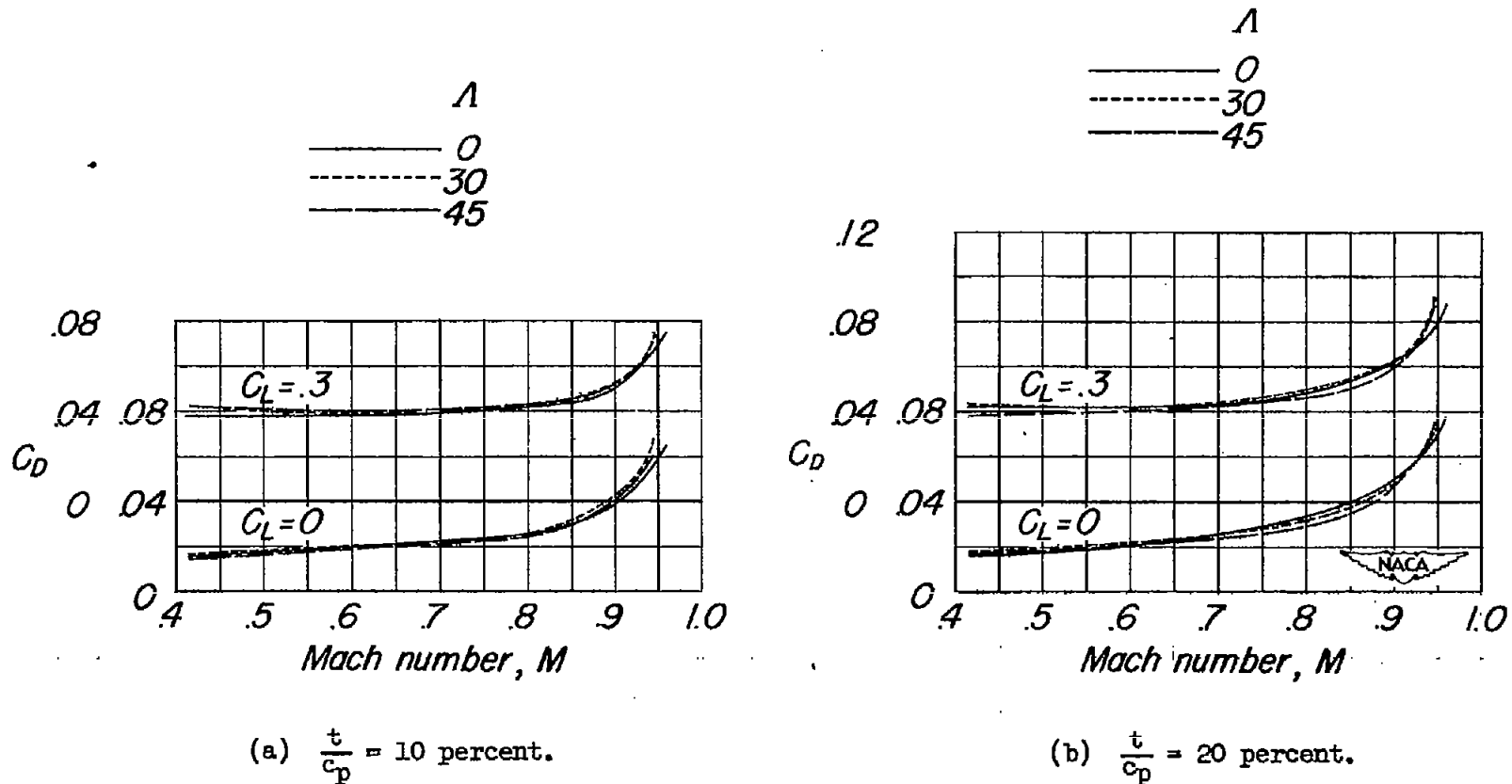
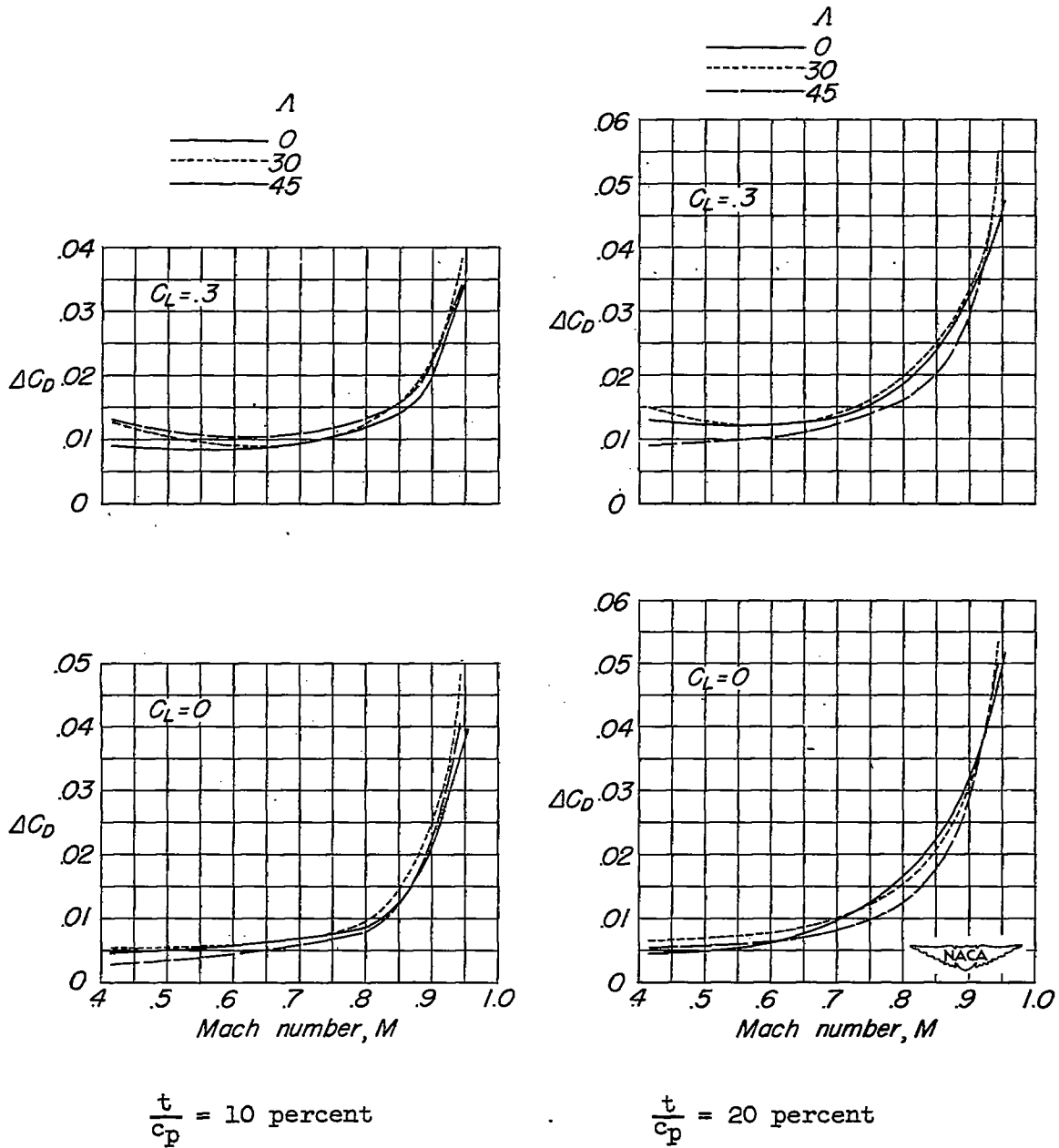
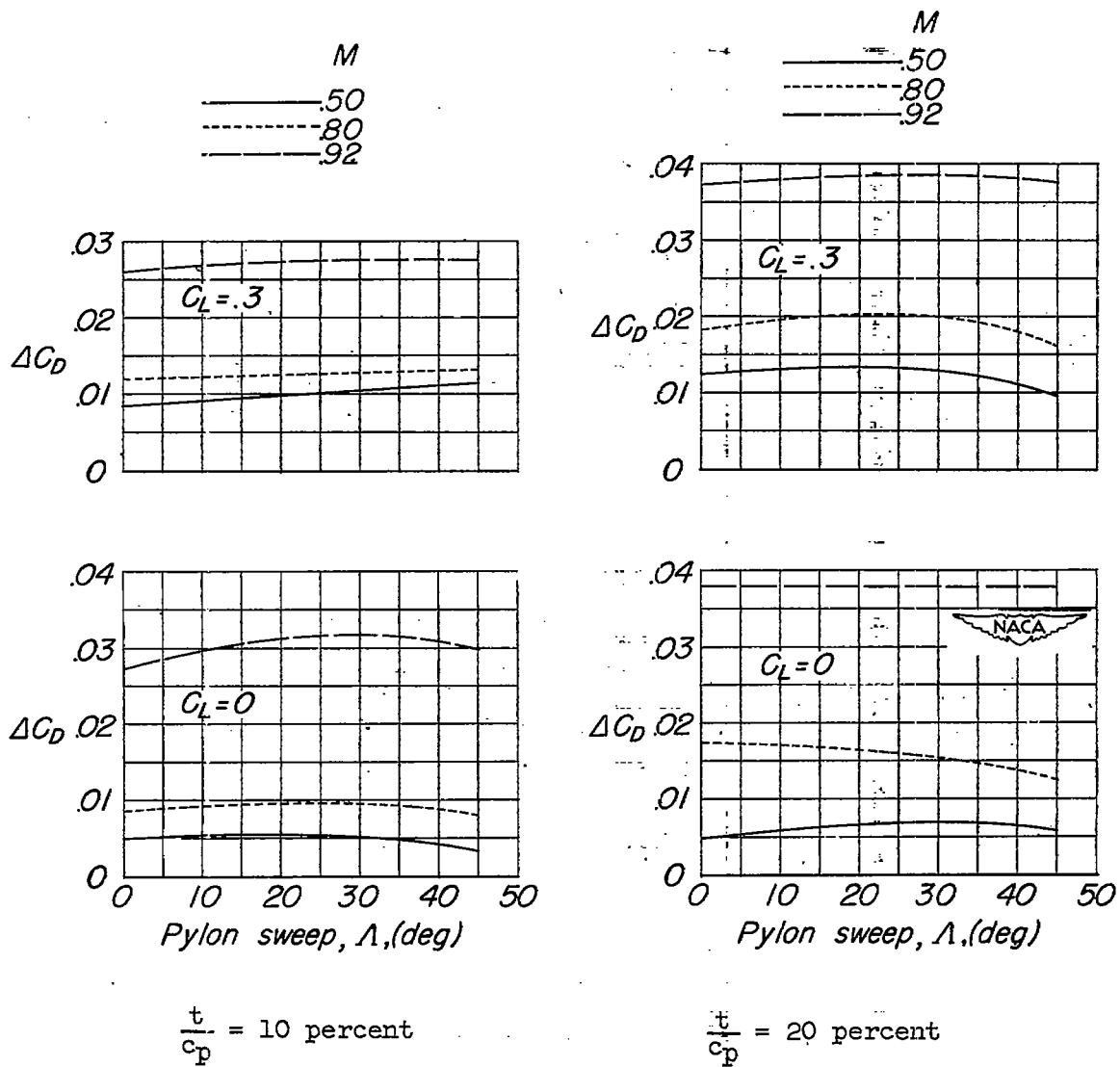


Figure 42.- Effect of Mach number on the drag characteristics of the basic model with an external-store installation showing the effects of variations in pylon sweep angle; $\frac{l_B}{d} = 6$; $\frac{l_p}{c} = 18.9$ percent; $c_p = 1.5$ inches.



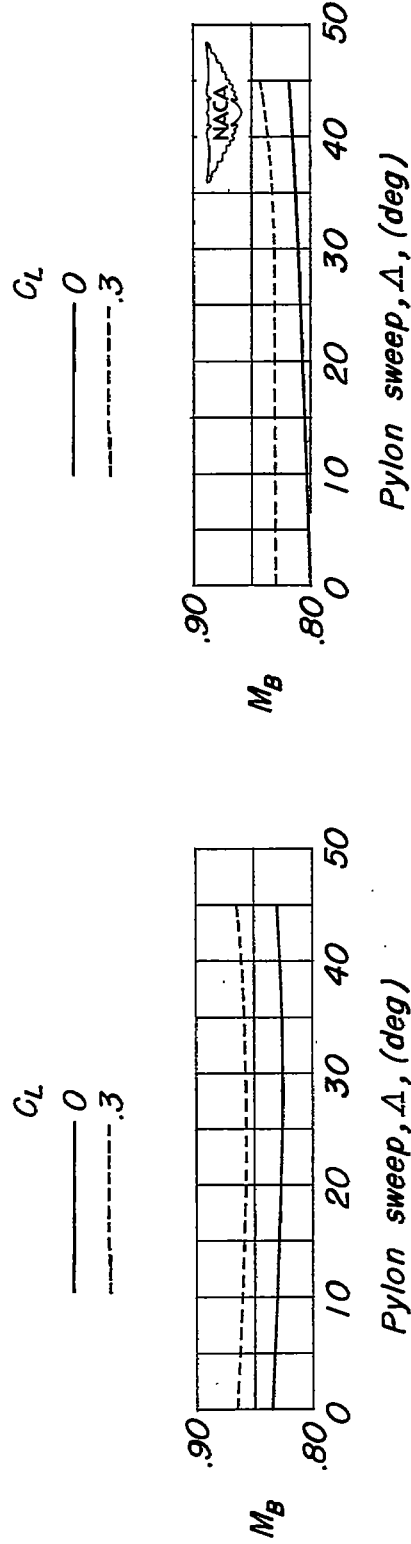
(a) ΔC_D against M.

Figure 43.- Effect of variations in pylon sweep angle on the drag characteristics of the basic model; $\frac{l_s}{d} = 6$; $\frac{l_p}{c} = 18.9 \text{ percent}$; $c_p = 1.5 \text{ inches}$.



(b) ΔC_D against Λ .

Figure 43.- Concluded.



(a) $\frac{t}{c_p} = 10$ percent.

(b) $\frac{t}{c_p} = 20$ percent.

Figure 44.- Effect of variations in pylon sweep angle on the drag-break Mach numbers of the basic model; $\frac{l_B}{d} = 6$; $\frac{l_p}{c} = 18.9$ percent; $c_p = 1.5$ inches.

~~CONFIDENTIAL~~

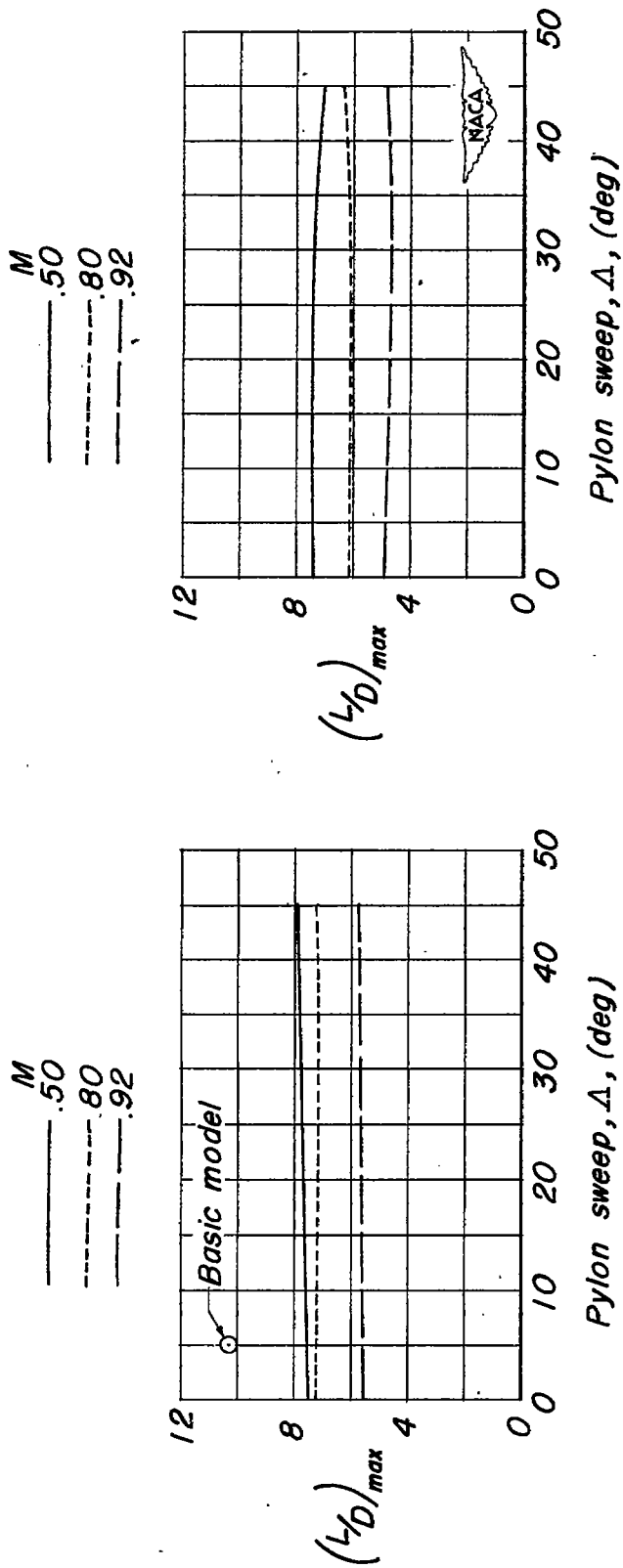
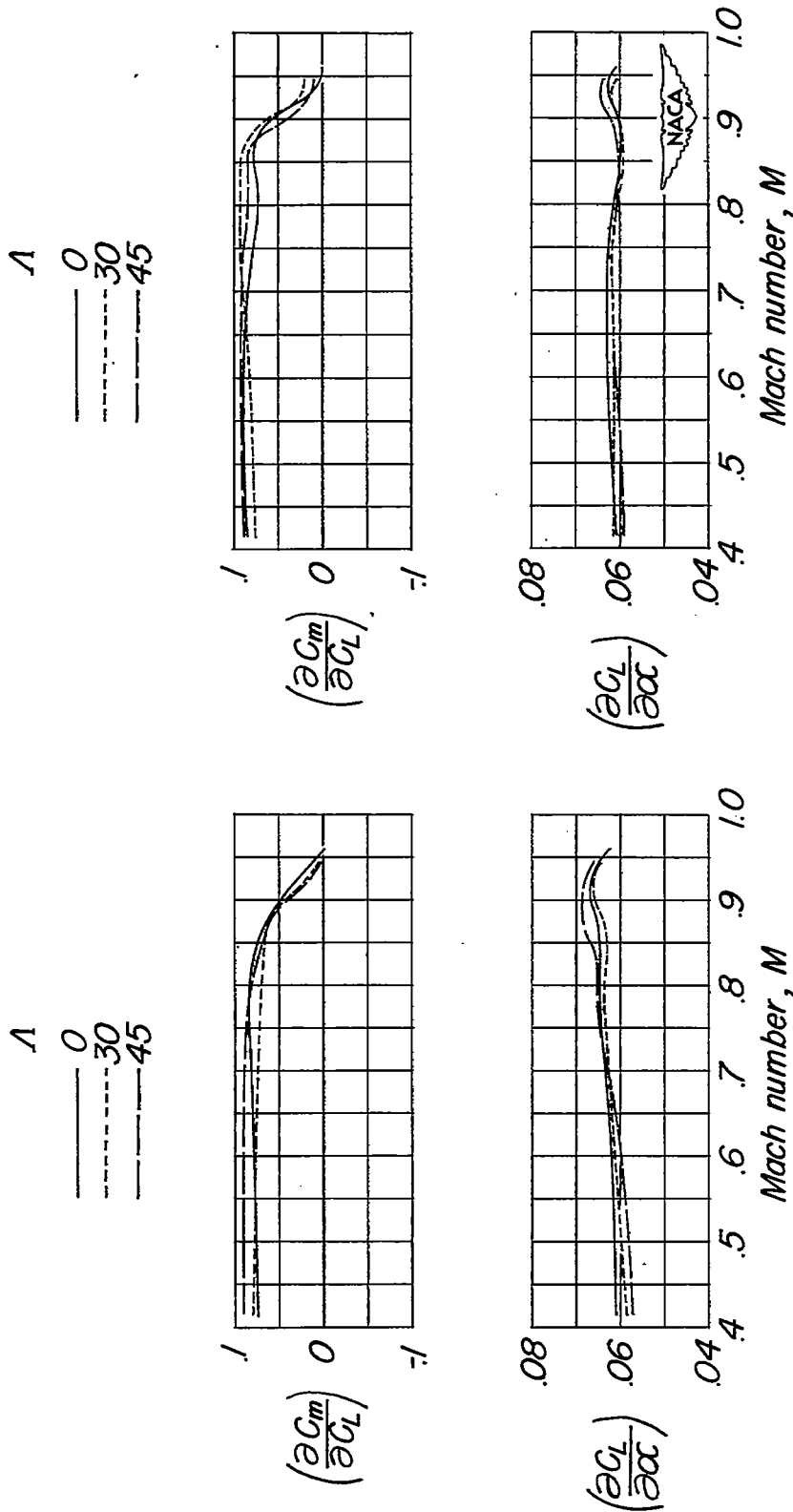


Figure 45.- Effect of variations in pylon sweep angle on the maximum lift-drag ratios of the basic model; $\frac{l_s}{d} = 6$; $\frac{l_p}{c} = 18.9$ percent; $c_p = 1.5$ inches.

~~CONFIDENTIAL~~

~~CONFIDENTIAL~~



(a) $\frac{t}{c_p} = 10$ percent.

(b) $\frac{t}{c_p} = 20$ percent.

Figure 46.- Effect of Mach number on the aerodynamic-center location and lift-curve slope of the basic model with an external-store installation showing the effects of variations in pylon sweep angle; $\frac{l_p}{c} = 6$; $\frac{l_p}{c} = 18.9$ percent; $c_p = 1.5$ inches.

~~CONFIDENTIAL~~